MODELING AND MEASUREMENT OF AIRPLANE FLUTTER PHENOMENON ON VHF TELEVISION SIGNAL

ANUCHIT WONGKEERATIKUL

A THESIS SUBMITTED IN PARTIAL FULFILLMENT

OF THE REQUIREMENT FOR THE DEGREE OF

DOCTOR OF ENGINEERING IN ELECTRICAL ENGINEERING

SCHOOL OF GRADUATE STUDIES

KING MONGKUT'S INSTITUTE OF TECHNOLOGY LADKRABANG

2008

KMITL-2008-EN-D-018-334

หัวข้อวิทยานิพนธ์	การจำลองและการวัดการเกิดปรากฏการณ์รบกวน จากเครื่องบิน ต่อคลื่นสัญญาณโทรทัศน์ย่าน VHF
นักศึกษา	นายอนุชิต วงศ์กีรติกุล
รหัสประจำตัว	45160316
ปริญญา	วิศวกรรมศาสตรดุษฎีบัณฑิต
สาขาวิชา	วิศวกรรมไฟฟ้า
พ.ศ.	2551
อาจารย์ที่ปรึกษาวิทยานิพนธ์	ผศ. ดร. สุทธิชัย นพนาคีพงษ์
อาจารย์ที่ปรึกษาวิทยานิพนธ์ร่วม	ผศ. ดร. พรชัย ทรัพย์นิธิ

บทคัดย่อ

วิทยานิพนธ์นี้ได้ทำการศึกษาการแพร่กระจายคลื่นของการส่งสัญญาณโทรทัศน์ ที่เกิดปัญหาจากการแพร่กระจายคลื่นโทรทัศน์ย่านความถี่ต่ำ และการเกิดปรากฏการณ์รบกวนจากเครื่องบิน โดยเฉพาะผลของการเกิดปรากฏการณ์รบกวนสัญญาณโทรทัศน์ย่านความถี่ VHF เนื่องจากเครื่องบิน ซึ่งเป็นปัญหาสำคัญอย่างหนึ่งของการรับสัญญาณโทรทัศน์ โดยการสร้างแบบจำลองบนหลักการพื้นฐานอยู่ 3 อย่างด้วยกัน คือ 1) ไบสตาติกเรดาห์ครอสเซคชั่น (Bistatic Radar Cross Section) ของวัตถุรูปทรงรี 2) การวิเคราะห์แบบ 3 มิติ ได้ถูกนำมาใช้เพื่อหาระยะห่างระหว่างคลื่นตรงและคลื่นสะท้อนจากเครื่องบินที่กำลังบินอยู่ 3) ทฤษฎีของเรย์ (Ray Theory) ที่มีพื้นฐานบนกายภาพและเรขาคณิตวิเคราะห์ ได้ถูกนำมาใช้ในการพิจารณา ผลลัพธ์ของแบบจำลองที่ได้จะนำไปเปรียบเทียบกับผลที่ได้จากการวัดจริง ซึ่งจะมีพารามิเตอร์ต่างๆ เช่น ความสูงของเครื่องบิน ระยะห่างจากสนามบิน มุมของการบิน ชนิดของเครื่องบิน รวมถึงความเร็วของเครื่องบิน เป็นต้น พารามิเตอร์เหล่านี้เป็นตัวแปร ที่ทำให้เกิดรูปแบบต่างๆ ของการรบกวน โดยได้ทำการเปรียบเทียบผลทั้งสองที่ความถี่ 60.75 MHz และ 208.75 MHz ซึ่งเราพบว่ารูปแบบของการเกิดปรากฏการณ์รบกวนมีความสอดคล้องกันอย่างมากระหว่างการจำลองและการวัดจริง

Thesis	Modeling and Measurement of Airplane Flutter Phenomena on VHF Television Signal
Student	Mr. Anuchit Wongkeeratikul
Student ID	45160316
Degree	Doctor of Engineering
Program	Electrical Engineering
Year	2008
Thesis Advisor	Asst. Prof. Dr. Suttichai Noppanakeepong
Thesis Co-advisor	Asst. Prof. Dr. Pornchai Supnithi

ABSTRACT

The thesis studies radio wave propagation on television broadcasting. Some problems of broadcasting such as Low Band Broadcasting, and Airplane Flutter Phenomena are described, in particular, airplane flutter phenomena on television broadcasting at VHF frequency band. The thesis presents a novel approach to model TV signal due to airplane flutter phenomena. The three components of the modeling are based on 1) Bistatic radar cross sections (RCS) of an ellipsoid, 2) 3-dimensional geometry consideration technique to calculate the distance difference between direct and reflected waves due to airplane, and 3) Ray theory, based on physical and geometrical consideration. Unlike previous works, the model takes into account of realistic parameters such as flying height, distance from the airport, flying angle, altitude, aircraft body type among others. The simulation results are then compared with measurement results at 60.75 MHz and 208.75 MHz. The results show good agreement between simulation and measurement patterns.

Acknowledgment

I would like to express my deepest and sincere gratitude to my advisor, Prof. Dr. Yoshiaki Moriya and Asst. Prof. Dr. Suttichai Noppanakeepong, for kindly providing me a good opportunity to study in this field, helpful guidance, valuable suggestions, kindness, thoughtful discussions and continuous encouragement throughout the course of study.

I would also like to express my sincere appreciation to my co-advisor, Assoc. Prof. Nipa Leelaruji and Assoc. Prof. Narong Hemmakorn, and Asst. Prof. Dr. Pornchai Supnithi, for their invaluable advice, useful ideas, thoughtful discussions and entire criticism.

Thanks are extended to Mr. Tikumporn Boonsuck and Miss. Pattreya Trerapat, candidate doctor student and graduate student in the satellite communication laboratory, respectively for their support and helpful field measurements. I also would like to thank the Department of Air Traffic Control; Aeronautical Radio of Thailand Ltd., for their flight information.

Finally, I would like to deeply thank towards my parents and my wife Ms. Saisamorn Wongkeeratikul for their supports and encouragement throughout this thesis.

Anuchit Wongkeeratikul

Contents

Contents (cont.)

Contents (cont.)

List of Abbreviations

Abbreviation	Description
C/N	Carrier-to-noise ratio [dB]
FEC	Forward Error Correction
Ku-band	12-14 GHz satellite frequency
C-band	4-6 GHz satellite frequency
Tx	TV transmitter
Rx	TV receiver
EMI	Electromagnetic Interference
VHF	Very High Frequency
UHF	Ultra High Frequency
MCOT	Mass Communication Organization of Thailand
BEC	Bangkok Entertainment Company Limited
PRD	Government Public Relations Department
T_{sun}	Sun brightness temperature [K]
f	Frequency
p	Single polarization attenuation factor
B_N	Usable noise bandwidth [dBHz]
L_S	Free space loss
r	Distance from earth to satellite
PSK	Phase Shift Keying
BER	Bit Error Rate
FM	Frequency Modulation
S/N	Signal-to-noise ratio
f_{max}	Highest frequency in the base band modulation signal

List of Abbreviations (cont.)

Δf_{peak}	Peak deviation frequency
B_{IF}	IF bandwidth
E_b	Average bit energy
P_b	Probability of bit error
M	M-symbol phase shift keying
T_o	duration time
B	Pre-detection bandwidth
D	Antenna diameter (m)
T_{ant}	Antenna noise temperature [K]
C/N_{up}	Up-link carrier-to-noise [dB]
C/N_{down}	Down-link carrier-to-noise [dB]
C/N_{down_sun}	Down-link carrier-to-noise (when sun transit)
$EIRP$	Effective Isotropic Radiated Power [dBw]
G_r	Receive antenna gain [dBi]
T_s	System noise temperature [dBK]
LNB	Low Noise Block
QPSK	Quadrature Phase Shift Keying
m	Modulation index
QP	Quasi-periodic fluctuation
NEC	Numerical Electromagnetic Code
RCS	Radar Cross Section
$E(r)$	Total electric field strength at receiving antenna at a radial distance r
E_o	Electric field strength of the direct wave at a radial distance r

List of Abbreviations (cont.)

R_1	Distance traveled by direct wave between source and point
R_2	Distance traveled by ground reflected wave between source and point
R_{ra}	Distance from airplane to receive antenna
h_{Tx}	Transmitter antenna height (m)
h_{Rx}	Receiver antenna height (m)
r	Distance between source and field point measured on the plane
y_{Tx}, y_{Rx}	Distance from transmitter and receiver antennas to airplane in y plane, respectively
e_1	Direct wave electric field strength
e_2	Ground reflected wave electric field strength
e_3	Airplane reflected wave
P_o	Output power of transmitter
k	Relative permittivity of the earth
P_{Dr}	Power density of wave at the receive antenna due to scattered by airplane
P_t	Transmitted power
G_t	Transmit antenna gain
G_r	Receive antenna gain

List of Symbols

Symbol	Description
λ	Wave length
θ and ϕ	Spherical coordinate
η	Antenna efficiency
$G(\theta, \phi)$	Antenna gain pattern [dBi]
θ_e	Half power beam width
$\sigma = \sigma_B$	RCS back scattered of ellipsoid
β	Free space wave number or phase constant
$D(\theta, \phi)$	Direct gain pattern
$S(\theta, \phi)$	Far field power density
ρ	Magnitude of reflection coefficient
Γ_{airp}	Percentage of reflection by airplane
$\sigma_{airp} = \sigma = \sigma_B$	RCS back scattered of airplane
$D(\theta, \phi)$	Directivity of antenna
$G(\theta, \phi)$	Antenna gain pattern
ε	Permittivity of the earth [F/m]
ρ_{gro}	Reflection coefficient by ground
φ_1, φ_2	Reflection coefficient phase by ground and airplane
θ_{Tx}, θ_{Rx}	Angle between antenna and reflected wave by airplane in vertical plane at transmit and receive side in degrees, respectively

Chapter 1

Introduction

Broadcasting has the communicative function for the public as a mass media. Variously information can be transmitted to the audience compared with other mass media. According to social influence is large. The subject of broadcasting is Television Broadcasting now. Television broadcasting is widely used as important media in worldwide.

The television signal transmits to receiver by the radio wave. The radio wave normally propagates into the space. Therefore, the propagation medium has influence on the radio wave at times. The problem of the television broadcasting technology often depends on the frequency. As for television broadcasting, the VHF and UHF bands are used for terrestrial broadcasting. The satellite broadcasting is used for the large coverage area. As for the range of the frequency, satellite broadcasting is used 1~20 GHz. The ionosphere influences in a low frequency band, and the rainfall attenuation is generated in a high frequency band. It is hoped that the excellent television broadcasting could be received anywhere in the stable footprint.

Wireless method is used for the majority of television broadcasting. Therefore, a lot of radio wave propagation problems occur. Even if, a new improvement technology has been used for the television reception up to now but some problems still occur. This thesis presents radio wave propagation problems of TV broadcasting and a new modeling approach.

1.1 Statement and Significance of the Problem

Some problems still occur in the TV broadcasting system such as noise interference in low channel receiving signal, solar noise, airplane flutter phenomena, and

etc. These problems are annoys to TV watching. The following shows significance of these problems.

Electromagnetic Interference (EMI): electromagnetic interference causes high interference to television reception, in particular, at low frequency band such as 47-68 MHz. This EMI is generally generated by man-made effects such as interference from high voltage transmission line (corona or leakage noise), transient switch, motor commutator sparking, automobile ignition, airplane scattering and sometimes from natural phenomena such as atmospheric noise [1] [2]. This interference will cause horizontal interference lines across the screen and the Buzz or Cracking sound at the TV speaker. At times the picture is collapsed or disappears.

Airplane flutter phenomena: The airplane flutter occurs when an airplane flies across TV transmitter and TV receiver antenna [5]. The reflected signal from airplane reaches the receiving antenna at the same time as the direct signal but with a phase delay. The phenomena naturally affect the signal quality of both analog and digital transmission systems [6]. In the previous works, a lot of researchers tried to analyze scattering events by the airplane. However, the analysis was not able to be done. We propose a novel approach to simulate the flutter phenomena based on physical and geometrical parameters. Accurate model of the signal variation caused by the phenomena is thus necessary for flutter prediction and compensation. The signal measurement is crucial for comparison with the simulation results of the developed model.

1.2 Goals and Objectives

- To study causes of interference generated of low band receiving, solar noise and airplane flutter phenomena.

- To create an accurate model of the signal variation caused by the airplane flutter phenomena necessary for flutter prediction and compensation. The airplane flutter signal measurement is crucial for comparison with the simulation results of the developed model.

1.3 Hypothesis to be tested

- Low frequency interference and solar noise interference are dependent on frequency. The interference can be reduced when higher frequency is used.

- The Airplane flutter modeling is based on Bistatic radar cross section of an ellipsoid, Ray theory and 3-dimensions consideration. It is suitable for use to analysis of these phenomena.

1.4 Scope of the Study

- To study causes of EMI and problem solving methods.

- To measure airplane flutter phenomena and crate an accurate prediction model.

1.5 Process of the Study

EMI:

- To study EMI interference on TV signal.

- Equipment setups and perform an experiment.

- Measure TV field strength signal and EMI signal.

- Consideration effects of EMI on TV reception.

Airplane Flutter:

- To study causes of airplane flutter.

- Equipment setups and take an experiment.

- To measure signal variation caused by airplane. The audio frequency of TV ch3 and ch9 are used for testing purpose.

- To create modeling of airplane flutter phenomena based on Bistatic radar cross section, Ray theory and 3-dimensional consideration.

- To compare between measurement and simulation results.

1.6 Limitation of the Study

- Due to measurement performed on open field, but some reflected wave from building causes of some patterns of airplane flutter fluctuation are complexes.

- Due to an airplane has not only body reflected but wings and tail could reflect the signals. In these cases, the special pattern of signal variation occurs.

- In this thesis, an only signal reflected by the airplane body is considered.

Chapter 2

Some Problems on Television Broadcasting Reception

This chapter investigated the problem that the television broadcasting signal is encountered on the propagation path. The trouble of television broadcasting seen in the radio wave propagation reaches many topics. The majority of the troubles are generated by interference by other radio sources. The trouble can be caused by electrical devices such as electrical motor, tools and appliances. Moreover, the interference occurs when TV signal reflects from an obstacle, such as building, mountains or airplane. Another trouble is weakening of reception signal. The weak reception signal causes of noise increased. Background theory of radio wave on TV transmission signal is show on the next section.

2.1 Ground Wave of Television Broadcasting System

The frequency of VHF and UHF bands are used for the ground wave broadcasting. The amplitude modulation is used for visual of television broadcasting. The frequency modulation is used for aural section. Power ratio of aural and visual signal is 1/10. When input signal is low, snow noise appears in the AM modulation part. Ground wave broadcasting obtains an excellent picture under the best reception input signal level. Normally, the best reception condition occurs when input signal level is 60 dBμV to 80 dBμV.

To understand the signal level behavior, the reception signal level can obtained from electric field strength E in a free space of the ground wave by [7]

$$E = \sqrt{30P}/d \text{ ,} \qquad \text{V/m} \qquad (2.1)$$

when d is distance between the transmitting and the receiving antenna in meter, P is transmission power in watt. Usually, electric field strength E_o (V/m) is shown by the isotropic gain of the half wavelength dipole antenna as

$$E_o \cong 7\sqrt{GP}/d, \qquad \text{V/m} \qquad (2.2)$$

here G is relative gain of the antenna.

Electric field strength E at television reception point is summation of the direct wave and the ground-reflected wave. Thus, it becomes an addition with the phase of two waves.

$$E = E_o\left(2\left|\frac{\sin 2\pi h_1 h_2}{\lambda d}\right|\right), \qquad \text{V/m} \qquad (2.3)$$

where h_1 and h_2 are the height of transmitting and receiving antennas, respectively.

An actual television reception signal is measured at KMITL. The channel 3 frequency is not transmitted now. The measurement is performed on rooftop of telecommunication engineering department (about 12 meters above ground) and main building of engineering faculty (about 52 meters above ground). Table 2.1 shows measured data of television broadcasting signal from Bangkok and Nakornratjasima stations. When antenna height is low, we found that the high frequency signal from Bangkok station has extremely decreased. This may be due to screening effect of many high building in Bangkok province. For a common problem of each channel, the measured value at the rooftop of the 3 floor is lower than the theory value. In addition, the measured value by half wave dipole antenna with 2 meters height above ground is about 40 dBμV/m (Reference: Figure 5.10-5.20 in Chapter 5). This shows that when the antenna height is low, the reception signal level has extremely lower.

Table 2.1 Measurement results of signal strength

Channel	Antenna height above ground (m)		Difference (dB)
	52 meters (dBμV/m)	12 meters (dBμV/m)	
Bangkok station			
Ch 3	78.5	63.8	15.2
Ch 5	83.0	58.2	24.8
Ch 7	91.3	71.3	20.0
Ch 9	78.3	51.1	27.2
Ch 11	94.2	71.5	22.7
Nakornratjasima station			
Ch 2	54.9	34.2	20.7
Ch 6	28.0	-	-
Ch 8	43.8	23.0	20.0
Ch 12	32.2	21.4	10.8

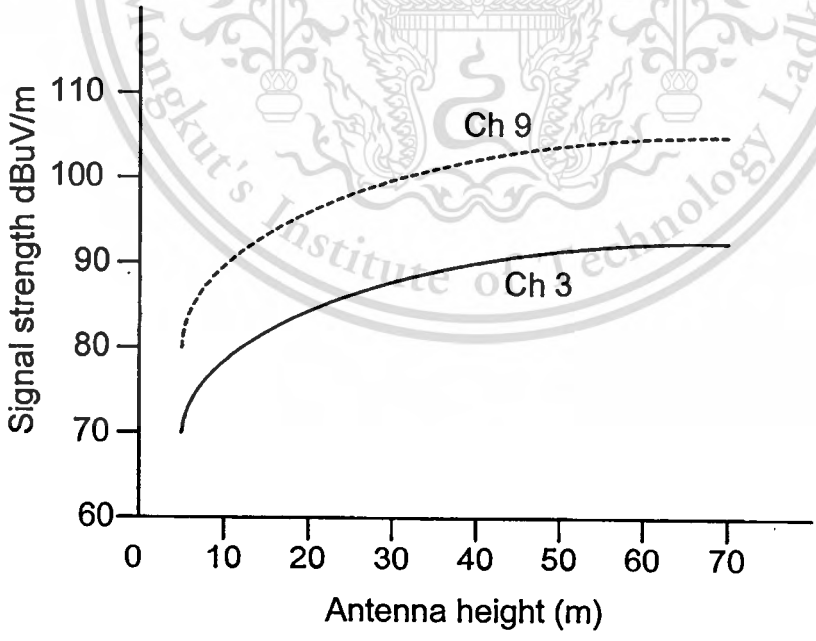

Fig. 2.1 Electric field strength characteristic of channel 3 and channel 9 when the receiving antenna height is changed

Figure 2.1 shows the electric field strength characteristic of channel 3 and channel 9 when the receiving antenna height is changed. The signal strength at reception point is calculated from Eq.(2.3). We find that the signal strength increased when antenna height increased but the signal level is increased in exponential shape. This shows that when antenna height is high rate increases, the signal level is only a little rate increases. The signal levels difference of channel 3 and channel 9 is about 10 dBμV/m.

Some problem of TV receiving is illustrated in the following section. The Interference degrades both picture and sound qualities of TV reception.

2.2 Electromagnetic Interference (EMI) on Low-band Reception

Fig. 2.2 Examples of Electromagnetic Interference (a) Digital TV (b) Analog TV

Many interference problems can be traced to domestic electrical equipment or appliances in home or a neighboring property. Electrical/impulse interference is usually more noticeable with digital reception [8]. For the reception will appear to be breaking up or look like a mosaic pattern as shown in Fig. 2.2(a) and (b). Television reception of VHF frequency channel 2 and 3 (47-68MHz), the received signal is easier interfered by EMI than the high frequency channel. In the case of Analog system, this interference will cause horizontal interference lines across the screen and the Buzz or cracking sound at the TV speaker is illustrated in Fig. 2.2(c). Sometimes the picture is collapsed or disappears. Moreover, this EMI can be generated by man-made effects such as interference from high voltage transmission line (corona or leakage noise), transient switch, motor commutator sparking, automotive ignition and airplane: and sometimes from natural phenomena such as atmosphere noise and signal fade. If it generated, the best solution is an aerial with a balun and a double screened coaxial cable. Analogue cures below could cure the problem. If this type of interference appears on digital reception all the time, and also freezes, the reason is that the signal is not strong enough.

Some causes of electrical/impulse Interference - Type 1 include Vacuum cleaners, Fans, Electric drills, Electric trains, Electric razor, and Sewing machines.

Some causes of electrical/impulse Interference - Type 2 include Automatic switches, Central heating thermostats, Refrigerators and Freezers.

This type of interference is normally caused by switches or thermostats especially thermostats in central heating systems. It appears on the screen as a dense white band of spots or on digital pictures as a mosaic effect, but only for a short period of time.

In many cases the source of the interference will be obvious because the interference appears when an item such as an electric drill is being used. Where the source of interference isn't obvious, try to locate it by switching off everything in the home one item at a time while another person monitors the effect on the TV screen.

Alternatively, if you have a portable radio and can hear the interference on it, take the radio from room to room to find where the interference is loudest. All modern electrical equipment is manufactured to regulations requiring that interference suppressors be fitted.

To problem solving is shown in the following. 1) Always install an aerial with a balun, 2) Combine a balun fitted aerial to good quality double-screened type coaxial cable, 3) Avoid coupling joints in the cable; always aim to have one solid piece of cable to each outlet point and 4) Do not run coaxial cable near to any source of electrical interference such as a thermostat or a motor.

2.3 Solar Noise Interference

Fig. 2.3 Example of solar noise interference on Analog TV

Solar noise interference disturbs on satellite broadcasting system in both digital and analog versions. It occurs when the sun is just behind the spacecraft when viewed from the ground antenna system. At that moment, the temperature of receiving antenna rises abruptly and the communication link fails due to the noise from the sun. For geostationary broadcasting satellite system, the solar noise interference happens once a

day for several minutes during a few day near the spring and fall equinoxes. The number of sun interference and their duration depend on the minimum tolerable carrier-to-noise (*C/N*) ratio. When the transit time, the TV screen shows a mixture of picture and snow as shown in Fig 2.3. As strong solar noise, only snow occurs.

The interference level that will be experienced depends upon the frequency of operation, the antenna beam width, the receiver bandwidth, the acceptable signal to noise ratio, and the level of solar activity at the time. These parameters must be used with caution to reduce the solar noise effects. We can use Ku-band instead of C-band or use Digital system with FEC (Forward Error Correction) instead of Analog system while the solar noise occurs to solve the problems.

2.4 Interference Trouble by Airplane

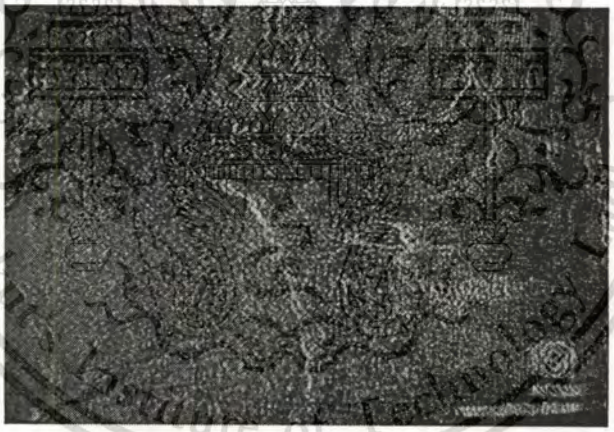

Fig. 2.4 Example of airplane flutter interference on Analog TV

Airplane flutter phenomena occur when an airplane flies across transmitting and receiving antenna. The reflected signal from airplane reaches the receiving antenna at the same time as the direct signal but with a phase delay. The phenomena naturally affect the signal quality of both analog and digital transmission systems. The reflected wave by airplane is can be disturb both picture and sound of television when an airplane flies across the direction of receiving signal. Result of two signals is ghosting, fading, sometime

collapse and distortion of picture on TV screen as shown in Fig. 2.4. We perform measurement and modeling of this phenomenon on TV signal when the airplane flies across and range Tx (transmitter) and Rx (receiver). The Yagi antenna is used for improving the airplane flutter phenomena problem due to both high gain and directivity. The model of signal variation caused by these phenomena is thus necessary for flutter prediction and compensation. In chapter 4 we study in the details of these phenomena.

2.5 Ghosting

(a) (b) (c)

Fig. 2.5 Ghosting interference (a) normal picture (b) an example of "Ghosting" and (c) when Ghosting occurs

Ghosting is the sort of picture experienced see when the TV signal is reflected from a large building or other structure in your locality as shown in Fig. 2.4. The problem is caused when both the direct signal and a reflected signal from the transmitter are received [9]. Because the reflected signal travels a greater distance before it arrives, it produces a picture shifted to the right of the normal picture.

Digital television employs a modulation system with strong protection against multipath reception (ghosting). In most cases when ghosting occurs on an analogue picture, the digital reception will be fine. However, if the digital reception seems to be affected due to the ghosting seen on the analogue pictures, the cures for analogue ghosting should in turn cure the digital reception as well. Solutions for ghosting can be done with fact that. 1) Better picture can usually be obtained by altering the direction in which the

aerial is pointing or 2) One can adjusting the height of the aerial is usually the best method to adopt or 3) If ghosting is severe and persistent, a more directive aerial such as a high gain aerial or a log periodic type should be used. Another aerial that has been known to eliminate ghost signals is a Grid type aerial.

2.6 Poor picture (Weak signal) on Digital or Analog System

Some poor pictures are illustrated in Fig. 2.6. The picture on the left shows a normal picture for comparison. The pictures on the right are the type that will be received if you are far away from the TV station or if there is a building or hill between antenna and the TV station. The same effect may be caused if one live in a valley where shielded from the signal. Each TV station has a defined service area where the strength of the TV signal is adequate to give good reception. Just beyond the boundary of the service area is a fringe area where the signal will be weaker and reception quality will be poorer. Solutions to poor picture can be archived are in the following. 1) Once one has checked that the weak signal is not due to a defective or badly pointed aerial, poor connection, broken or disconnected lead, one could improve the signal strength by: Changing the coax cable to a double-screened type, 2) One can increase the height of the aerial if possible, 3) Install a higher gain aerial, and 4) Installing a masthead or setback amplifier to boost the signal. 5) If there are many splits of the signal around the home using standard coaxial cable splitter units, it could be that the signal has been reduced too much, in cases where 2 or more TV sets are to be fed it is recommended that a distribution amplifier be used rather than splitting the signal. This method is especially essential for digital reception.

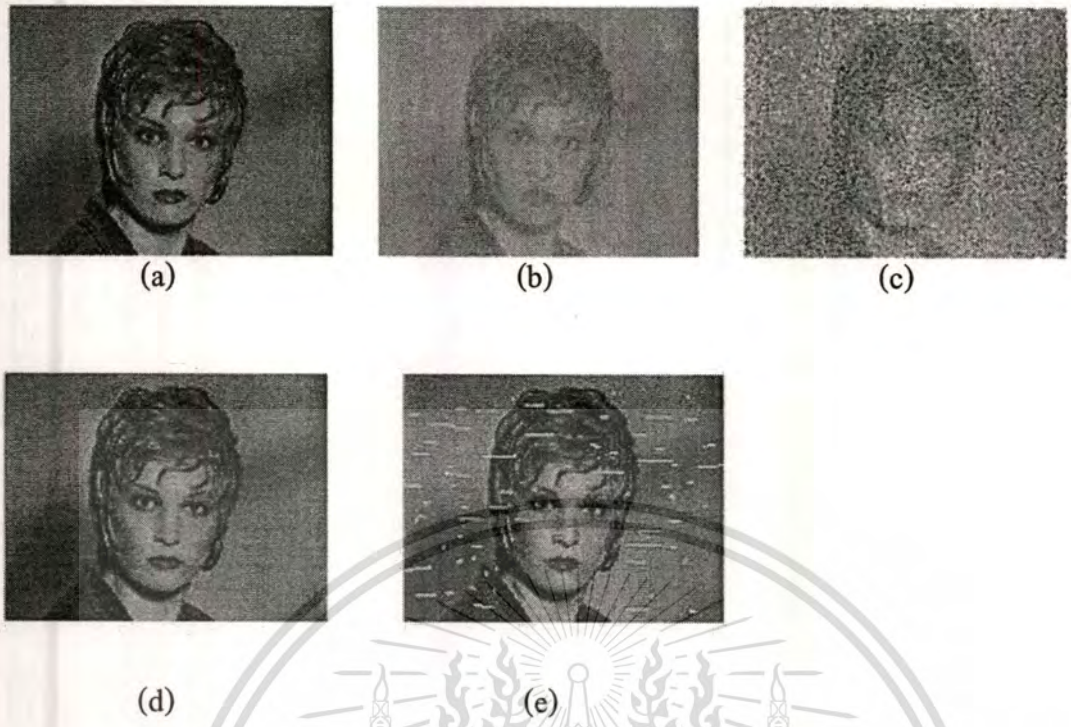

(a) (b) (c)

(d) (e)

Fig. 2.6 Poor pictures (a) Normal analog picture (b) (c) progressively weaker analog signal (d) a normal digital picture and (e) a weak digital signal

2.7 Co-channel Interference

(a) (b)

Fig. 2.7 Two examples of Co-channel interference

A distant transmitter usually causes co-channel Interference, because it transmits on the same channel as the local transmitter where the main signal is being received. This problem is rare, but unfortunately can happen due to the channel allocations of the vast amount of transmitters nationwide as illustrated in Fig. 2.7. Co-channel interference can affect digital reception by overloading; in this case the following analogue cures could cure the problem. Solution to co-channel interference can be done by the following steps. 1) It can be that the aerial installed has a very large viewing angle/beam width; an aerial such as a high gain that has a narrow viewing angle could solve the problem, 2) Adjustments in height and left to right (azimuth) as per the ghosting example could solve the problem, 3) If the problem is severe, it could be that the location of the property is on a bearing with the required transmitter that will always have the problem. In a case like this it is often required that the aerial be pointed in a different direction to receive from an alternative transmitter. This alternative transmitter could be further away from the original; therefore amplification or a higher gain aerial may be required and 4) Monitor the polarity of the aerial when searching for an alternative signal as the alternative transmitter may transmit a vertically polarized signal; this means that the orientation of the aerial will need to be vertical.

2.8 Radio Interference

Effects of radio interference on the TV screen include 1) moving, wavy or herringbone patterns, 2) a 'waffle' effect, 3) S patterns or 4) loss of color as illustrated in Fig. 2.8. This type of interference is usually caused by equipment that emits radio waves, as used by taxis and emergency services, amateur and citizens' band radio, and mobile phone services. Most of this equipment is properly licensed and filtered, though some is not. Radio interference can also be caused by equipment connected to your TV set, such as a video or DVD recorder or a signal booster [10].

Fig. 2.8 Example effects of radio interference on Analog TV

Solutions to poor picture can be archived are in the following. 1) You can cure many cases by fitting a simple plug-in high-pass filter between the plug on the end of the aerial lead and the aerial socket on the back of the TV set. A variety of suitable filters are available and your dealer will advise you which ones to try, 2) If the filter does not work, the TV set could require an internal modification to improve its immunity to interference, 3) Many aerials have well out of band rejection performance, so a change of aerial to one with good out of band rejection may be worthwhile, and 4) Also many masthead and distribution amplifiers have filters fitted, so a change of amplifier to one with included filters could also help.

2.9 Interference from a Neighboring channel

The transmitter of a television station in an area can cause problems with the reception of more distant stations transmitting on adjacent channels as shown in Fig.2.9. If, for example, one receiving both a weak channel 13 signal and a very strong channel 12 signal, the sound of the latter is likely to cause a grainy picture on channel 13 [11] [12]. To check this, tune another television to channel 12, if possible, while observing the interference on channel 13 of the original television set. If you are experiencing this type

of interference, there will be a correlation between the interference on channel 13 and the sound on channel 12. Solutions to interference from a neighboring channel can be archived are in the following. 1) Re-pointing your antenna may eliminate this type of interference; if not, proper filters will be necessary, and 2) A higher-gain Yagi or rear-screen antenna may also prove effective.

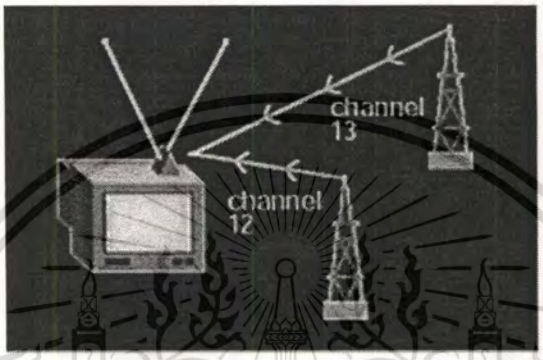

(a)

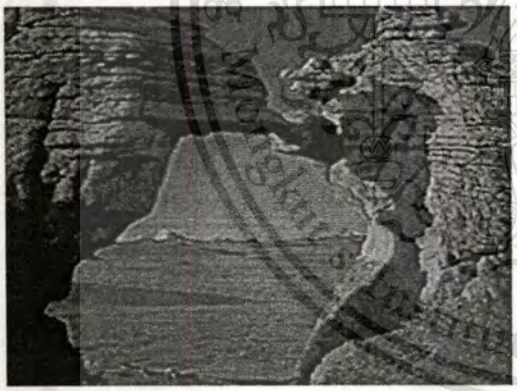

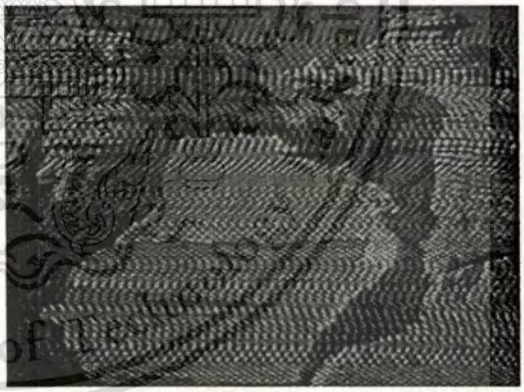

(b) (c)

Fig. 2.9 Interference from a Neighboring channel (a) causes of Neighboring channel (b) normal picture (c) example of neighboring interference

Chapter 3

Low-band Reception

3.1 Introduction

Electromagnetic interference (EMI) is the unintended radio frequency emissions from electrical and electronic products, which have the potential to interference with the operation of other products. EMI could high interference to television reception, especially at low frequency band such as 47-68 MHz. The EMI is generally generated by man-made activities such as interference from high voltage transmission line (corona or leakage noise), circuit changing switch, motor commutator sparking, automobile ignition and airplane: and sometimes from natural phenomena such as atmosphere noise [13] [14]. In addition, EMI is generated by computers, hair dryers or vacuum cleaners interfering with television/radio reception or telephones. While some EMI is a nuisance of industry plant, aircraft control systems, motor vehicles, or medical equipment, the Electromagnetic Compatibility (EMC) framework has been put into place to reduce the disturbances caused by EMI [15]. Electromagnetic Compatibility refers to the ability of an electrical or electronic device or system to function satisfactorily in its environment without interference to other devices in that environment. When VHF low-band (channel 2 and 3) signal is received, it is easier interfered by EMI rather than the higher frequency channel [16]. This interference will cause horizontal interference lines across the screen and the Buzz or Cracking sound at the TV speaker. Sometimes the picture is collapsed or disappears.

In this chapter, the characteristic of the electromagnetic interference effect generated by several sources discussed above at the television frequency channel 2-4 is presented. We propose the methods to avoid their effects on television reception on the VHF low band channels.

3.2 Experimental Details

3.2.1 Measurement Setup

The TV signal field strength has been measured by using Hewllet Packard (HP) spectrum analyzer model 8591C and using the HP antenna has correction factor setup. The measurement parameters are illustrated in Table 3.1.

The measurement is made at the 10 km point apart from the television transmitter station and move every 10 kilometers away until reaching the 100 kilometers point from the transmitter. The measurement range covers both in the urban area and the rural area where there is no interference effected from EMI. Signal strength is measured from MCOT, PRD and BEC station. The transmitter station CH2 of MCOT (Mass Communication Organization of Thailand) is located at Nongbua-Lumpu province. It uses NEC model PCN1410AL/1 VHF TV transmitter with 10 kW output power. This area is on small hill and the total height of antenna is 380 meters above sea level. The CH4 of PRD transmitter station is located at Khon Kaen province. It uses HARISS TV transmitter with 10 kW output power. The station is on the flat urban area (Muang district). TV transmitter antenna height is 150 meters above sea level. The CH2 transmitter station of BEC (Bangkok Entertainment Company) is on Kho-yai-ting, Srikute district, Nakornratjasima province. The TV transmitter of NEC model PCN1620SSL/1 with 20 kW output power is used. Its location is on the mountain. The total antenna and mountain height is 790 meters above sea level.

We also perform the EMI measurement on VHF low band channels with the receiving antenna heights of 6, 12 and 18 meters by setting up on open area and without any disturbance from other sources. The field strength for EMI is measured at every 2 meters increment for distance 1-40 meters. The spectrum analyzer of Hewllet Packard model 8591C is used to measure EMI signal levels. The measurement is done for 4-5 times for each point and the average value for better accuracy data is computed. The parameters of EMI measurement are illustrated in Table 3.2.

Table 3.1 Measurement setup for signal field strength

Frequency (MHz)	47-54 (MCOT, BEC) 61-68 (PRD)
Tx antenna height above see level (m) CH 2 (BEC) CH 2 (MCOT) CH 4 (PRD)	 790 (Nakornratjasima) 380 (Nongbua-Lumpoo) 150 (Khon Kaen)
Rx antenna height of standard dipole (m)	5

Table 3.2 EMI measurement parameters

Rx antenna heights (m)	6, 12, 18
Yagi low band antenna (CH 2 – CH 4) Gain (dB) VSWR F/B ratio (dB)	*MASPRO* 5 1.2 10
EMI generator	Motor cycle
Spectrum analyzer	Hewllet Packard model 8591C

3.2.2 Measurement Results

The results of TV signal field strength of CH2 (MCOT station) from Nongbua- lumpu province, CH4 (PRD station) from Khon Kaen province and CH2 (BEC station) from Nakornratjasima province are shown in Figure 3.1. We observe that the field strength of CH4 decrease on the faster rate than that of CH2 (MCOT and BEC stations). This is due to the fact that CH4 has the lower Tx (Transmitter) antenna and higher frequency than CH2.

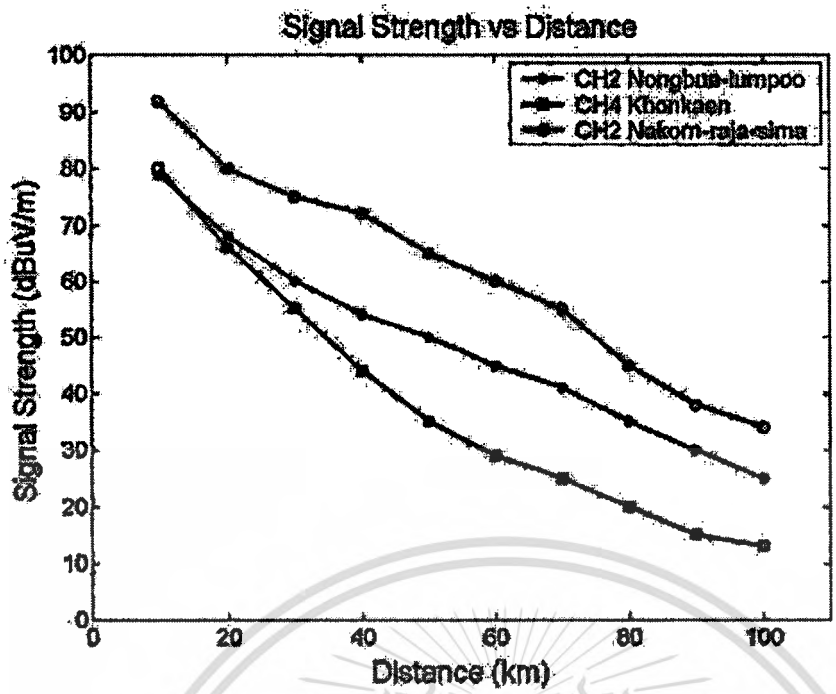

Fig. 3.1 The field strength results of CH2 (MCOT, BEC) and CH4 (PRD)

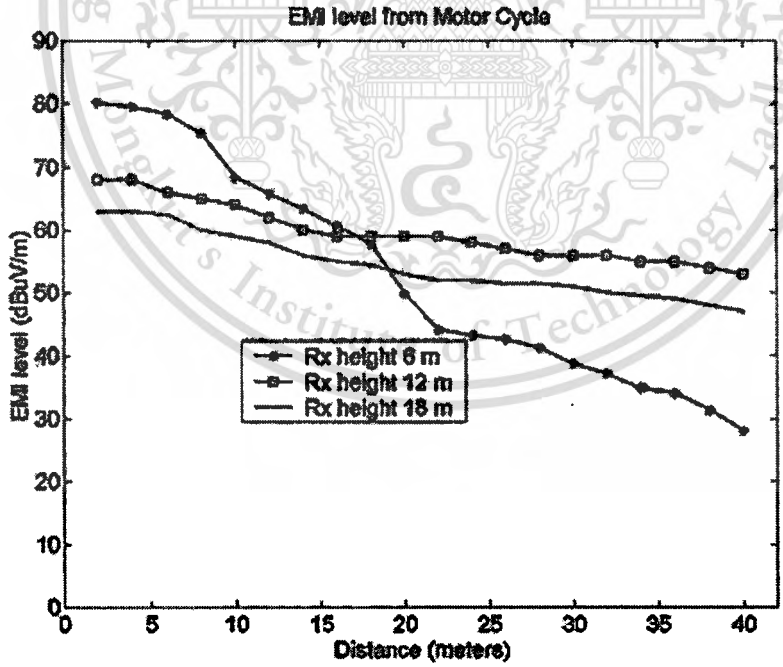

Fig. 3.2 EMI level generated by motor cycle at 6, 12 and 18 m of receiver antenna height

At the distance around 10 km from Tx antenna, both PRD and MCOT have similar field strength at around 80 dBμV/m. While BEC is 92 dBμV/m because it has higher both output power and antenna height. When the distance is further increased, the field strength of CH4 will decrease rapidly. At the distance 50 kilometers, Muang district, Kalasin province, the field strength of CH4 is dramatically decreased to 35 dBμV/m compared to CH2 of MCOT at the distance 70 kilometers, Pend district, Udon Thani province, the field strength decrease slightly to 44 dBμV/m. It can be seen that for CH2 with longer distance, its field strength is still higher than CH4.

The measurement results of EMI generated by motor cycle are illustrated in Fig. 3.2. It shows the EMI generated by motor cycle at 6, 12 and 18 meters of Rx antenna height. At 2 meters apart from source the measurement results are 80, 68 and 63 dBμV/m, respectively and at the 40 meters apart from source are 28, 54 and 47 dBμV/m, respectively. We find that at low receiving antenna height, for example 6 meters, the interference will be high level when EMI source is near Rx antenna but it decreases quickly when EMI source is far from the antenna.

The received signal from CH3 Nongkam, Bangkok at KMITL using the yagi antenna 5 elements of MASPRO with height of 40 meters above ground is illustrated in Fig. 3.3. The distance from TV station is around 40 kilometers. We could see the snows affected on TV picture screen. Figure 3.4 shows line scan signal number 12 to 22 by VM700T of Textronix. We find the noise signal on line 12 to 16. Line 18 to 19 had shown the vertical interval test (VIT) signal.

Figure 3.5 illustrate of the spectrum of EMI generated by motor cycle, spectrum of CH4 TV frequency response and spectrum of FM radio broadcasting frequency response. They are spread in the range of 24-124 MHz frequency band. The center frequency is 74.3 MHz. We observe that the left hand portion of center frequency is EMI and it is easy to disturb the receiving signal CH2 to CH3 (47-61 MHz).

Fig. 3.3 EMI interference on TV screen of CH 3 (54-61 MHz) BEC, Bangkok

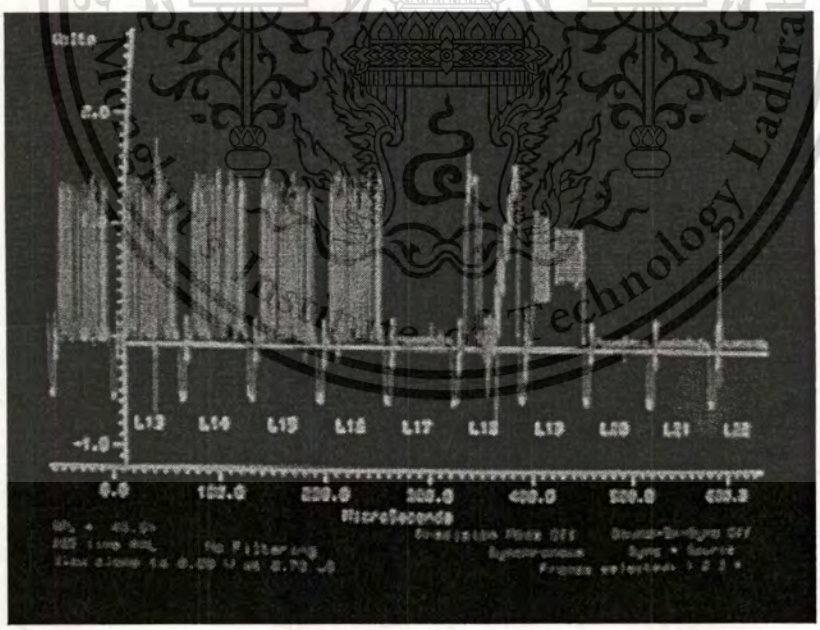

Fig. 3.4 Line scans number 13 to 22 of Figure 3.3 by VM700T video wave from analyzer of Textronix instrument

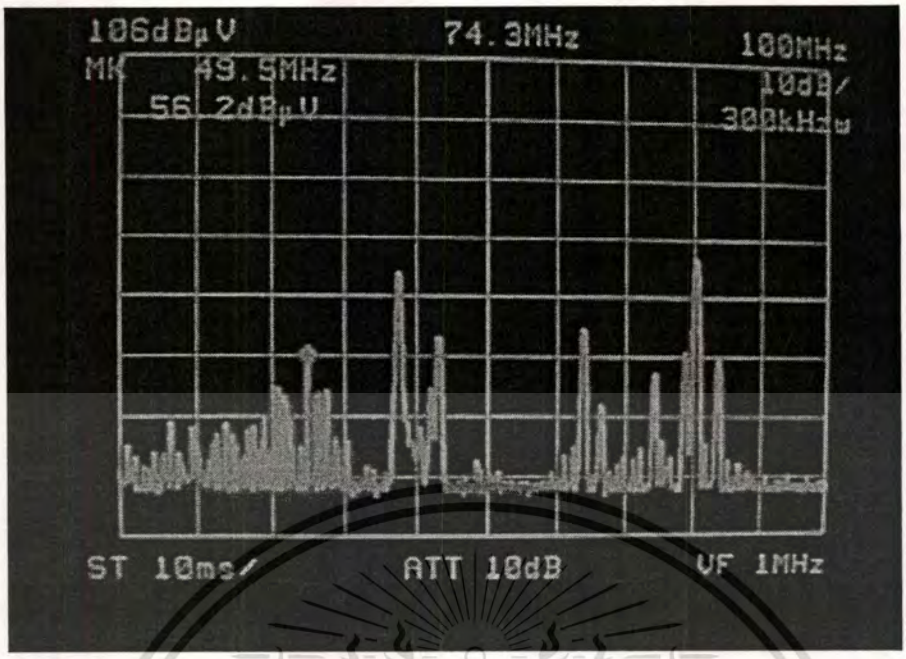

Fig. 3.5 Spectrum of EMI generated by motor cycle, CH4 (61-68 MHz) and FM radio broadcasting (88-108 MHz)

3.3 Discussions

The field strength of CH4 (PRD) decreases on the faster rate than CH2 (MCOT) may be due to transmit antenna is low level as shown in Fig. 3.1. Even if the output power of both channels is at same level (10 kW). The EMI is at high level when used with low receive antenna and quickly decreases when apart from EMI source as illustrated in Fig. 3.2. Normally, the higher antenna can be used to reduce disturbance from EMI source. We find that although the TV field strength of CH3 (BEC), Bangkok station is at high level around 60 dBμV/m (40 kilometers from transmit antenna) with 40 meters receiver antenna height but it is still easily disturbed by EMI as shown in Fig. 3.3.

The signal strength of CH2 (BEC) is at high level, but is very easily disturbed by EMI, but with little effects on CH4 and higher channel. By measurement, the distance around 60 kilometers from transmitting station at Sri-bun-rung district, Nongbua-lumpu

province, signal strength of CH2 (MCOT) about 45 dBμV/m. The EMI is about 20-30 dBμV/m and can observe the effects on TV screen. We find the horizontal interference line across the screen from a few lines to several lines, sometimes loses the sync signal makes the picture flip and also introduces Buzz or Cracking sound on loud speaker. While the receiving signal of CH4 (PRD) at Nond-sa-ard district, Khon Kaen province, the distance around 60 kilometers away from transmitter, does not show any interference effects. Even though the signal field strength is lower than of CH2. Figure 3.5 shows EMI signal causes interference at low frequencies band of around 30-54 MHz, but affect slightly or none at higher frequencies.

3.4 EMI Filters

When the source of the signal noise cannot be eliminated, filtering is recommended as the last resort. EMI filter is commonly available filters. As EMI filters are commercially available to eliminate high frequency noise in power lines. They not only stop the noise from entering the system, they also the noise manufactured by the system to leave the system and reach other parts of the bigger system. This effect is called bidirectional. A combination of inductors and capacitors make up the EMI filters. The EMI filters can also be in configurations such as feedthrough capacitors, L-circuits, PI-circuit, and T-circuits. The component of a feedthrough capacitor component is a capacitor. Feedthrough capacitors are good choice when the impedance connected to the filter is high. The L-circuit has an inductor on one side of the capacitor. This configuration works best for the line and load that have a large difference in impedance. The inductive element gets connected to the lowest impedance. For PI-circuit, two capacitors surround an inductor. When the line and load have a large difference in impedance, the PI-circuit is the most suitable. The PI-circuit also is used when high levels of attenuation are needed. The T-circuit has inductors on either side of the capacitor. It works best when both line and load impedances are low.

However, feedthruough caused of low frequency response is not so good. In practical, we must choose suitable type of feedthrough for high quality of circuits.

3.5 Conclusions

In the study of low-band frequency reception, we find that lowest channel of TV broadcasting (CH2 frequency of 47-54 MHz) in the VHF frequency low band such as BEC Nakornratjasima province or MCOT Nongbua-lumpu province is most affected by EMI although the received signal field strength is high. The PRD Khon-Kaen, which has higher frequency of CH4 (61-68 MHz), is slightly affected or almost unaffected even though the received signal field strength is lower.

We may change the antenna direction to avoid EMI source path or change the position of the receiving antenna or using the noise canceller is installed in the noise generator such as appliances to reduce effects of EMI.

3.6 Acknowledgements

The authors are grateful to Dr. Kanok Janchitrapongrej for his kind support for providing the Textronix VM700T measurement equipment.

Chapter 4

Airplane Flutter Phenomena

4.1 Literature Review

Airplane flutter phenomena [16][17] occurs when an airplane flies across transmitting and receiving antenna. The reflected signal from airplane reaches the receiving antenna at the same time as the direct signal but with a phase delay. The phenomena naturally affect the signal quality of both analog and digital transmission systems [18]. Accurate model of the signal variation caused by the phenomena is thus necessary for flutter prediction and compensation. The signal measurement is crucial for comparison with the simulation results of the developed model.

Previous works on flutter modeling can be found in [16][19][20][21]. In [16], the reflected signal from aircraft is measured from different angles using scaled aircraft in an echoic chamber. A Quasi-periodic (QP) fluctuation of signals is observed. In [20], a sinusoidal approach is used to replicate the signal attenuation in the VHF and UHF band as a result of the airplane flying near an airport. It indicates that directivity of the antenna does not affect the pattern of received TV signal. In [16], a geometrical aspect is, however, not used to generate the signals.

To obtain more accurate flutter models, aircraft modeling is required. Radar cross section (RCS) technique has been used to model complexes objects. In [22], approximation of an airplane dimensions based on bistatic RCS of spheres and cylinder agree approximately with predictions obtained via exact techniques. In [23], the RCS of Boeing 747-200 aircraft is developed using the Numerical Electromagnetic Code (NEC). The paper presents RCS variations of an aircraft along different flight routes at the 20-60 MHz frequency band. The simulation result is not compared with the actual flying route, but with the experiment of scaled aircraft in the echoic chamber. In this case, although the

experiment offers better understanding of fluttering, it is based on unrealistic parameter values. For example, the airplane is scaled to 1:100 operating at frequency of 2-6 GHz instead of 20-60 MHz. In addition, the speeds under study differ from actual values at 400-500 km/hour.

The signal variation from fluttering is the result of multipath propagation of direct waves, reflected waves from the airplane and ground. Multipath propagation from the airplane fluttering has recently been discussed in the literature [19][20][24]. In [19-20], a single scatter multipath model and Doppler shift effect are included to model the VHF signal. In [24], the modeling of fading and ghosting of both digital and analog signals are reported. The paper describes simulation of multipath effects with the result of picture distortion in various environment conditions ranging from fixed path between transmitters and receivers to moving reflectors with and reception under mobile condition, but the paper does not compare simulation from equipment with measurement data.

In this chapter, we develop a novel model to produce signal fluctuation due to the airplane flutter phenomena. Our contributions are three folds. Firstly, the bistatic *ellipsoid* RCS backscattered method is used to approximate the airplane body. Secondly, the distance and phase difference between direct and reflected waves are computed using the 3-dimensional geometrical technique. Finally, we calculate the total electric field strength at the receiving antenna by modifying the Ray theory and using multipath propagation. Most importantly, realistic parameters such as flight altitude, speed, direction, body type, frequency among others are included in the model. The simulated results are compared against the measured data with the actual flying routes based on two modes of flying patterns: cross and cross-range pattern. Furthermore, the model clearly shows the effect of airplane fluttering on low frequency signal.

4.2 Background Theory

In this section, the radar cross section (RCS) back scattered of a simple object and wave propagation on the plane earth are reviewed in relation with the flutter phenomena.

4.2.1 Bistatic Radar

Radar systems that use the same antenna for both transmitting and receiving are called mono-static radars. Bistatic radar uses transmit and receive antennas that are placed in different locations. Under this difinition CW radar, although they use separate transmit and receive antennas, are not considered bistatic radar unless the distance between the two antennas is considerable. The angle between wave from transmitting antenna to target and reflected wave from target to receiving antenna is called bistatic angle. A synchronization link between the transmitter and receiver is necessary in order to maximize the receiver's knowledge of the transmitted signal so that it can extract maximum target information.

The synchronization link may provide the receiver with the following information: (1) the transmitted frequency in order to compute the Doppler shift; and (2) the transmit time or phase reference in order to measure the total scattered path (direct wave + reflected wave). Frequency and phase reference synchronization can be maintained through line-of-sight communications between the transmitter and receiver. However, if this is not possible, the receiver may use a stable reference oscillator for synchronization.

4.2.2 Radar Cross Section (RCS)

The electromagnetic waves with any specified polarization diffract scattered signals in all directions when incident on a target. These scattered waves are broken down into two parts; the first part is made of waves that have the same polarization as the receiving antenna, the other has a different polarization to which the receiving

antenna does not respond. These two polarizations are orthogonal. The target RCS is defined as effective cross section of the target causing the intensity of the back scattered energy with the same polarization as the radar's receiving antenna. It is expressed with the unit of m^2. An approximate method is often used to predict RCS of complexes and extended targets such as aircraft, ships, and missile [25]. When experimental results are available, they can be used to validate and verify the approximations.

We consider using RCS of ellipsoid with dimensions (width and length) relative to the body of an airplane. In fact, other shapes of objects such as spheres and cylinders have been used to model the airplane flutter, but the case in this paper produces results closer to measured data.

4.2.3 RCS Back Scattered of Ellipsoid

The RCS back scattered determines the proportion of intensity of waves reflected from the target. Consider an ellipsoid centered at the coordinate (0,0,0) as shown in Fig.4.1. It is used to model the body part of an airplane defined by

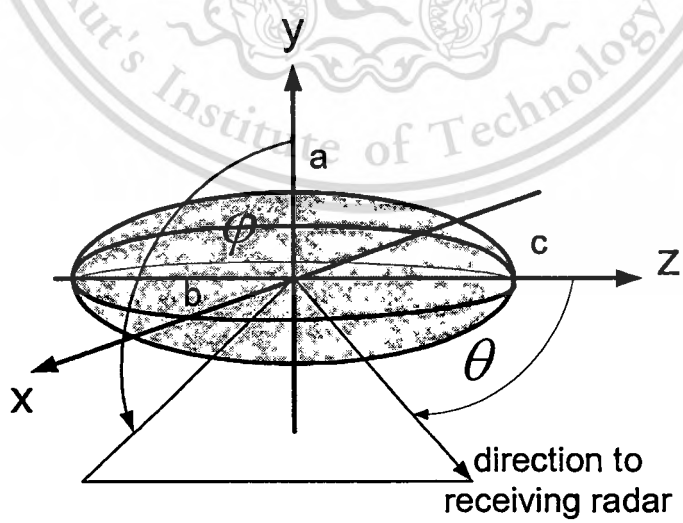

Fig. 4.1 Geometry of ellipsoid RCS back scattered

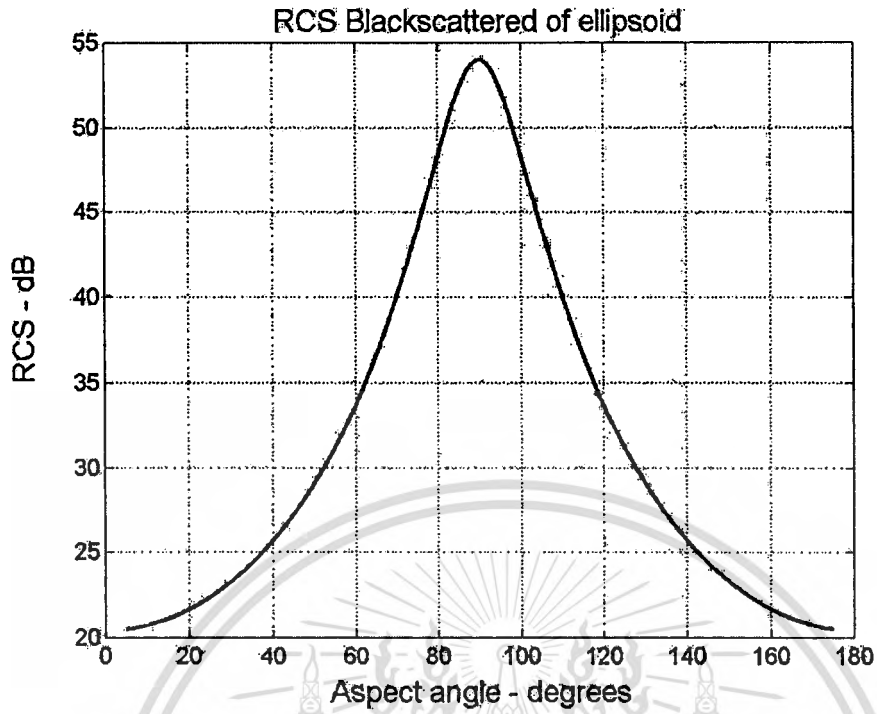

Fig. 4.2 The RCS back scattered of ellipsoid size are a=10 m, b=10 m, and c=70 m

$$\left(\frac{x}{a}\right)^2+\left(\frac{y}{b}\right)^2+\left(\frac{z}{c}\right)^2=1, \tag{4.1}$$

where a and b are the widths and c is the length of an ellipsoid.

The direction to the receiving signal has aspect angle θ from the z-axis, and φ is the angle between the y-axis and the incoming wave incident on the ellipsoid. One widely accepted approximation RCS back scattered of ellipsoid (σ) is given by [26]

$$\sigma=\frac{\pi a^2b^2c^2}{\left(a^2\sin^2\theta\cos^2\varphi+b^2\sin^2\theta\sin^2\varphi+c^2\cos^2\theta\right)^2}. \tag{4.2}$$

When $a = b$, the ellipsoid becomes roll symmetric, thus, the RCS back scattered is independent of φ, and Eq (4.2) is reduced to

$$\sigma = \frac{\pi a^4 c^2}{\left(a^2 \sin^2\theta + c^2 \cos^2\theta\right)^2}. \tag{4.3}$$

In Fig.4.2, the plot of the ellipsoid RCS back scattered in dB versus θ with φ = 45°, a = 10 m, b = 10 m, and c = 70 m is shown. This dimension in fact approximates the body of a Boeing 747-200. The aspect angle θ ranges from 0 to 180 degrees. Observe that the peak of ellipsoid RCS back scattered occurs at about 54 dB for the aspect angle θ at 90°, *i.e.*, when the waves are transmitted directly to the target.

4.2.4 Radio Wave Propagation

Free space propagation: Consider an isotropic radiator in free space. By definition, an isotropic radiator produces identical radiation intensity in all directions. In free space, the resultant spherical wave spreads out with uniform intensity in all directions. If Po is the power radiated from the isotropic source, the electric field strength (E_o) at a radial distance r is given by [26]

$$E_o = \frac{\sqrt{30P_o}}{r}\varepsilon^{-j\beta r} \quad \text{V/m}, \tag{4.4}$$

Where $\beta = 2\pi/\lambda$ is the free-space wave number or phase constant, the subscript on E_o denotes the free space field. Note that the electric field strength E_o scales with $1/r$.

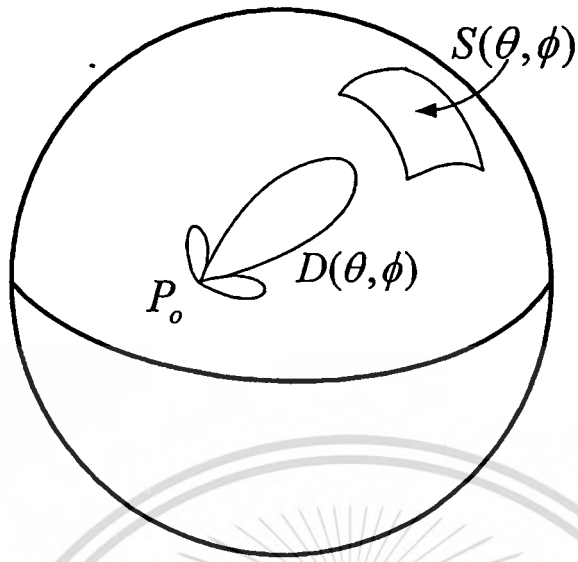

Fig. 4.3 Radiator with directional gain pattern.

Consider a source with a directional gain pattern $D\ (\theta,\phi)$ and surface area far field power density is related by $S\ (\theta,\phi)$ as shown in Fig.4.3. In this case, the radiated power is concentrated in some direction as it spreads out over the surface of a surrounding imaginary sphere. The far-field electric field strength is given by

$$E_o(\theta,\phi) = \frac{\sqrt{30 P_o D(\theta,\phi)}}{r} \varepsilon^{-j\beta r} \quad \text{V/m.} \tag{4.5}$$

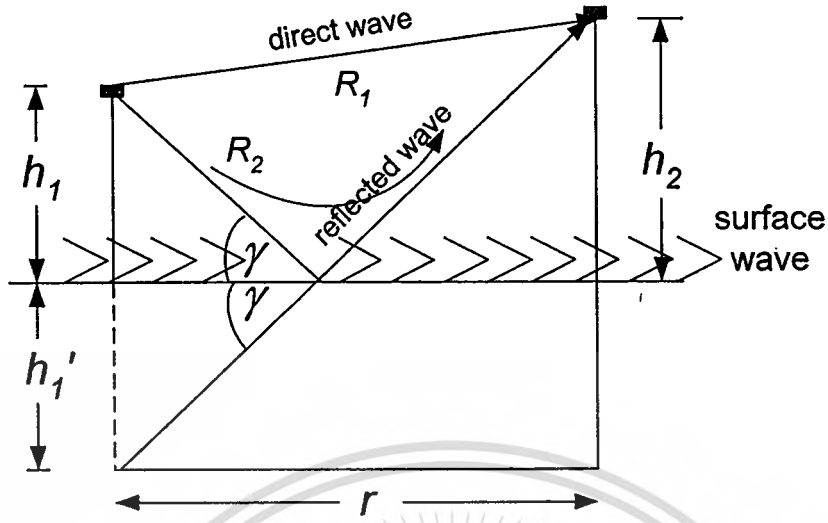

Fig. 4.4 R_1 and R_2 are geometry of direct wave and reflected wave distance, respectively

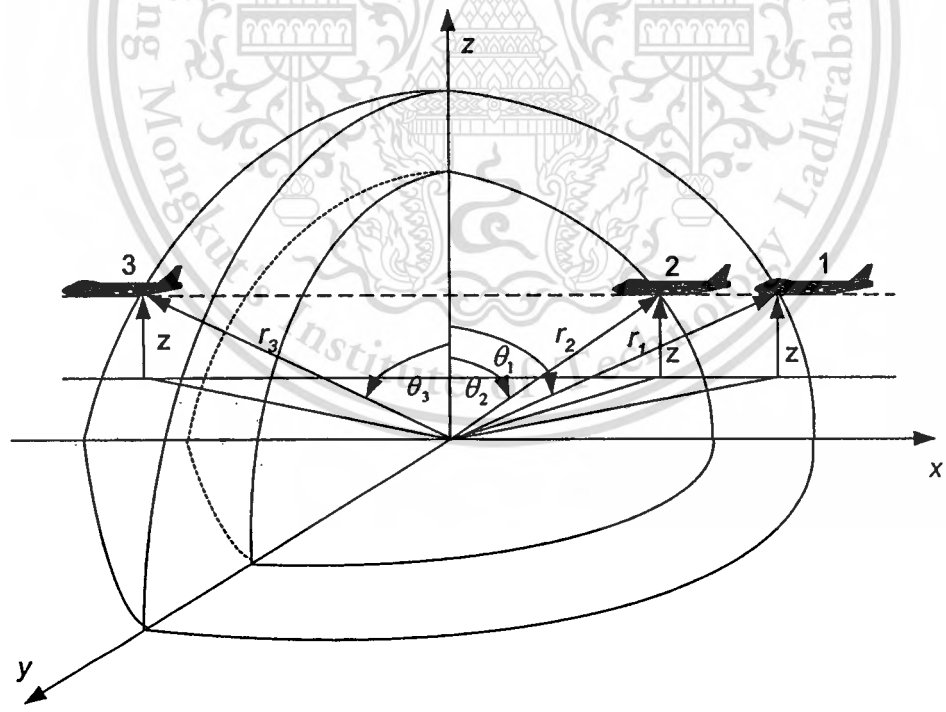

Fig. 4.5 The geometry of distance from airplane to receiving antenna $r = z / Cos\theta$

4.2.5 Geometry of Reflected Wave

In this part, the distance of direct wave between transmitting antenna to receiving antenna, distance of reflected wave by ground, and distance of reflected wave by airplane are described. The 3-dimension method is used for calculation in case of reflected by airplane due to airplane moving during the entire time the effect occurs.

Direct wave and reflected wave by ground could be found by geometry is illustrated in Fig.4.4. The direct wave distance $R_1 = [r^2+(h_1-h_2)^2]^{1/2}$. The geometry of reflected wave distance by ground R_2 shows that the value of h_1' is mirror-reflected value of h_1. From geometry, the distance of $R_2 = [r^2 + (h_1+h_2)^2]^{1/2}$.

Geometry of reflected wave distance by airplane could be obtained by spherical coordinate theory [27], $r = z / \mathrm{Cos}\theta$ is illustrated in Fig.4.5. Airplane flies from position 1 to 2 and reach position 3, thus value of angle θ changes all time depending on position of airplane. The altitude and speed of airplane (z) are from Aeronautical Radio of Thailand. This method could be used to calculate both distances from transmitting antenna to airplane and distance from receiving antenna to airplane.

4.2.6 Ground-wave Propagation Over Plane Earth

The geometry for ground wave propagation over plane earth is used for analysis of airplane flutter phenomena as both direct and indirect wave of multipath interfering signal. For the method used to calculate the ground wave electric field strength $E(r)$ depends on the geometry and wavelength given by [26]

$$E(r) = E_o(R_1) + \rho E_o(R_2) \tag{4.6}$$

where

$E(r)$ = total electric field strength at receiving antenna at a radial distance r,

E_o = electric field strength of the direct wave at a radial distance r,

R_1 = distance traveled by direct wave between source and point,

R_2 = distance traveled by ground reflected wave between source and points,

ρ = magnitude of reflection coefficient.

4.3 Proposed Method

In this section, we explain a proposed method to compute the electric field strength of the ground wave based on two techniques: 3-dimensional geometry and ellipsoid RCS back scattered. The RCS of ellipsoid with appropriate dimensions (width and length) relative to the body of an airplane can be used in the model of flutter phenomena. In this paper, we focus on the body part of airplane only because it is the biggest part and scatters most of the signals. The signal is, in fact, scattered from the body at all time, independent of the direction and pattern of the flying routes. For other parts such as wing and tail, however, the amount of reflected waves is typically quite small and dependent on the flying angles. They do not always affect the TV signal due to the flatness and relatively small size [16].

4.3.1 Basic Parameters

The basic parameters, which affect the signal variation patterns, can be classified into 3 categories as follow.

a) Amplitude of variation depends on the parameters including percentage of reflection by airplane (Γ_{airp}), RCS back scattered (σ), size of airplane, and distance from airplane to receiving antenna (R_{ra}).

b) Frequency of variation pattern depends on the wavelength (λ) of the TV signal.

c) Duration time of variation pattern depends on the parameters including speed, altitude, directivity of antenna, and direction of airplane.

A simple multipath scattering model is used to describe the airplane flutter phenomena. It is formulated with the objectives of increasing the understanding of some of the measured signal behavior and also predicting its patterns. This requires a fundamental description of the causes of the signal variation and is the reason why this model is based on both physical and geometrical considerations. The method used to calculate the field strength at the receiving antenna is modified from Ray theory by A. A. Smith Jr. [26], which depends on the geometry and signal wavelength. In the case of reflection by airplane, some parameters such as radar cross section (RCS), airplane altitude, speed and direction of airplane are considered.

4.3.2 Cross Pattern

Consider the geometry of wave propagation reflected from airplane flying with *cross pattern* as shown in Fig. 4.6 (a), (b), and (c). The signal multipath is composed of the direct wave (e_1), reflected wave by ground (e_2), and reflected wave from airplane (e_3), respectively. Figure 4.6(a) is a front view showing the transmitted and received angle θ and the signal at receiving antenna that is composed of e_1, e_2 and e_3, respectively. Fig 4.6(b) is a top view showing the angle ϕ at receiving and transmitting sites and Fig 4.6(c) shows a 3-dimensional geometry.

For the cross pattern, vertical angle θ on the receiving side during interference is constant at 45 degrees, while the horizontal angle ϕ varies from around 45 to 135 degrees as shown in Fig.4.6 (a), (b), and (c).

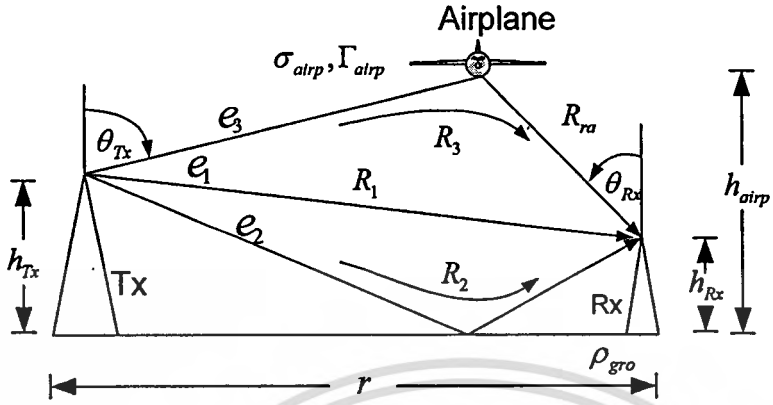

(a)

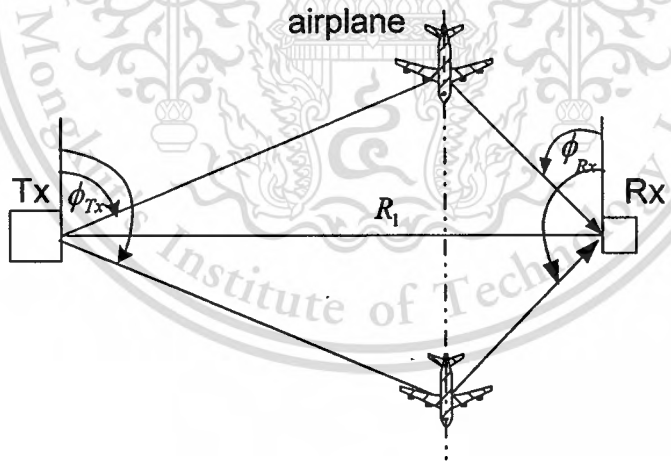

(b)

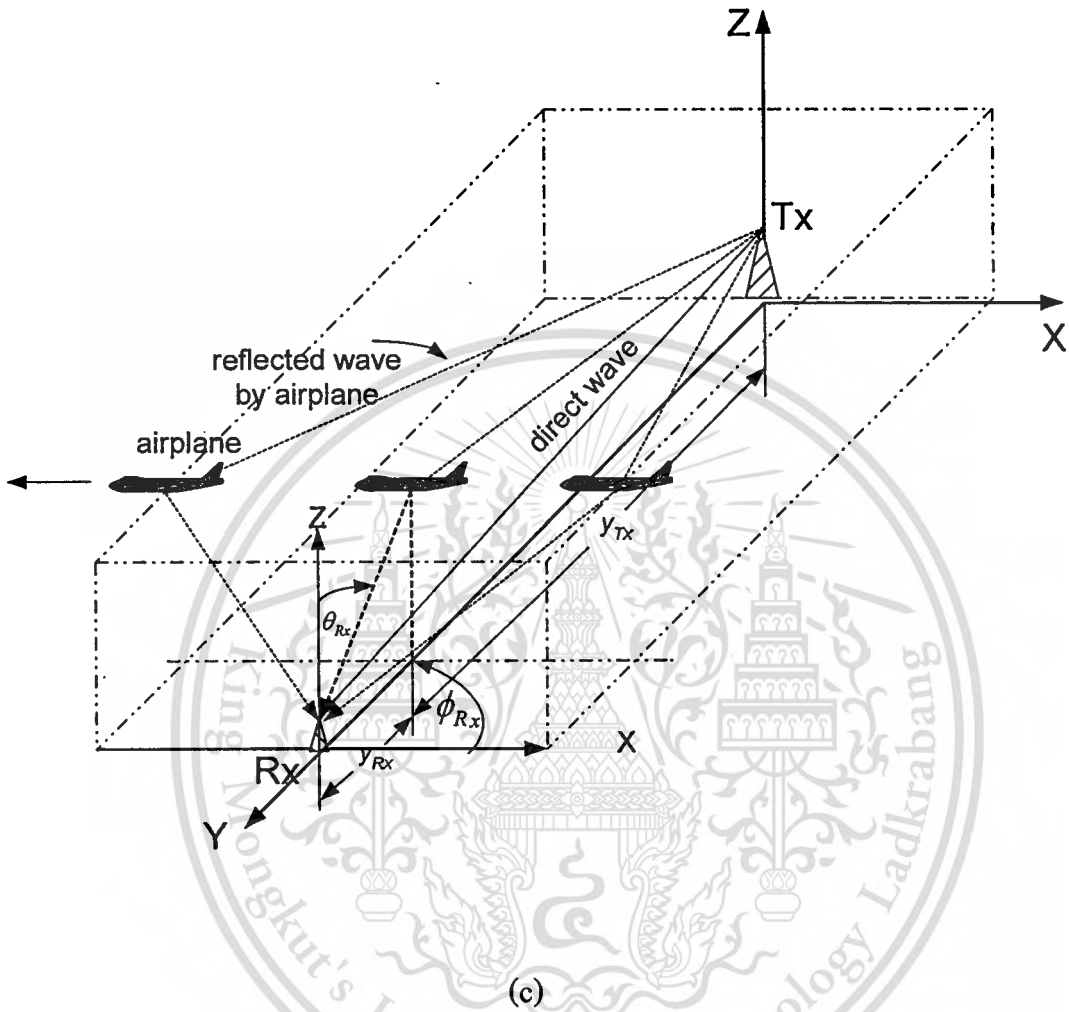

Fig. 4.6 The geometry of the wave propagation in the airplane flutter, composed of the direct wave (e_1), reflected wave by ground (e_2), and reflected wave by airplane (e_3). (a) front view, (b) top view, and (c) 3-dimensional view

In Fig. 4.6,

R_1 is distance traveled by direct wave between source and field point by [26]
$= \left[r^2 + (h_{Tx} - h_{Rx})^2\right]^{\frac{1}{2}}$,

R_2 is distance traveled by ground reflected wave between source and field points and can be computed = $\left[r^2 + (h_{Tx} + h_{Rx})^2\right]^{\frac{1}{2}}$,

R_3 is distance traveled by airplane reflected wave between source and field points can be computed = $(z / \text{Cos}\ \theta_{Tx}) + (z / \text{Cos}\ \theta_{Rx})$,

y_{Tx}, y_{Rx} is distance from transmitting and receiving antennas to airplane in y plane, respectively,

r is distance between source and field point measured on the plane,

h_{Tx} is height of transmitting antenna above earth plane,

h_{Rx} is height of receiving antenna above earth plane,

θ_{Tx}, θ_{Rx} is angle between antenna and reflected wave by airplane in vertical plane at transmitting and receiving side (degrees), respectively,

ϕ_{Tx}, ϕ_{Rx} is angle between antenna to reflected wave by airplane in horizontal plane at transmitting and receiving side (degrees), respectively, and

R_{ra} is distance between receiving antenna to airplane given = $z / \text{Cos}\ \theta_{Rx}$.

The total electric field strength at the receiving antenna $E(r)$ can be computed from the sum of the direct wave (e_1), ground reflected wave (e_2), and airplane reflected wave (e_3), each of which can be computed based on Eq.(4.5), *i.e.*,

$$E(r) = e_1 + e_2 + e_3$$

$$= \sqrt{(30 P_o D(\theta,\phi))}\left[\frac{\varepsilon^{-j\beta R_1}}{R_1} + \left|\rho_{gro}\right|\frac{\varepsilon^{-j\beta R_2}\varepsilon^{-j\varphi_1}}{R_2} + \left|\sigma_{airp}\right|\left|\Gamma_{airp}\right|\frac{\varepsilon^{-j\beta R_3}\varepsilon^{-j\varphi_2}}{R_3}\right], \quad (4.7)$$

where

P_o is output power of transmitter,

$D(\theta,\phi)$ is directivity of antenna,

ε is permittivity of the earth [F/m],

ε_0 is permittivity of free space = $8.854*10^{-12}$ F/m,

k is $\varepsilon/\varepsilon_0$ = the relative permittivity of the earth (k=15 for good earth),

β is $2\pi/\lambda$,

ρ_{gro} is reflection coefficient by ground ≅ 0.8% for VHF [26],

φ_1, φ_2 is reflection coefficient phase by ground and airplane, respectively,

σ_{airp} is RCS back scattered of an airplane, and

Γ_{airp} is percentage of reflection by airplane [%].

Equation (4.7) can be used to calculate the signal variation caused by airplane at the receiving antenna. The RCS back scattered σ_{airp} is based on an ellipsoid of dimension relative to the body of an airplane. The phase difference (φ) is determined from the different paths of direct and reflected wave and based on 3-dimensional geometry due to the airplane movement at all time. Percentage of airplane reflection (Γ_{airp}) is dependent on the size of airplane, R_{ra}, and frequency of signal. The directivity (D) depends on the type of antenna, for high-gain transmitting and receiving antennas, the directivity needs to be accounted for in Eq.(4.7).

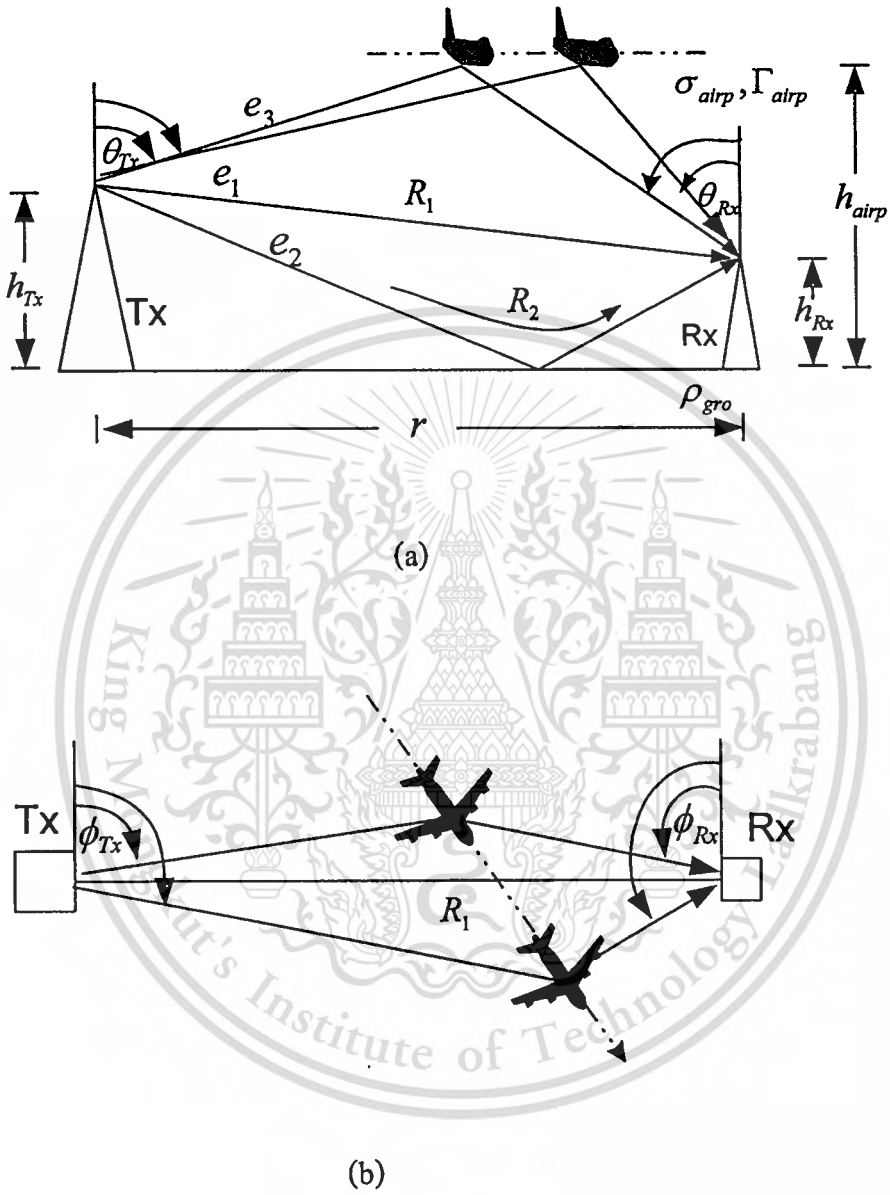

Fig. 4.7 The flying geometry of cross-range pattern. The direction of the flying airplane did not fly perpendicular with the line-of-sight signal (a) front view and (b) top view

4.3.3 Cross-range Pattern

In Fig.4.7 (a) and (b), the geometry of cross-range pattern of an airplane is shown. The airplane makes an angle that is not perpendicular to the line-of-sight signal. In this case, both angle of θ_{Rx} and ϕ_{Rx} vary, while for the case of cross pattern, θ_{Rx} is constant. From the view of receive antenna, the angle θ_{Rx} decreases as the plane approaches the antenna, while, the angle ϕ_{Rx} increases.

4.3.4 Percentage of Reflection Wave Caused by Airplane (Γ_{airp})

The power density of wave at the receiving antenna due to scattered by airplane (P_{Dr}) by [25] is

$$P_{Dr} = \frac{G_r \lambda^2 P_t G_t \sigma_B}{(4\pi)^3 R_t^{\,2} R_{ra}^{\,2}} \tag{4.8}$$

where P_t is transmitted power, R_{ra} is distance between receiving antenna to airplane, G_t and G_r are transmitting and receiving antenna gain, respectively, σ_B is the radar cross section, in this case with $\sigma_B = \sigma = \sigma_{airp}$, and R_t is the range from the transmitting antenna to a target.

The percentage of reflection of wave by airplane is defined as

$$\Gamma_{airp} = \frac{P_{Dr}}{P_{Dr(\max)}} \times 100\ (\%), \tag{4.9}$$

The $P_{Dr(max)}$ is maximum power intensity of reflected wave from the airplane measured at the receiving antenna. The relationship between Γ_{airp} and R_{ra} is illustrated in Fig.4.8 at the frequency of 60 MHz, 74 MHz, and 209 MHz, respectively.

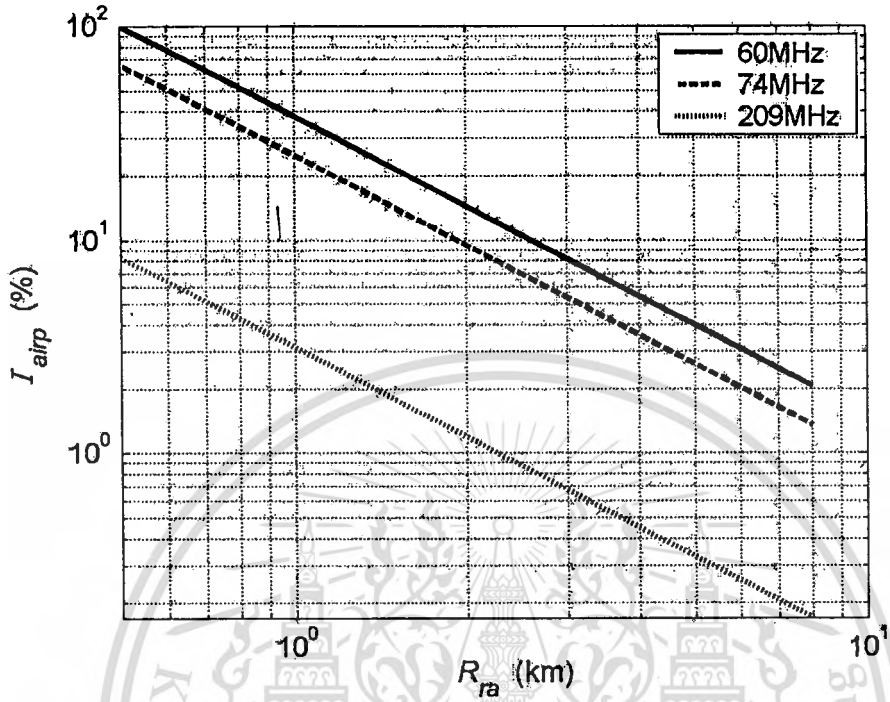

Fig. 4.8 The percentage of reflection from airplane (Γ_{airp}) at the frequency of 60 MHz, 100 MHz, and 209 MHz

From the figure, it can be observed that at the distance of R_{ra} equal to 1400 m (equivalent to the altitude of 1000 m in cross pattern experiment), the percentages of reflection at 60 MHz and 209 MHz are 25 % and 2 %, respectively. The higher frequency, the lower proportion of reflection Γ_{airp} is found. The value of Γ_{airp} is an essential parameter used in the airplane flutter model in Eq.(4.7).

Chapter 5

Measurement and Simulation Results on Airplane Flutter

5.1 Measurement and Simulation Results

In this section, the measurement and simulation results of airplane flutter phenomena on TV signals are presented. The signal variation caused by airplane was measured at King Mongkut's Institute of Technology Ladkrabang (KMITL) campus, Bangkok, Thailand. The airplane took off from Donmuang International Airport and flew pass the line-of-sight signal between Tx and Rx points at KMITL. The obtained data were then compared with the simulation results using the parameters relevant to the measurement.

5.1.1 Measurement Setup

The measurement parameters are listed in Table 5.1. The TV signals from local stations of channel 3 (Ch3) at 60.75 MHz and channel 9 (Ch9) at 208.75 MHz are selected in the test. For Ch3, the output power is 60 kW with 230-m height antenna and for Ch9, the output power is 20 kW with 250-m antenna height. Both channels are transmitted from the same antenna tower at Nongkam station, located on the western rim of the city. On the receiving side, Anritsu WI-208 field strength meter is used with standard 3-meter and 3.5-meter dipole antennas above ground for Ch3 and Ch9, respectively. The received signal is collected using Keyence data acquisition system, and Yokogawa Hokushin Electric paper recorder as shown in Fig. 5.1. The data acquisition rate is 100 samples per second. The equipment is setup in the middle of the football field on KMITL campus, located on the eastern rim of the city the football field location is chosen to prevent signal reflection from the buildings in the vicinity.

The TV signals of Ch3 and Ch9 were recorded as the airplane flied over the observation point. The receiving antenna Rx at KMITL is approximately 45 km from transmitting antenna Tx at Nongkam station. Note that strong line-of-sight signals exist.

In Fig.5.3, two possible airplane routes over KMITL measured points are shown. The Boeing 747 typically flies with cross (Route 1) and cross-range (Route2) patterns between the Tx and Rx antennas. There are many flights per day. The flight information such as airplane altitude, speeds, of model is obtained from Aeronautical Radio of Thailand, Ltd.

TABLE 5.1 MEASUREMENT PARAMETERS

Transmitting side	
Ch3 frequency	60.75 MHz
Ch9 frequency	208.75 MHz
Ch3 transmitting antenna height	230 m
Ch9 transmitting antenna height	250 m
Output power of Ch3	60 kW
Output power of Ch9	20 kW
Antenna gain	13 dB
Polarization	Horizontal
Receiving side	
Distance from Tx (Nongkam) to Rx(KMITL)	45 km
Field strength meter	Anritsu(WI-208)
Data acquisition	Keyence(NR-2000)
Paper recorder	Yokogawa- Hokushin Electric
Standard dipole height,(60.75 MHz and 208.75 MHz, with gain of 2.15 dB)	3 m, 3.5 m
Polarization	Horizontal
Airplane parameters	
Airplane	Boeing747
Altitude	1000-2000m
Speed	400-500km/h
Direction	cross, cross-range

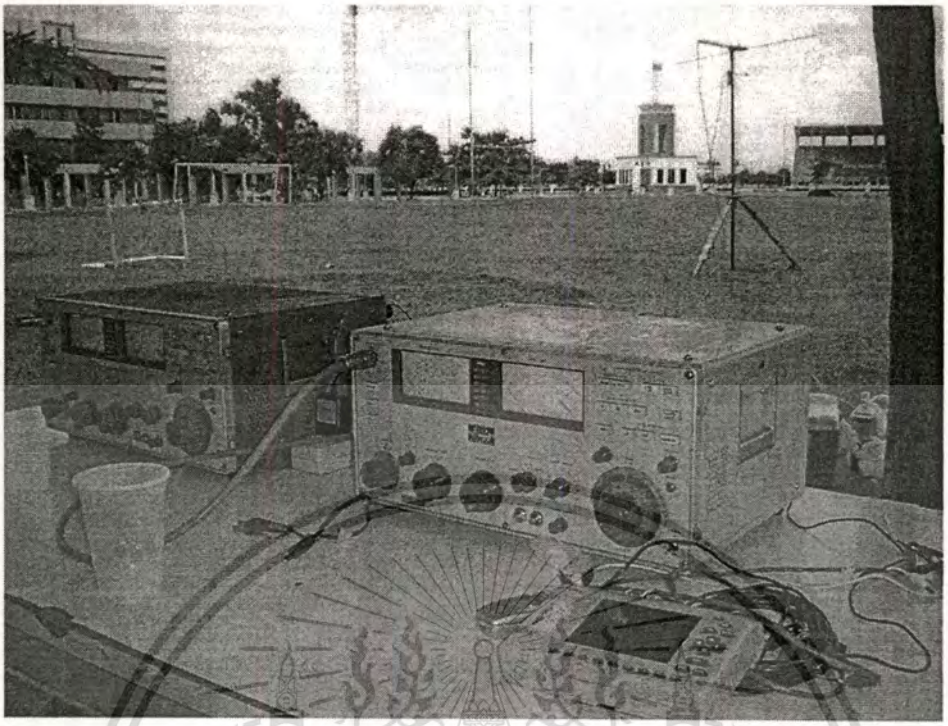

(a)

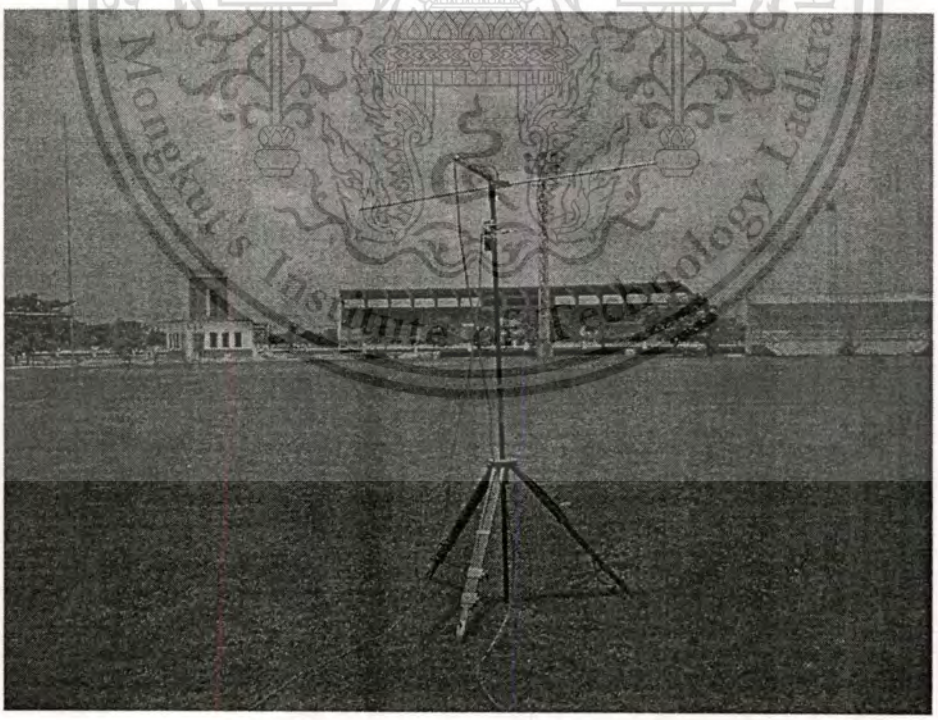

(b)

Fig. 5.1 Instrument setups for airplane flutter phenomena measurement at KMITL football field. (a) Field strength meters (b) Standard dipole antennas

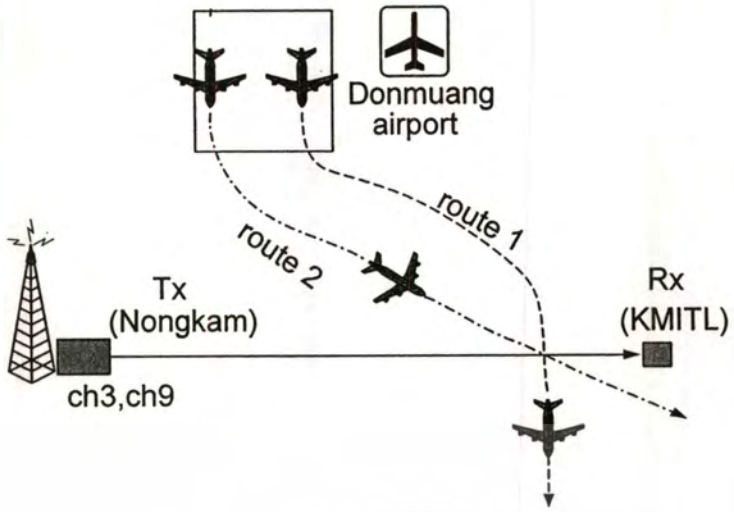

Fig. 5.2 Airplane route of cross and cross-range patterns at KMITL measured point

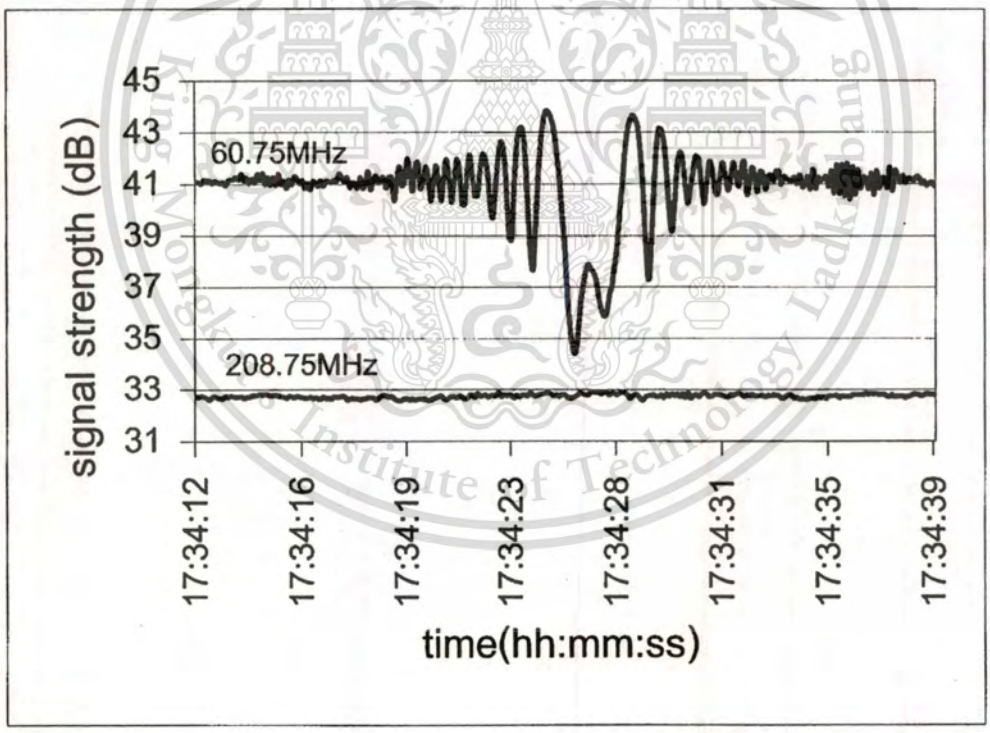

Fig. 5.3 Measured signal strengths of Ch3 (60.75 MHz) and Ch9 (208.75 MHz) for cross airplane route

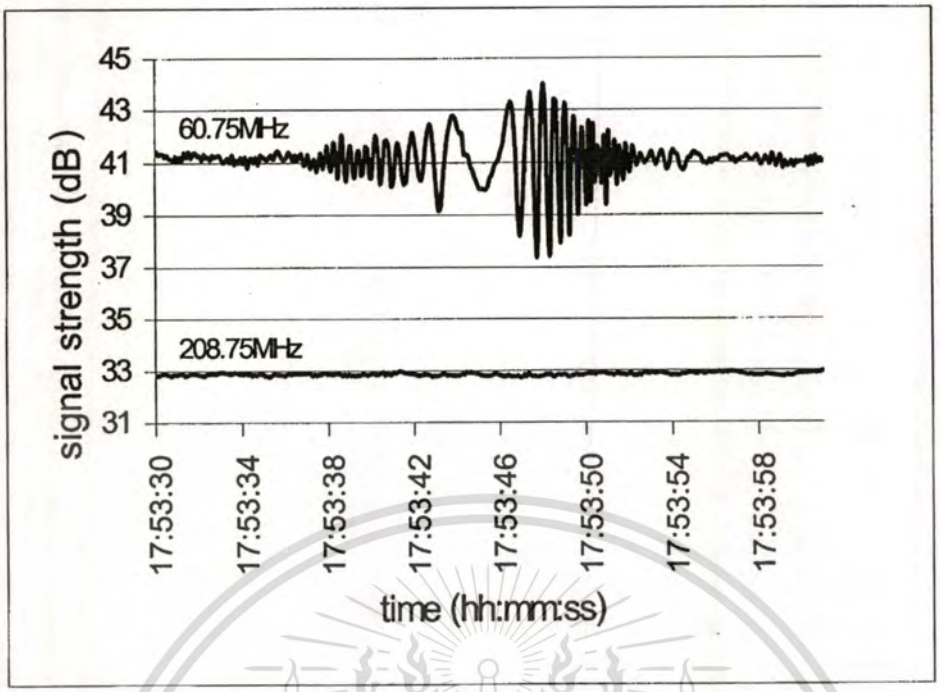

Fig. 5.4 Measured signal strengths of Ch3 (60.75 MHz) and Ch9 (208.75 MHz) for cross-range airplane route

5.1.2 Measurement Results

The TV signal strengths of the cross, and cross-range patterns are shown in Fig.5.3, and Fig.5.4, respectively. The signal variations of both patterns shown here are typical among all the collected data.

5.1.2.1 Cross Pattern

In Fig.5.3, the measured signal of the cross-pattern flight on Oct 28, 2003 from 17:34:12 to 17:34:39 hr is shown. The airplane took off from Donmuang International Airport and flied across the line-of-sight signal between Tx and Rx antennas (direction is perpendicular with the line-of-sight signal). The speed and altitude of the aircraft are approximately 450 km/h and 1,000 m, respectively. Typical signal levels of Ch3 and Ch9 are about 41 dB and 33 dB, respectively. With fluttering phenomena,

however, the maximum signal variation of Ch3 was 9.9 dB over a 14-second interval, while the signal of Ch9 is relatively unaffected. Observe that symmetry of the signal patterns exists in this case.

5.1.2.2 Cross-range Pattern

In Fig.5.4, the measured data from the cross-range pattern on Oct 28, 2003 from 17:53:30 to 17:53:58 hr is shown. The airplane took off from Donmuang airport and flied cross-range over the line-of-sight signal. The speed of airplane was 450 km/h with an altitude of 1800 m. Maximum signal variation of Ch3 was 7.2 dB over a 15-second interval. Similar to the cross pattern case, the signal at 208.75 MHz was, not noticeable.

5.1.3 Simulation Results

The signal levels of cross and cross-range flying patterns at KMITL depending on the geometry of the airplane and related flight parameters can be simulated.

5.1.3.1 Cross Pattern Simulation

The simulation of TV signals due to cross pattern route is done using the RCS of ellipsoid with dimension of 10x10x70 m. The altitude is 1,000 m (R_{ra} = 1400 m) with the aircraft speed of 450 km/h. The percentage of reflection for Ch3 and Ch9 are computed using (2), (8) and (9) to yield 25 % and 2 %, respectively. The vertical angle θ on the receiving side during interference is constant at 45 degrees, while the horizontal angle ϕ varies from 45 to 135 degrees. From Fig.5.5, the simulated signal variation of Ch3 is around 9 dB over a 14-second time interval, while the Ch9 signal shows some signal variation but with very small proportion to the Ch3 case. The simulated patterns closely resemble the measured patterns in Fig.5.3.

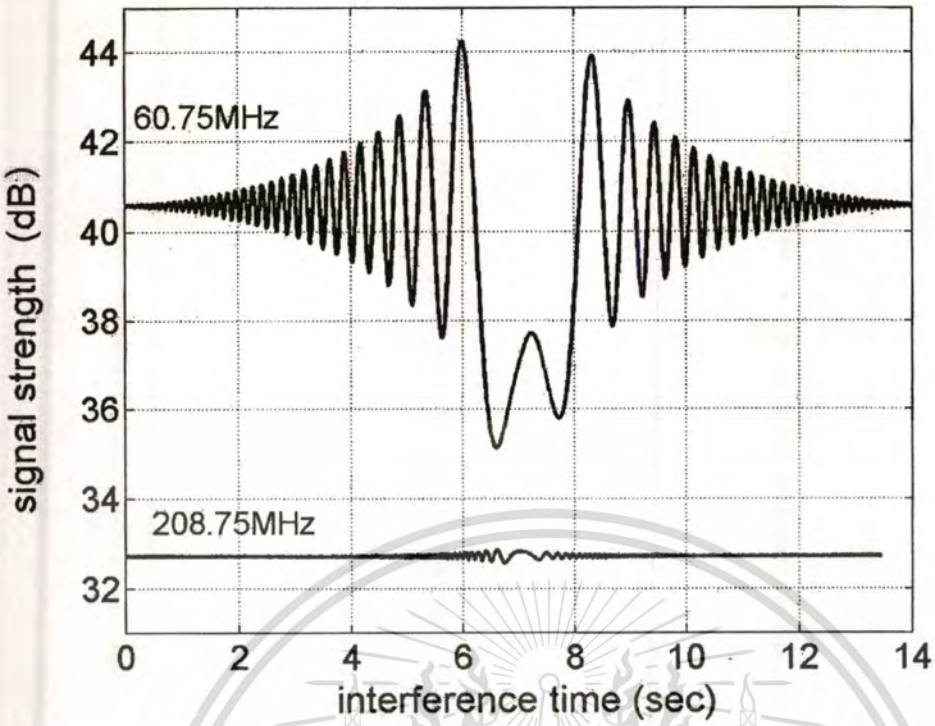

Fig. 5.5 Cross-pattern simulation results of Ch3 (60.75 MHz) and Ch9 (208.75 MHz)

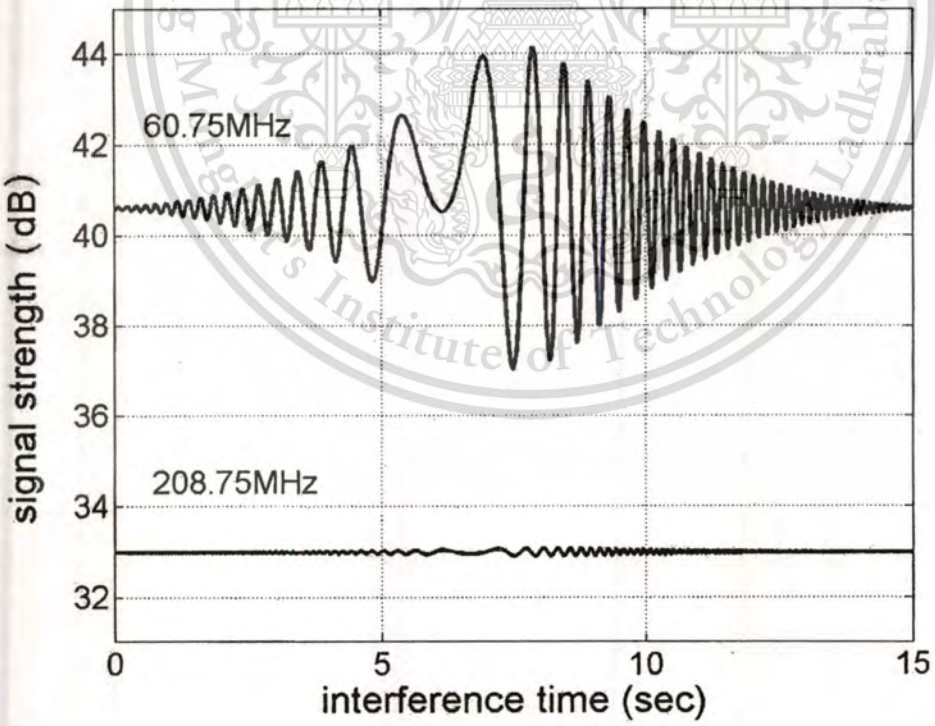

Fig. 5.6 Cross-range pattern simulation results of Ch3 (60.75 MHz) and Ch9 (208.75 MHz)

5.1.3.2 Cross-range Pattern Simulation

The simulation of TV signals due to a cross-range pattern route is done using the same size of RCS back scattered. The altitude is 1,800 m (R_{ra} = 2100 m) with the aircraft speed of 450 km/h. The percentage of reflection for Ch3 and Ch9 are similarly computed to yield 15% and 1.1%, respectively. The ellipsoid makes the vertical angle θ at the receiving side during interference from 28 down to 24 degrees, while the horizontal angle ϕ on receiving side varies from 55 to 120 degrees. From Fig.5.6, the simulated signal variation of Ch3 is 7 dB over a 15-second time interval. The Ch9 signal shows small change of amplitude.

Figure 5.7, we study the effects of speed and altitude on the characteristics of simulated flutter signal on cross pattern route. For all four cases, The vertical angles are roughly fixed, while the horizontal angle varies, specifically, $Rx(\theta,\phi)_{in}$ = [45°, 48°] and $Rx(\theta,\phi)_{out}$ = [44.9999 °, 133 °]. The frequency of Ch3 and the distance d_0 = 45 km is used.

From Fig. 5.7(a), with the speed of 450 km/h and altitude of 1,000 m, the duration time of signal variation is around 14 seconds and the maximum variation is around 9.1 dB. As the speed is reduced to 350 km/h with same altitude, the duration time is increased to 18 seconds as seen in Fig. 5.7(b). When altitude is increased to 2,000 m with the speed of 450 km/h, the maximum signal variation reduces to 3.5 dB but the duration time increases to 29 seconds as shown in Fig. 5.7(c). As the altitude is increased to 3,000 m with the speed of 450 km/h, the maximum signal variation reduces to 2.028 dB but the duration time increases to 43.9 seconds as shown in Fig. 5.7(d).

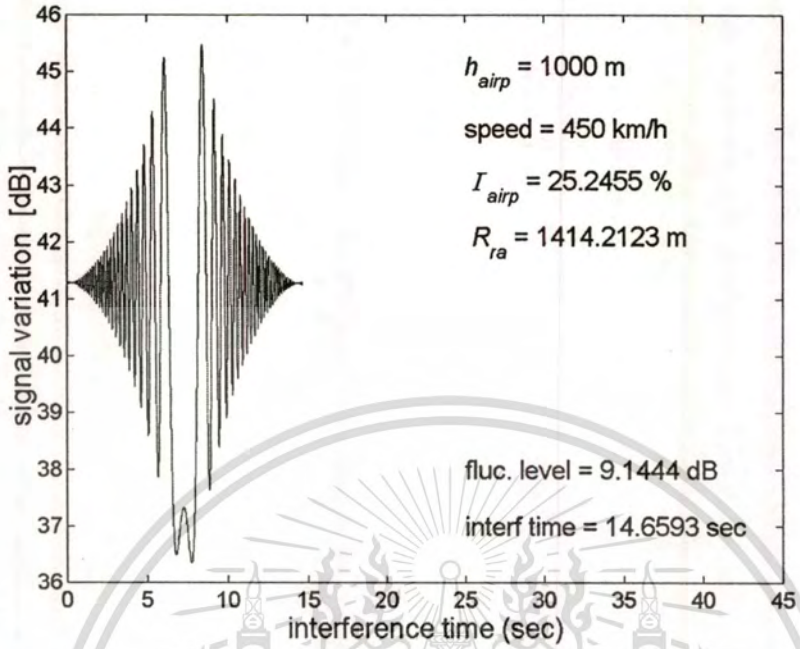

(a)

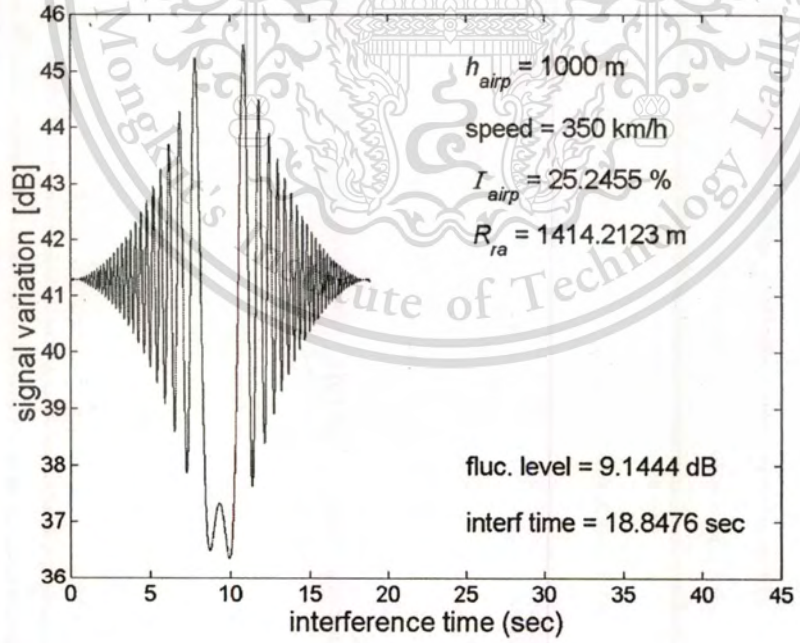

(b)

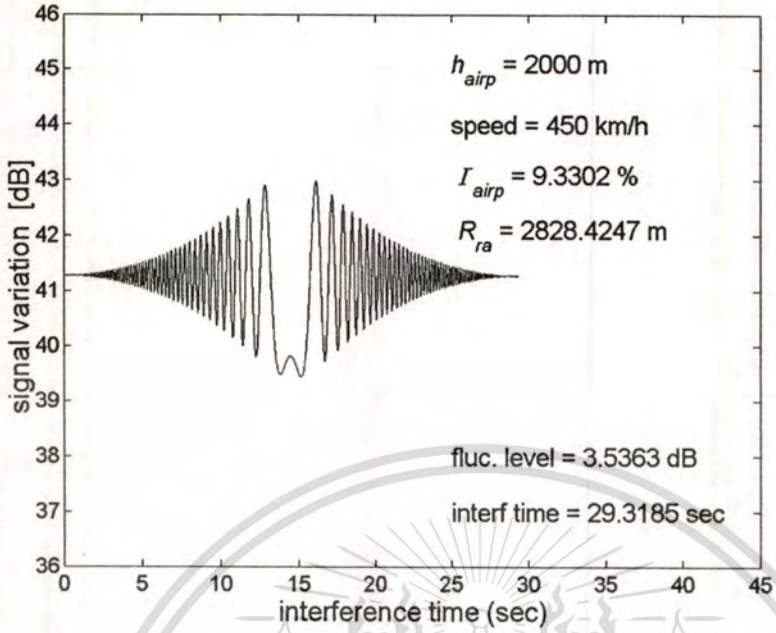

(c)

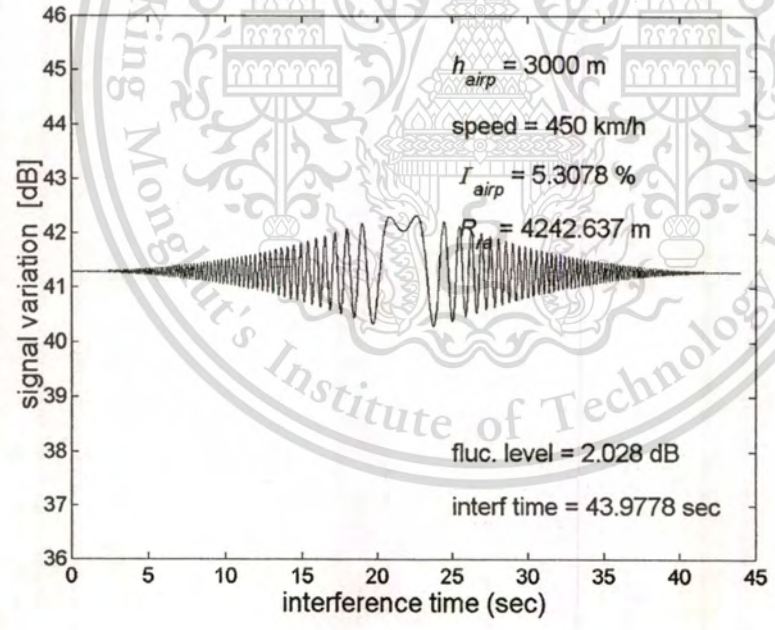

(d)

Fig. 5.7 Simulation results of cross flutter pattern of Ch3 when parameters are changed. (a) The speeds of 450km/h with altitude of 1000 m, (b) The speeds of 350km/h with altitude of 1000 m, (c) The speeds of 450km/h with altitude of 2000 m, and (d) The speeds of 450km/h with altitude of 3000 m

The relationship of between the simulated maximum signal variation and the distance R_{ra} can be seen in Fig. 5.8. The maximum signal variation is dependent on the TV frequency. In this figure, four frequencies 61, 74, 181, and 209 MHz are plotted. The measured maximum signal levels at 61MHz (denote by ●) and 209MHz (denoted by ×) at the R_{ra} of 1,400 m (at altitude of 1,000 m) are plotted and compared with the simulation results. For Ch3 (61 MHz) and Ch9 (209 MHz), the signal variation levels are around 9.9 dB and 0.3 dB, respectively. With R_{ra} of about 2100 m (at altitude of 1,800 m), the signal variation levels are around 7 dB and 0.2 dB, and_at R_{ra} of about 3,200 m the signal variation levels are around 3 dB and 0.1 dB, respectively. The measured values are close to the simulated ones. In addition, measured data of maximum signal variation of Ch3 on chapter 5 are also plots into the graph. We find that total of 18 data are closely calculated data of Ch3 frequency.

A 3-dimensional simulation plot of relationship between maximum signal variation, frequency and R_{ra} is also shown in Fig. 5.9. The frequency varies from 50 to 300 MHz, and R_{ra} ranges from 500 to 8,000 m. The figure shows that as R_{ra} and frequency increase, the maximum signal variation decreases. The KMITL measured points of R_{ra} equal to 1,400 m, 2,100 m, and 3,200 m of 61 MHz and 209 MHz, respectively are also plotted. It is evident that the measured results are close to the simulation results.

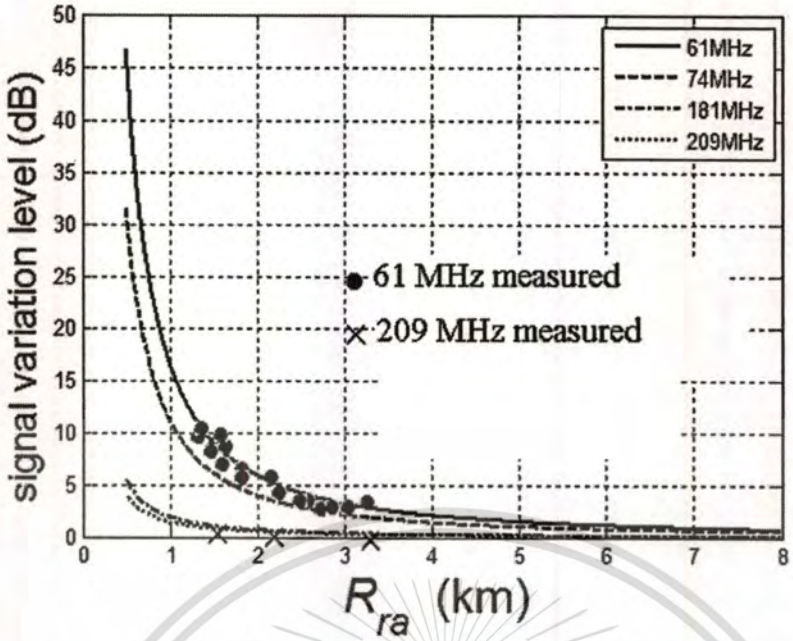

Fig. 5.8 Simulation of maximum signal variation for the frequencies of Ch3 (61 MHz), Ch5 (74 MHz), Ch7 (181 MHz) and Ch9 (209 MHz) to compare with measured data of 61 MHz and 209 MHz

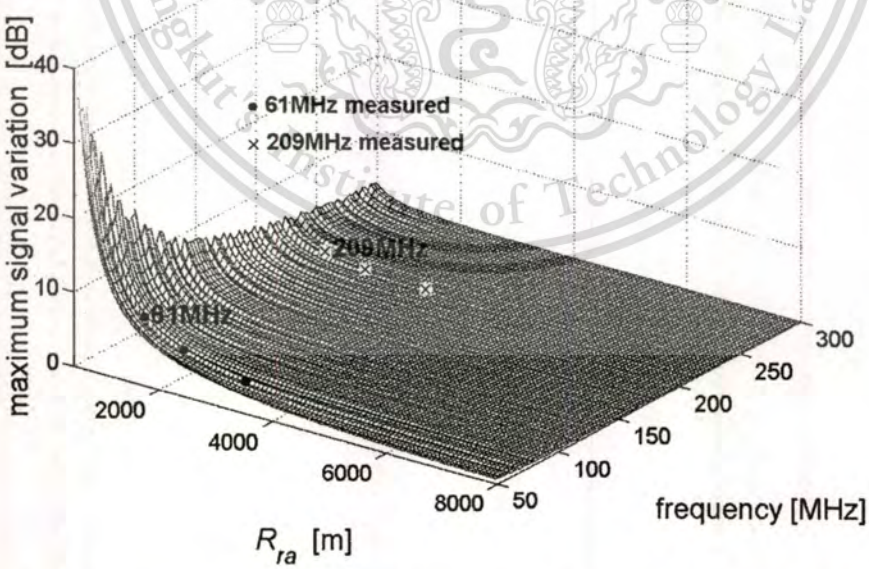

Fig. 5.9 A 3-dimensional plot of relationship between maximum signal variation, frequency and R_{ra}

5.1.4 Additional Measurement and Simulation Results

In the following, we show many case of airplane flutter phenomena is measured at KMITL to compare with simulation results. Parameters of airplane flight from Department of Air Traffic Control such as speed, altitude, and type of airplane together with angle of θ and ϕ at receiving side are input to the model. The experimental set up on Oct 28-29, 2003. Total of 15 figures are illustrated in the following can found both cross and cross-rang patterns of Boeing 747 airplane. The speed and altitude of airplane is around 400-450 km/h and 900-2500 m, respectively. The frequency of 60.75 MHz is used for observation.

In Fig. 5.10 (a), the measured signal of the cross-rang pattern flight on 15:32:54 to 15:33:19 hr is shown. The speed and altitude of airplane are approximately 450 km/h and 2,500 m, respectively. A typical signal level of Ch3 is 40 dB. With fluttering phenomena, however, the maximum signal variation of Ch3 is 3.5 dB over a 9-second interval. The simulation of Fig. 5.10 (a) shows in Fig 5.10 (b). The vertical angle θ on receiving side varies from 25 degrees to 10 degrees, while the horizontal angle ϕ varies from 50 to 100 degrees. The simulated signal variation is around 3.51 dB over a 10.2-second time interval. The simulated shows signal variation is closer to measured pattern but slightly difference of time interval.

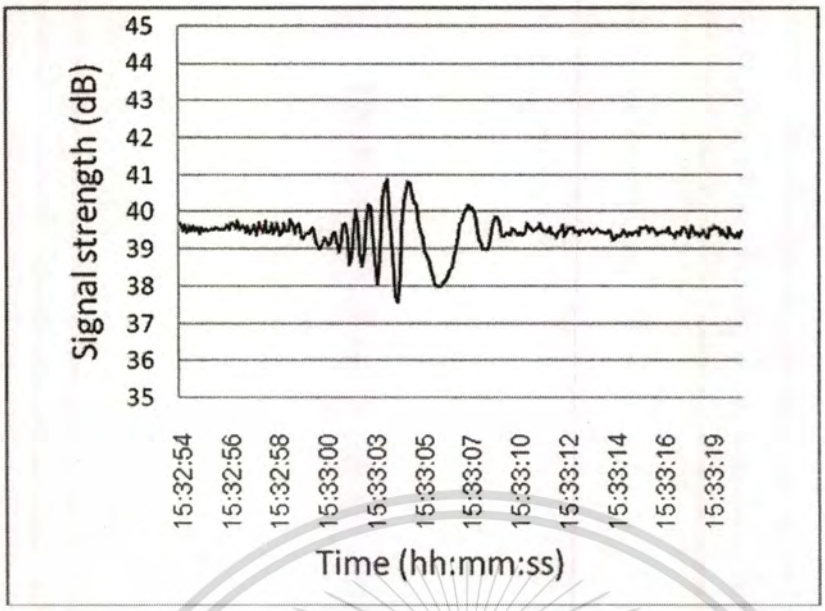

(a)

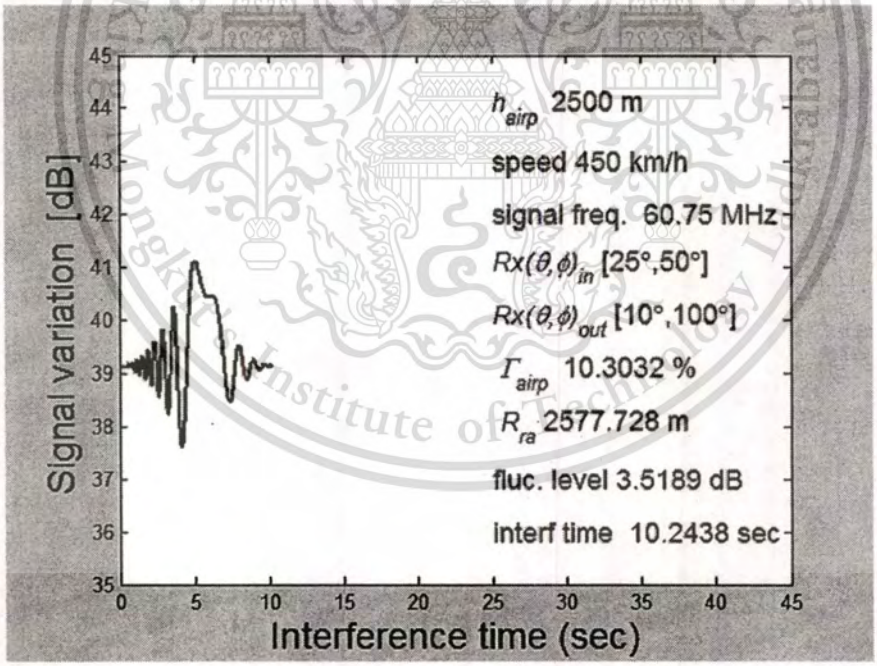

(b)

Fig. 5.10 Cross-range pattern of Boeing 747 with altitude of 2500 m, speed 450 km/h, $Rx(\theta,\phi)_{in}$ [25°,50°] , and $Rx(\theta,\phi)_{out}$ [10°,100°] (a) measured pattern (b) simulated pattern

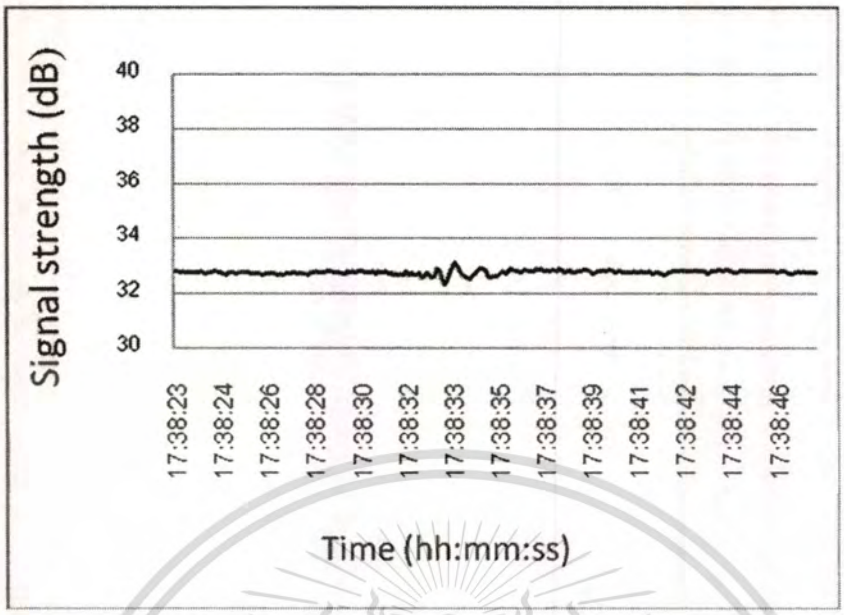

(a)

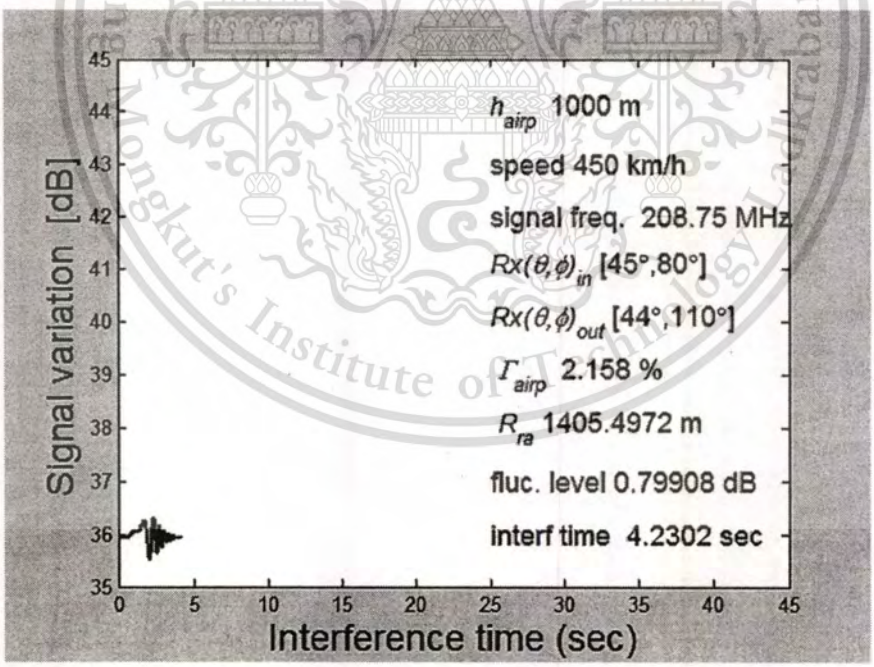

(b)

Fig. 5.11 Signal variation on Ch9 frequency when altitude of airplane is 1,000 m with speed of 450 km/h (a) measured pattern (b) simulated pattern

In Fig. 5.11(a), the measured signal of the cross-rang pattern flight on 17:38:23 to 17:38:46 hr is shown. The speed and altitude of airplane are approximately 450 km/h and 1,000 m, respectively. A typical signal level of Ch9 is 32 dB. With fluttering phenomena, however, the maximum signal variation of Ch9 is 1 dB over a 3-second interval. The simulation of Fig. 5.11(a) shows in Fig 5.11(b). The vertical angle θ on receiving side a little varies from 45 degrees to 44 degrees, while the horizontal angle ϕ varies from 80 to 110 degrees. The simulated signal variation is around 0.79 dB over a 4-second time interval. The simulated shows slightly difference both signal variation and time interval. These may be some parameters such as angles value are slightly mistake assigned.

In Fig. 5.12(a), the measured signal of the cross pattern flight on 17:55:49 to 17:56:12 hr is shown. The speed and altitude of airplane are approximately 450 km/h and 2,500 m, respectively. A typical signal level of Ch3 is 41 dB. With fluttering phenomena, however, the maximum signal variation of Ch3 is 2.2 dB over a 10-second interval. The simulation of Fig. 5.12(a) shows in Fig 5.12(b). The vertical angle θ on receiving side a little varies from 25 degrees to 23 degrees, while the horizontal angle ϕ varies from 63 to 120 degrees. The simulated signal variation is around 3.16 dB over a 9.6-second time interval. The simulated slightly difference both signal variation and time interval.

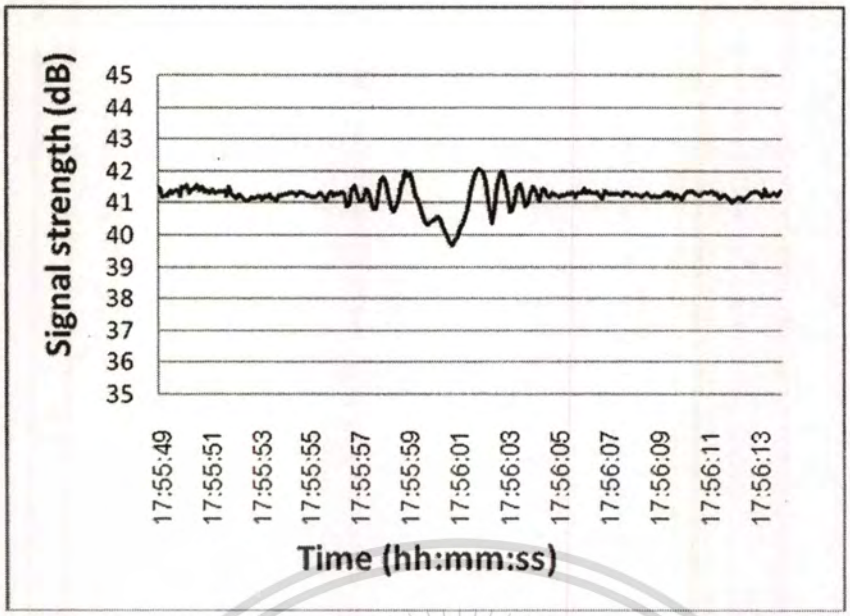

(a)

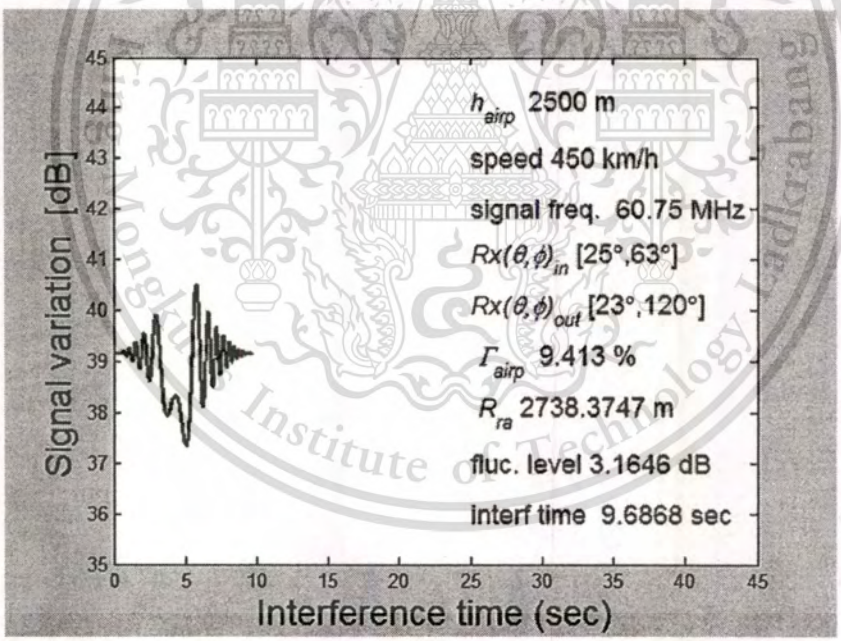

(b)

Fig. 5.12 Cross-range pattern of Boeing 747 with altitude of 2500 m, speed 450 km/h, $Rx(\theta,\phi)_{in}$ [25°,63°] , and $Rx(\theta,\phi)_{out}$ [23°,120°] (a) measured pattern (b) simulated pattern

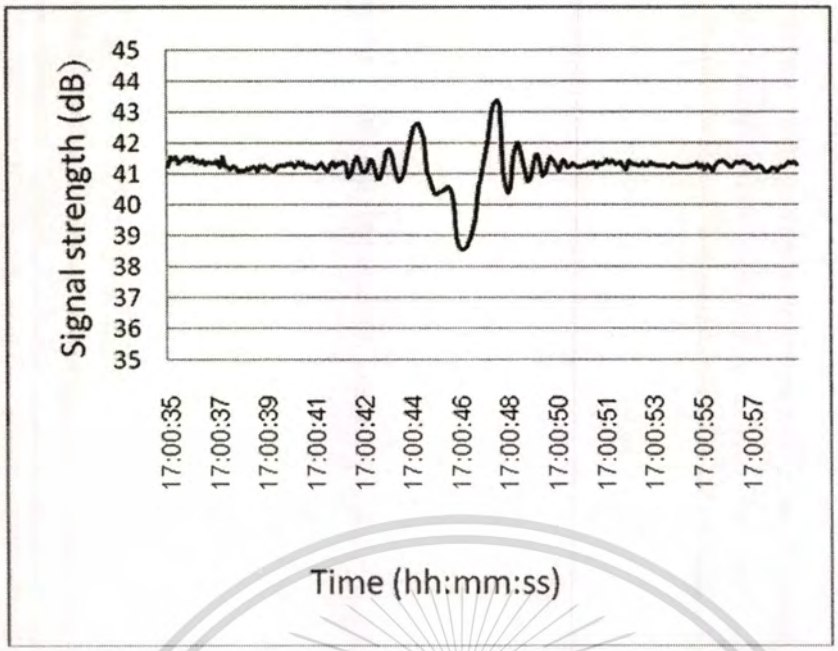

(a)

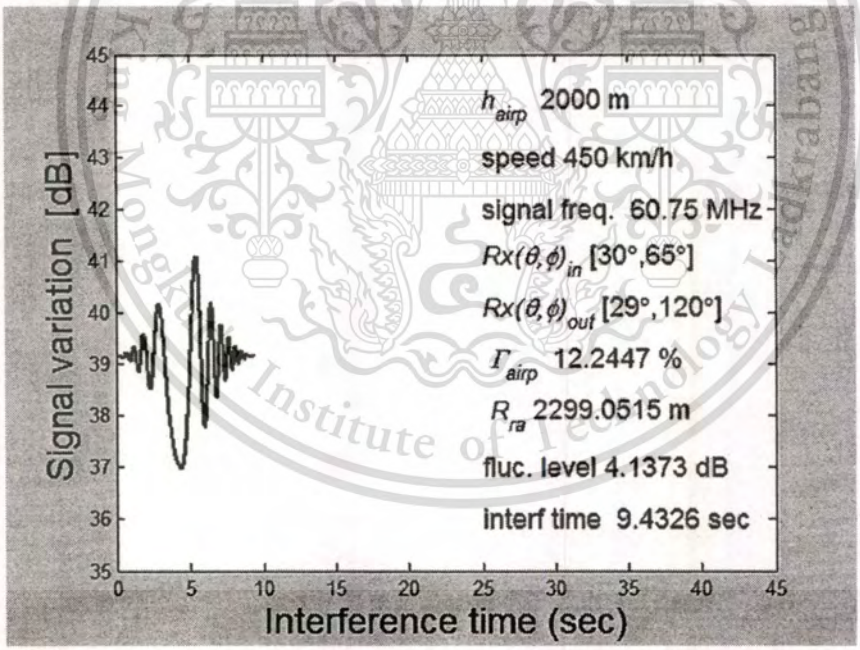

(b)

Fig. 5.13 Cross pattern of Boeing 747 with altitude of 2000 m, speed 450 km/h, $Rx(\theta,\phi)_{in}$ [30°,65°] , and $Rx(\theta,\phi)_{out}$ [29°,120°] (a) measured pattern (b) simulated pattern

In Fig. 5.13(a), the measured signal of the cross pattern flight on 17:00:35 to 17:00:57 hr is shown. The speed and altitude of airplane are approximately 450 km/h and 2,000 m, respectively. A typical signal level of Ch3 is 41 dB. With fluttering phenomena, however, the maximum signal variation of Ch3 is 4.7 dB over a 9-second interval. The simulation of Fig. 5.13(a) shows in Fig 5.13(b). The vertical angle θ on receiving side a little varies from 30 degrees to 29 degrees, while the horizontal angle ϕ varies from 65 to 120 degrees. The simulated signal variation is around 4.13 dB over a 9.4-second time interval. The simulated slightly difference both signal variation and time interval.

In Fig. 5.14(a), the measured signal of the cross-range pattern flight on 15:00:47 to 15:01:06 hr is shown. The speed and altitude of airplane are approximately 450 km/h and 1,400 m, respectively. A typical signal level of Ch3 is 40 dB. With fluttering phenomena, however, the maximum signal variation of Ch3 is 7 dB over a 10-second interval. The simulation of Fig. 5.14(a) shows in Fig 5.14(b). The vertical angle θ on receiving side varies from 35 degrees to 30 degrees, while the horizontal angle ϕ varies from 40 to 120 degrees. The simulated signal variation is around 7.6 dB over a 13.1-second time interval. The simulated slightly difference both signal variation and time interval.

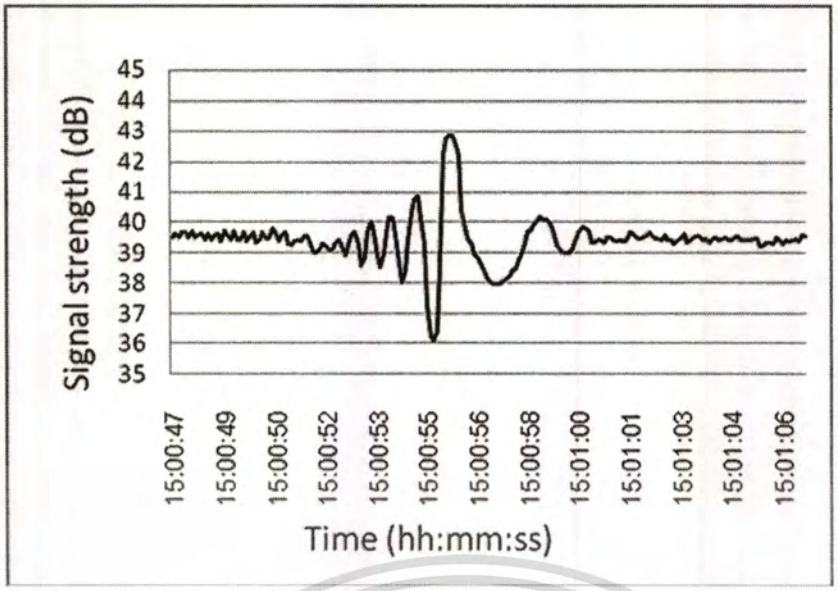

(a)

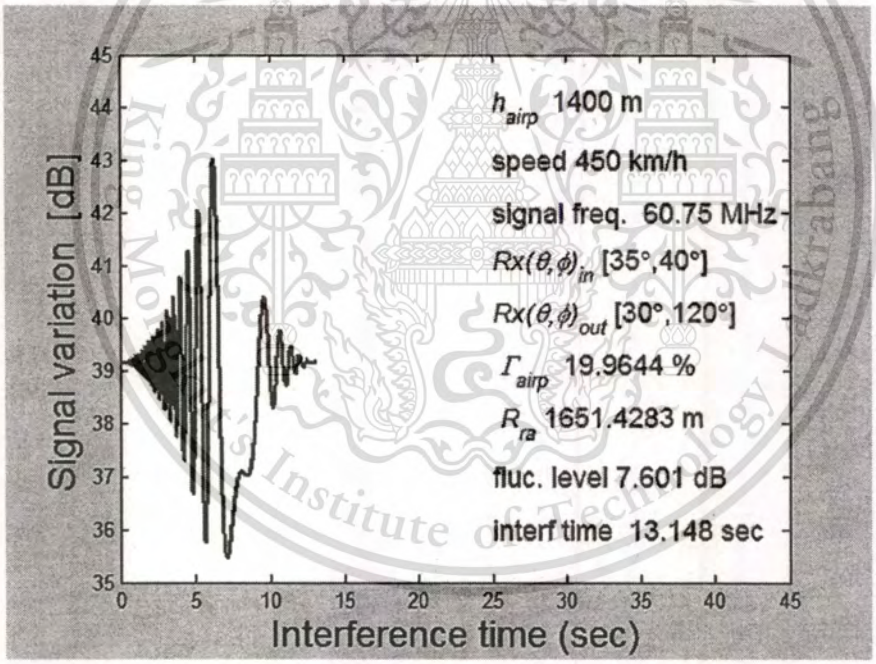

(b)

Fig. 5.14 Cross-range pattern of Boeing 747 with altitude of 1,400 m, speed 450 km/h, $Rx(\theta,\phi)_{in}$ [35°,40°] , and $Rx(\theta,\phi)_{out}$ [30°,120°] (a) measured pattern (b) simulated pattern

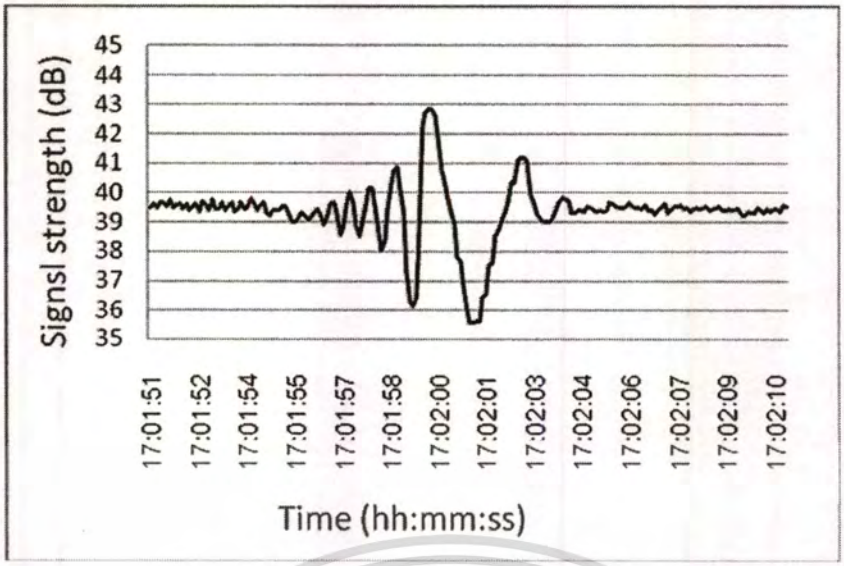

(a)

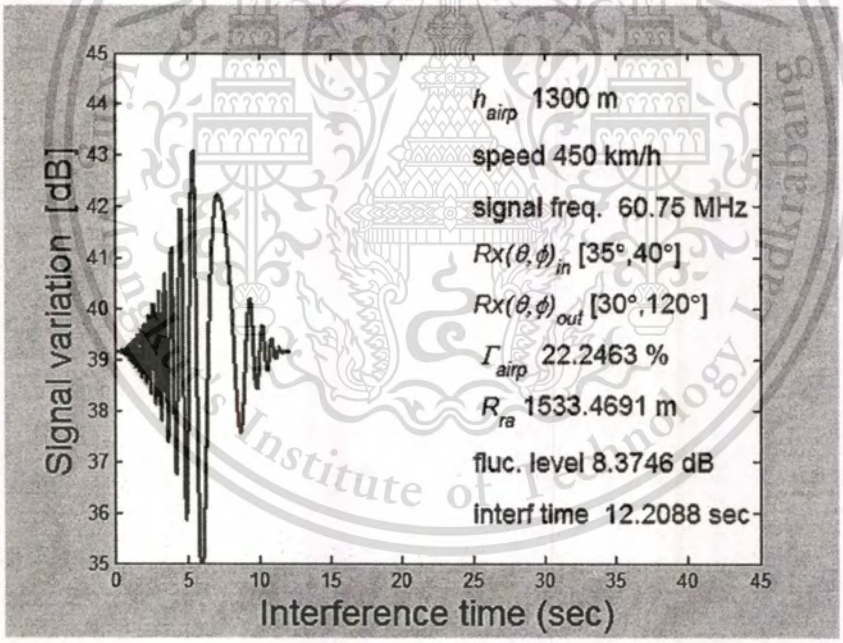

(b)

Fig. 5.15 Cross-range pattern of Boeing 747 with altitude of 1,300 m, speed 450 km/h, $Rx(\theta,\phi)_{in}$ [35°,40°] , and $Rx(\theta,\phi)_{out}$ [30°,120°] (a) measured pattern (b) simulated pattern

In Fig. 5.15(a), the measured signal of the cross-range pattern flight on 17:01:51 to 17:02:01 hr is shown. The speed and altitude of airplane are approximately 450 km/h and 1,300 m, respectively. A typical signal level of Ch3 is 40 dB. With fluttering phenomena, however, the maximum signal variation of Ch3 is 7.5 dB over a 10-second interval. The simulation of Fig. 5.15(a) shows in Fig 5.15(b). The vertical angle θ on receiving side varies from 35 degrees to 30 degrees, while the horizontal angle ϕ varies from 40 to 120 degrees. The simulated signal variation is around 8.37 dB over a 12.2-second time interval. The simulated slightly difference both signal variation and time interval.

In Fig. 5.16(a), the measured signal of the cross-range pattern flight on 17:00:36 to 17:01:02 hr is shown. The speed and altitude of airplane are approximately 450 km/h and 2,500 m, respectively. A typical signal level of Ch3 is 40 dB. With fluttering phenomena, however, the maximum signal variation of Ch3 is 2 dB over a 10-second interval. The simulation of Fig. 5.16(a) shows in Fig 5.16(b). The vertical angle θ on receiving side varies from 35 degrees to 20 degrees, while the horizontal angle ϕ varies from 50 to 70 degrees. The simulated signal variation is around 3.27 dB over a 11.3-second time interval. The simulated slightly difference both signal variation and time interval.

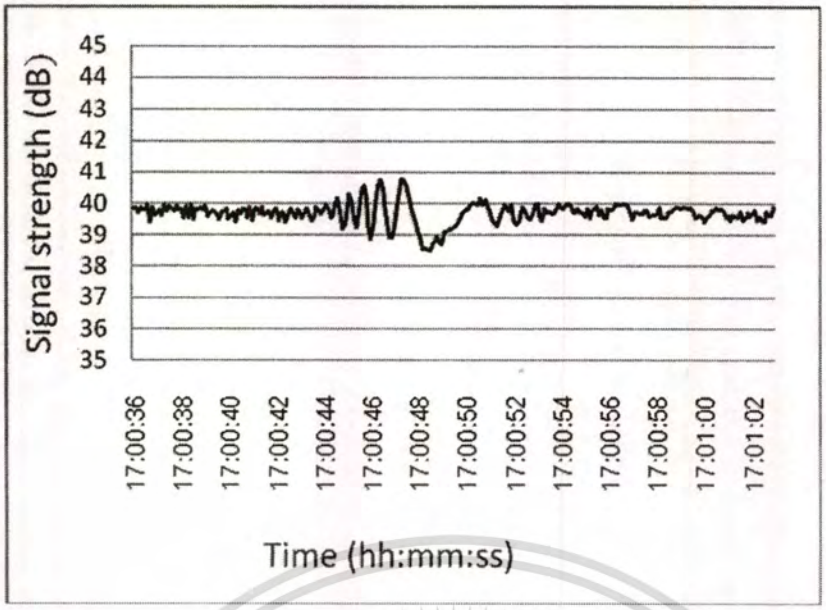

(a)

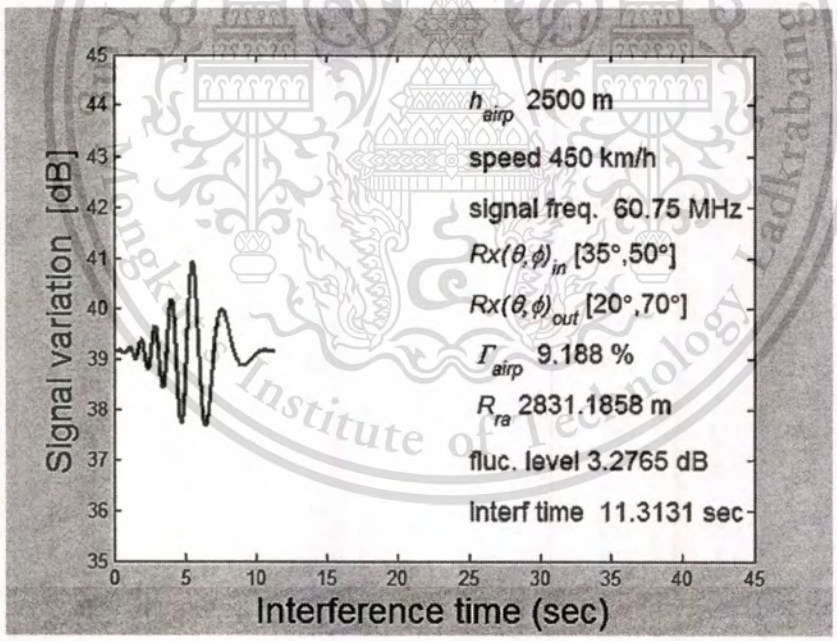

(b)

Fig. 5.16 Cross-range pattern of Boeing 747 with altitude of 2,500 m, speed 450 km/h, $Rx(\theta,\phi)_{in}$ [35°,50°] , and $Rx(\theta,\phi)_{out}$ [20°,70°] (a) measured pattern (b) simulated pattern

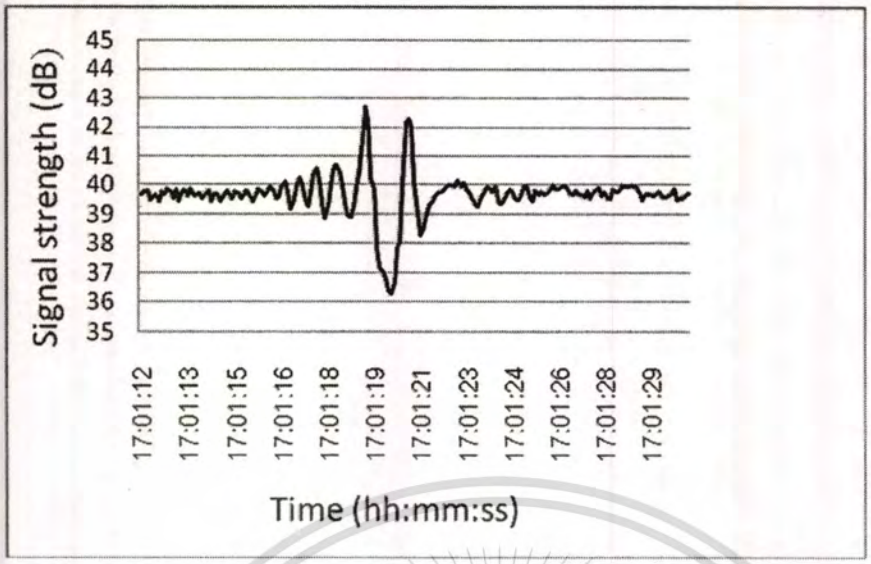

(a)

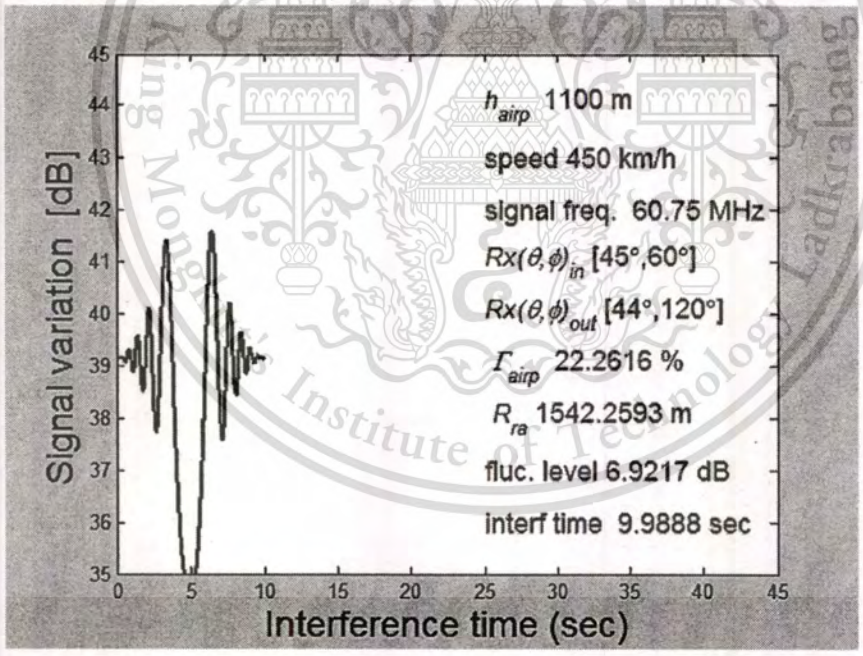

(b)

Fig. 5.17 Cross pattern of Boeing 747 with altitude of 1,100 m, speed 450 km/h, $Rx(\theta,\phi)_{in}$ [45°,60°] , and $Rx(\theta,\phi)_{out}$ [44°,120°] (a) measured pattern (b) simulated pattern

In Fig. 5.17(a), the measured signal of the cross-range pattern flight on 17:01:12 to 17:01:29 hr is shown. The speed and altitude of airplane are approximately 450 km/h and 1,100 m, respectively. A typical signal level of Ch3 is 40 dB. With fluttering phenomena, however, the maximum signal variation of Ch3 is 7 dB over a 9.9-second interval. The simulation of Fig. 5.17(a) shows in Fig. 5.17(b). The vertical angle θ on receiving side varies from 45 degrees to 44 degrees, while the horizontal angle ϕ varies from 60 to 120 degrees. The simulated signal variation is around 6.92 dB over a 9.98-second time interval. The simulated agreement with measured pattern both signal variation and time interval.

Figure 5.18(a) shows the measured signal of the cross pattern flight on 17:14:56 to 17:15:43 hr. The speed and altitude of airplane are approximately 450 km/h and 2,500 m, respectively. A typical signal level of Ch3 is 40 dB. With fluttering phenomena, the maximum signal variation of Ch3 is 2.7 dB over a 10-second interval. The simulation of Fig. 5.18(a) is illustrated in Fig. 5.18(b). The vertical angle θ on receiving side varies from 40 degrees to 39 degrees, while the horizontal angle ϕ varies from 70 to 110 degrees. The simulated signal variation is around 2.9 dB over a 9.61-second time interval. The simulated closely with measured pattern both signal variation and time interval.

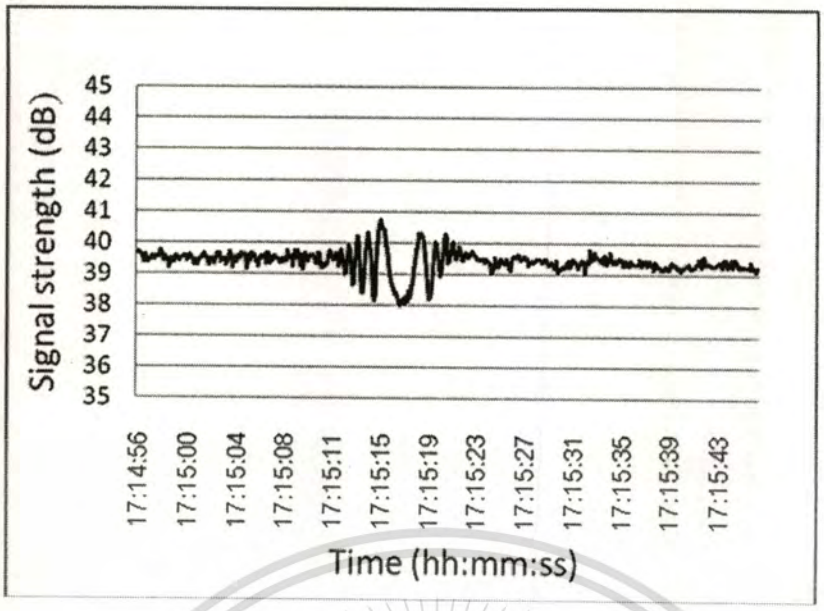

(a)

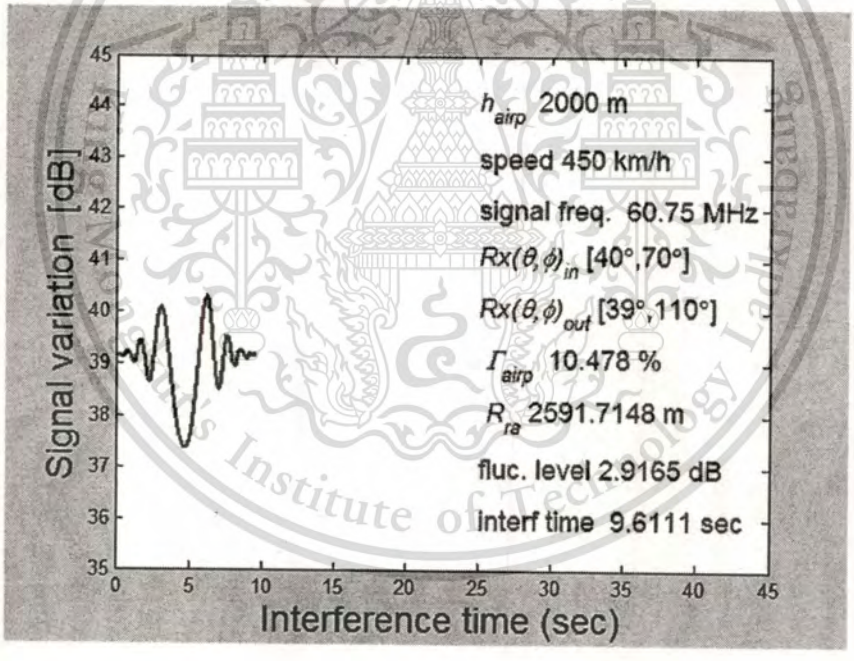

(b)

Fig. 5.18 Cross pattern of Boeing 747 with altitude of 2,000 m, speed 450 km/h, $Rx(\theta,\phi)_{in}$ [40°,70°] , and $Rx(\theta,\phi)_{out}$ [39°,110°] (a) measured pattern (b) simulated pattern

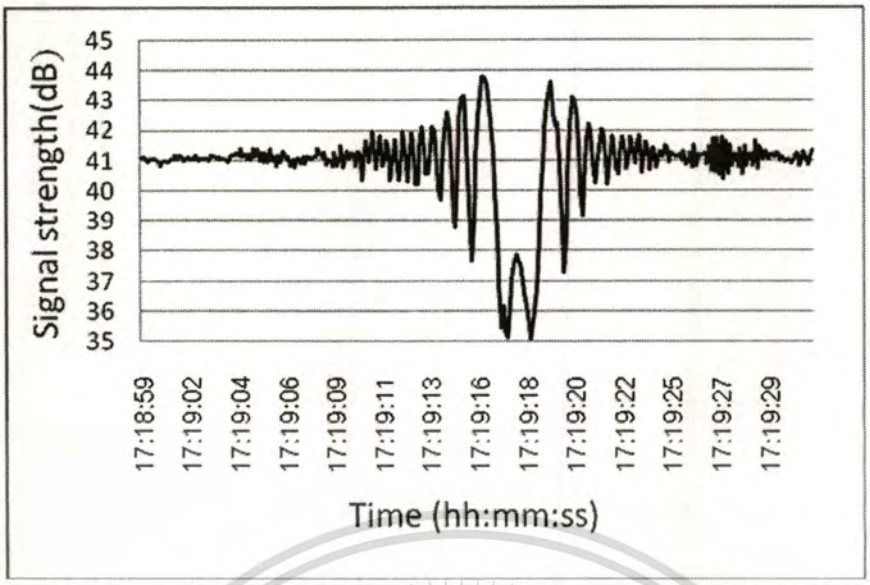

(a)

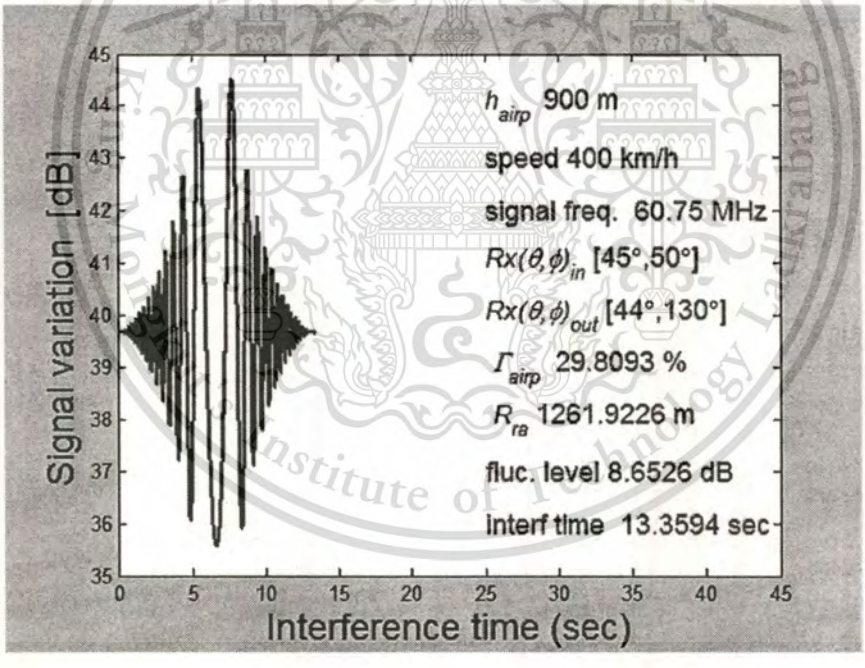

(b)

Fig. 5.19 Cross pattern of Boeing 747 with altitude of 900 m, speed 400 km/h, $Rx(\theta,\phi)_{in}$ [45°,50°] , and $Rx(\theta,\phi)_{out}$ [44°,130°] (a) measured pattern (b) simulated pattern

In Fig. 5.19(a), the measured signal of the cross pattern flight on 17:18:59 to 17:19:29 hr is shown. The speed and altitude of airplane are approximately 400 km/h and 900 m, respectively. A typical signal level of Ch3 is 41 dB. With fluttering phenomena, however, the maximum signal variation of Ch3 is 8.7 dB over a 13-second interval. The simulation of Fig. 5.19(a) shows in Fig. 5.19(b). The vertical angle θ on receiving side varies from 45 degrees to 44 degrees, while the horizontal angle ϕ varies from 50 to 130 degrees. The simulated signal variation is around 8.65 dB over a 13.35-second time interval. The simulated agreement with measured pattern both signal variation and time interval.

Figure 5.20(a) shows the measured signal of the cross pattern flight on 17:35:12 to 17:35:30 hr. The speed and altitude of airplane are approximately 400 km/h and 1,000 m, respectively. A typical signal level of Ch3 is 41 dB. With fluttering phenomena, the maximum signal variation of Ch3 is 8.5 dB over a 15-second interval. The simulation of Fig. 5.20(a) is illustrated in Fig. 5.20(b). The vertical angle θ on receiving side varies from 45 degrees to 44 degrees, while the horizontal angle ϕ varies from 50 to 130 degrees. The simulated signal variation is around 8.6 dB over a 14.84-second time interval. The simulated closely with measured pattern both signal variation and time interval.

Note: As you can see, the difference on Fig. 5.19 and Fig. 5.20 is altitude of airplane. The interference time increased when the altitude of airplane is increased.

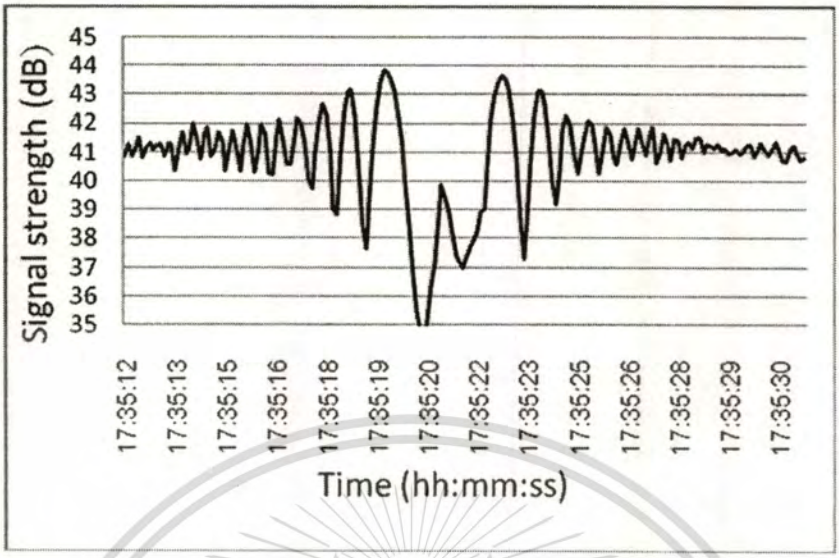

(a)

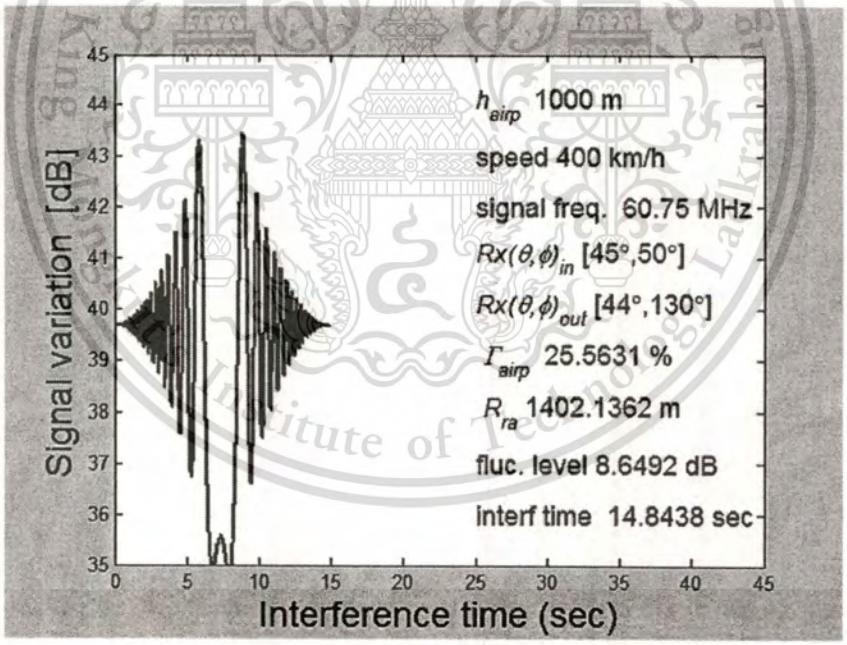

(b)

Fig 5.20 Cross pattern of Boeing 747 with altitude of 1,000 m, speed 400 km/h, $Rx(\theta,\phi)_{in}$ [45°,50°] , and $Rx(\theta,\phi)_{out}$ [44°,130°] (a) measured pattern (b) simulated pattern

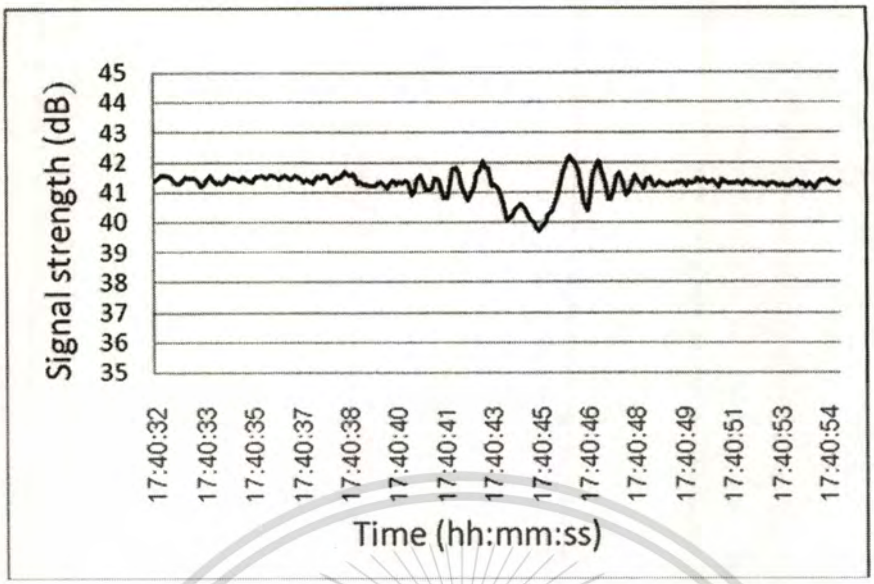

(a)

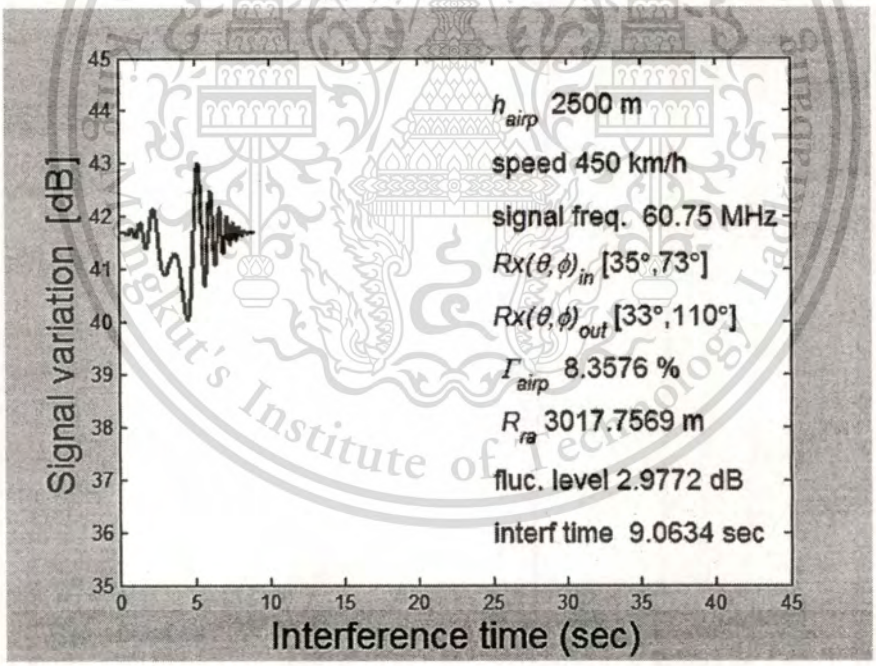

(b)

Fig 5.21 Cross-range pattern of Boeing 747 with altitude of 2,500 m, speed 450 km/h, $Rx(\theta,\phi)_{in}$ [35°,73°] , and $Rx(\theta,\phi)_{out}$ [33°,110°] (a) measured pattern (b) simulated pattern

In Fig. 5.21(a), the measured signal of the cross-range pattern flight on 17:40:32 to 17:40:54 hr is shown. The speed and altitude of airplane are approximately 450 km/h and 2,500 m, respectively. A typical signal level of Ch3 is 41 dB. With fluttering phenomena, however, the maximum signal variation of Ch3 is 2.2 dB over a 9-second interval. The simulation of Fig. 5.21(a) shows in Fig. 5.21(b). The vertical angle θ on receiving side varies from 35 degrees to 33 degrees, while the horizontal angle ϕ varies from 73 to 110 degrees. The simulated signal variation is around 2.97 dB over a 9.0-second time interval. The simulated agreement with measured pattern both signal variation and time interval.

Figure 5.22(a) shows the measured signal of the cross pattern flight on 17:06:19 to 17:06:51 hr. The speed and altitude of airplane are approximately 450 km/h and 1,500 m, respectively. A typical signal level of Ch3 is 41 dB. With fluttering phenomena, the maximum signal variation of Ch3 is 7.5 dB over a 15-second interval. The simulation of Fig. 5.22(a) is illustrated in Fig. 5.22(b). The vertical angle θ on receiving side varies from 38 degrees to 34 degrees, while the horizontal angle ϕ varies from 65 to 130 degrees. The simulated signal variation is around 6.5 dB over an 11.23-second time interval. The simulated slightly difference with measured pattern both signal variation and time interval.

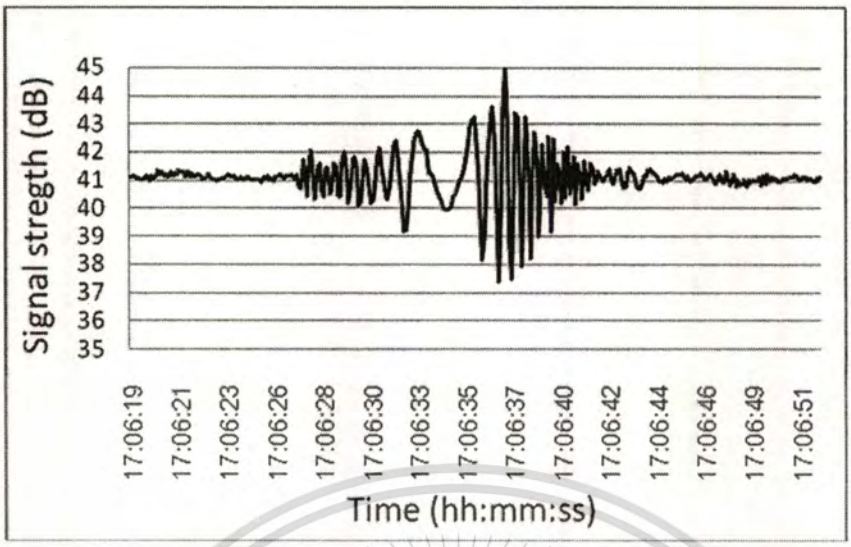

(a)

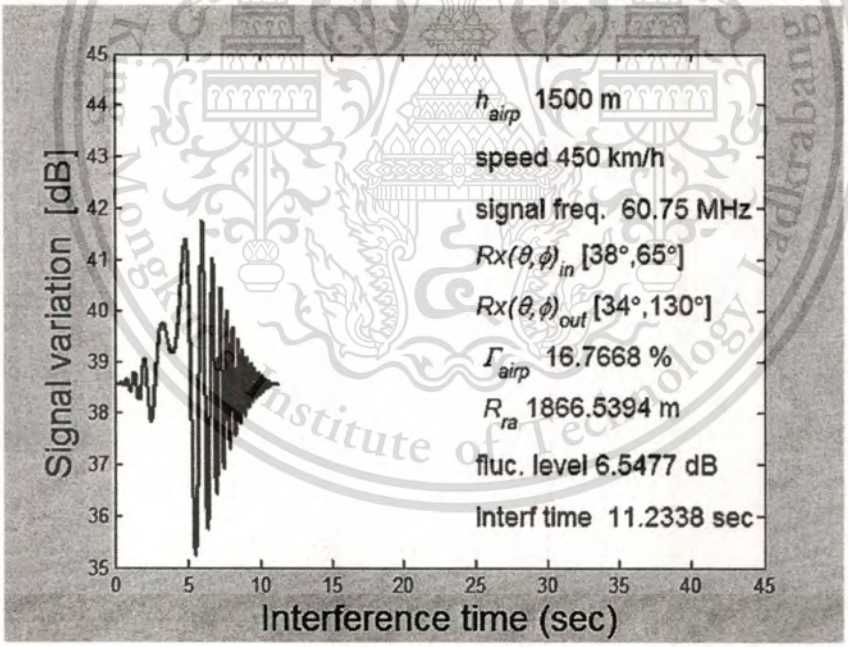

(b)

Fig. 5.22 Cross-range pattern of Boeing 747 with altitude of 1,500 m, speed 450 km/h, $Rx(\theta,\phi)_{in}$ [38°,65°] , and $Rx(\theta,\phi)_{out}$ [34°,130°] (a) measured pattern (b) simulated pattern

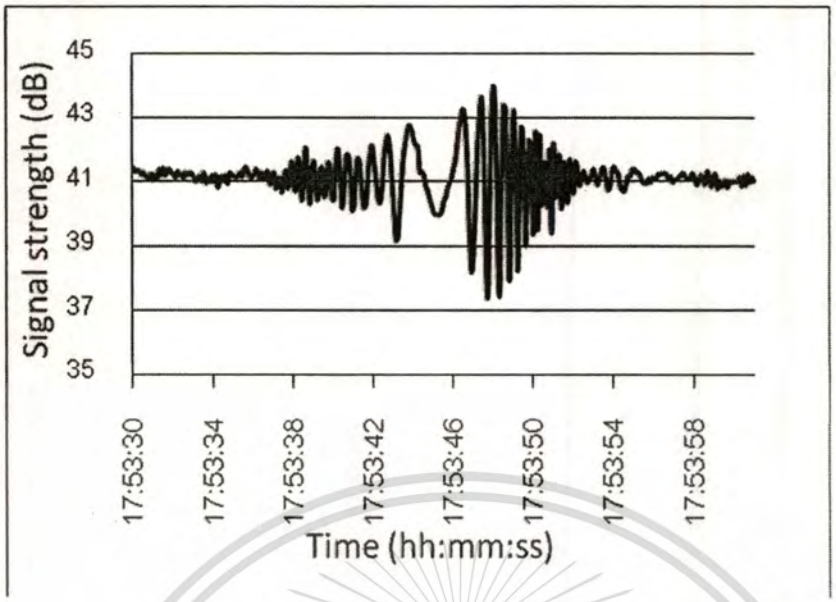

(a)

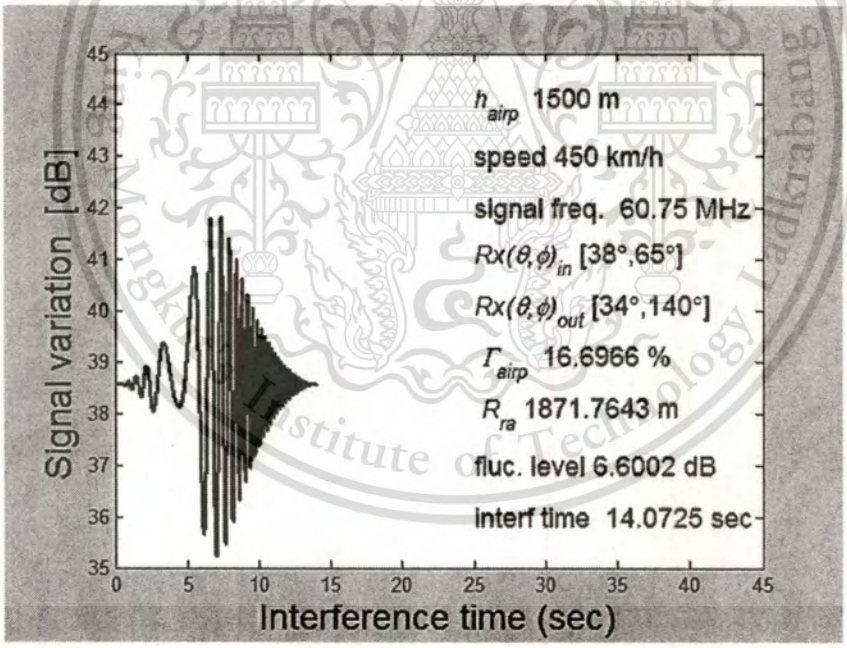

(b)

Fig 5.23 Cross-range pattern of Boeing 747 with altitude of 1,500 m, speed 450 km/h, $Rx(\theta,\phi)_{in}$ [38°,65°] , and $Rx(\theta,\phi)_{out}$ [34°,140°] (a) measured pattern (b) simulated pattern

In Fig. 5.23(a), the measured signal of the cross-range pattern flight on 17:53:30 to 17:53:58 hr is shown. The speed and altitude of airplane are approximately 450 km/h and 1,500 m, respectively. A typical signal level of Ch3 is 41 dB. With fluttering phenomena, however, the maximum signal variation of Ch3 is 6.3 dB over a 15-second interval. The simulation of Fig. 5.23(a) shows in Fig. 5.23(b). The vertical angle θ on receiving side varies from 38 degrees to 34 degrees, while the horizontal angle ϕ varies from 65 to 140 degrees. The simulated signal variation is around 6.6 dB over a 14.0-second time interval. The simulated slightly difference with measured pattern both signal variation and time interval.

Note: We can find that the difference on Fig. 5.22 and Fig 5.23 is angle ϕ at the receiving side. The interference time increased when the angle ϕ is increased.

Figure 5.24(a) shows the measured signal of the cross pattern flight on 17:20:02 to 17:20:33 hr. The speed and altitude of airplane are approximately 400 km/h and 900 m, respectively. A typical signal level of Ch3 is 41 dB. With fluttering phenomena, the maximum signal variation of Ch3 is 9 dB over a 15-second interval. The simulation of Fig. 5.24(a) is illustrated in Fig. 5.24(b). The vertical angle θ on receiving side varies from 45 degrees to 44 degrees, while the horizontal angle ϕ varies from 45 to 135 degrees. The simulated signal variation is around 9.09 dB over a 15.9-second time interval. The simulated closely with measured pattern both signal variation and time interval.

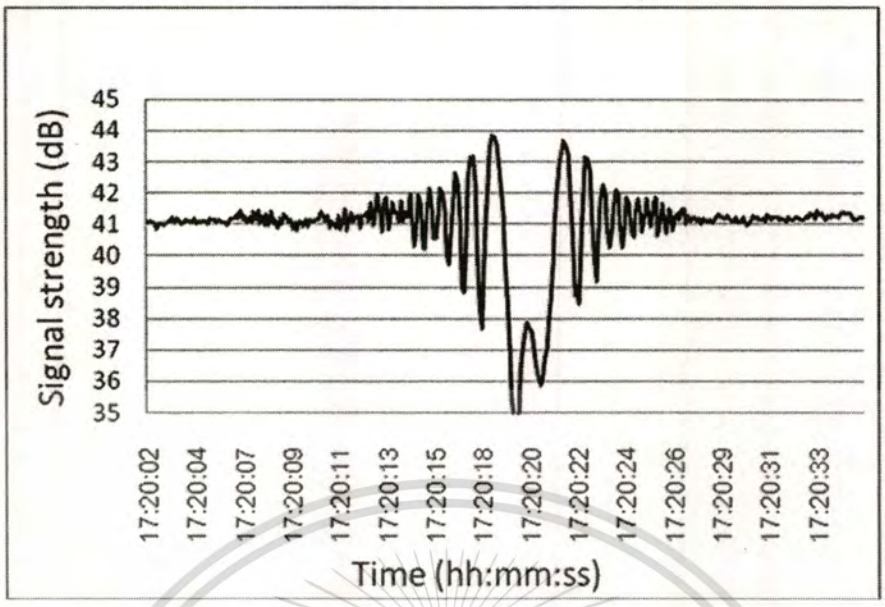

(a)

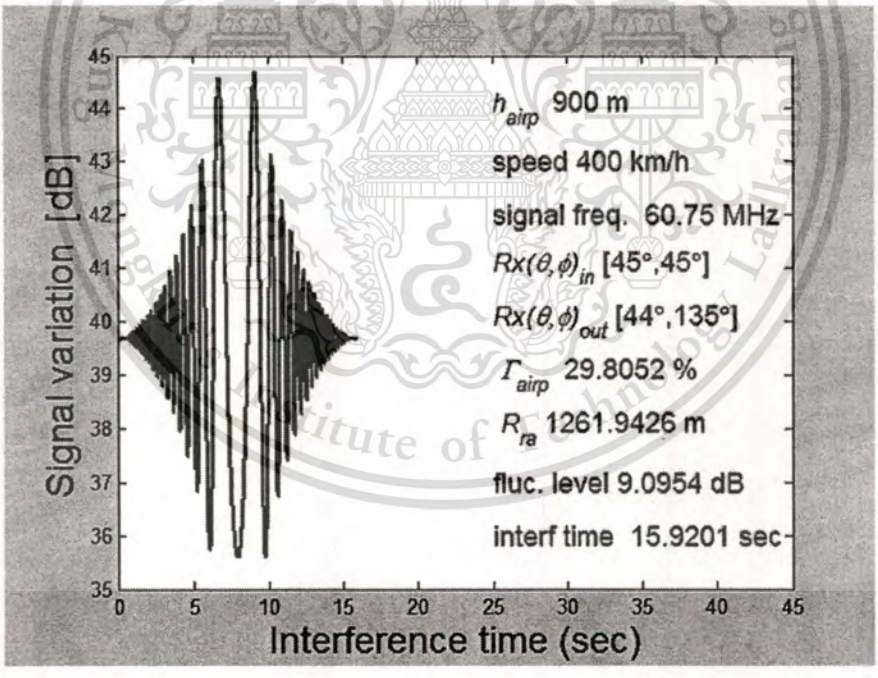

(b)

Fig. 5.24 Cross pattern of Boeing 747 with altitude of 900 m, speed 400 km/h, $Rx(\theta,\phi)_{in}$ [45°,45°] , and $Rx(\theta,\phi)_{out}$ [44°,135°] (a) measured pattern (b) simulated pattern

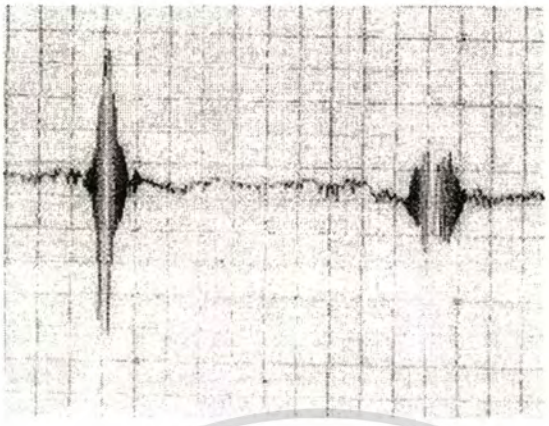

(a)

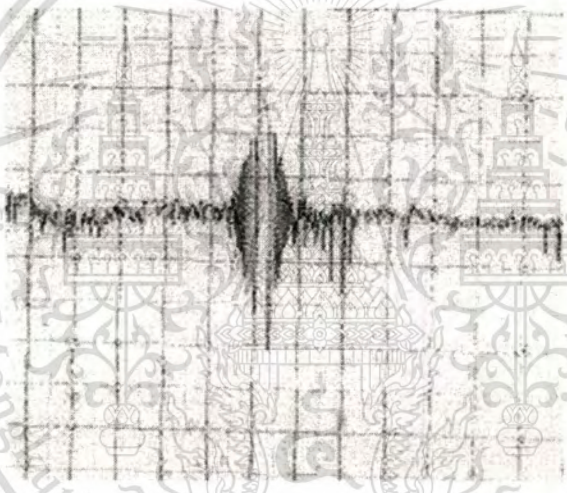

(b)

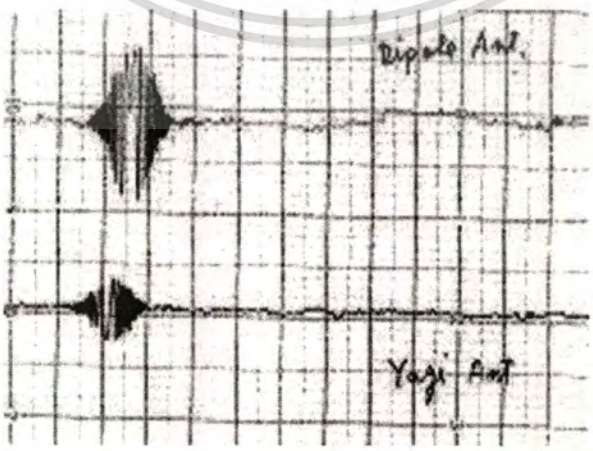

(c)

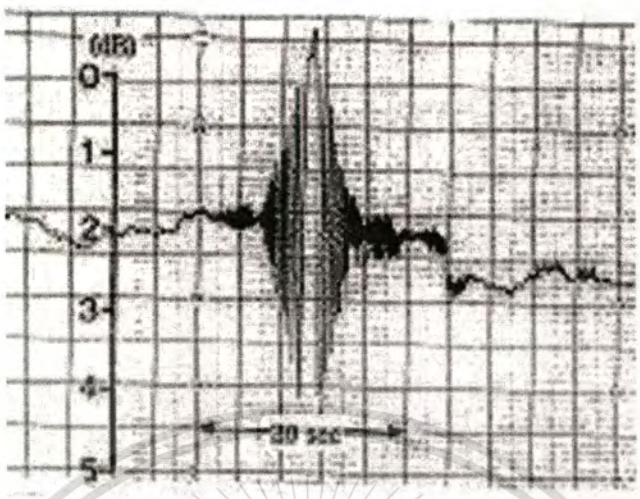

(d)

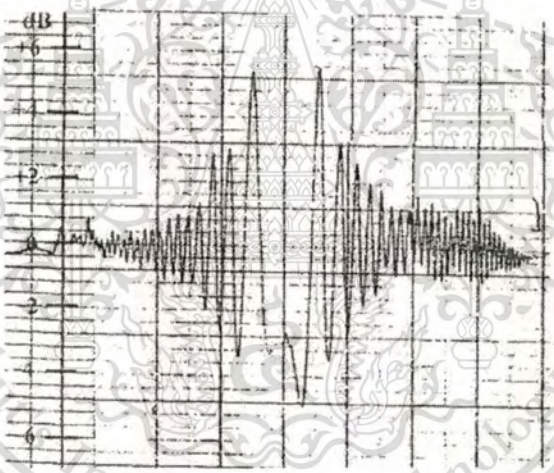

(e)

Fig. 15.25 Some airplane flutter patterns (a) two cross patterns but difference in altitude or size (b) cross pattern (c) when using difference type of receiving antenna, upper pattern is dipole antenna and lower pattern is yagi antenna (d) cross pattern with signal variation about 4 dB over 10-seconds (e) cross pattern with signal variation about 6 dB over 36-seconds

Some old airplane flutter patterns as shown in Fig. 5.25. Figure 5.25 (a) shows two cross patterns but difference in altitude or size. Figure 5.25 (b) shows cross pattern with signal variation around 3 dB over 10-seconds. Figure 5.25 (c) shows when using difference type of receiving antenna, upper pattern is using dipole antenna with around 2 dB of signal variation over 10-seconds and lower pattern is using yagi antenna with around 1 dB of signal variation over 9-seconds. We find that the signal variation is reduced when yagi antenna is used. Cross pattern with signal variation about 4 dB over 10-seconds as illustrated in Fig. 5.25 (d). Figure 5.25 (e) shows cross pattern with signal variation about 6 dB over 36-seconds. In addition, this figure shows long duration time affected on pattern.

5.2 Discussions

Flying object such as airplane could scatter wave from TV transmission signal. The scattered wave caused by airplane disturbs direct wave from transmission and the result appears in the reception of TV signals. The flutter phenomena also occur at a point considerably far from the airport. When the airplane flew across the line-of-sight path between the television signal and the receiving antennas, received signal strength cause a flutter or quasi-periodic fluctuation.

The observation and measurement of airplane flutter was performed at KMITL as the distance between transmitting and receiving side is 45 km. The signal was measured when the Boeing 747 flew with cross, and cross-range patterns between line-of-sight with altitudes of around 1,000-3,000 m and speeds of around 400-500 km/h. Symmetry of the variation pattern occurred when an airplane flew across between line-of-sight signal. Asymmetry of the variation pattern occurs as an airplane flew cross-range between the line-of-sight signals. The measurement pattern results, mostly 80% from about 100 measured data are cross and cross-range patterns are used in the analysis in this paper.

From the experimental results, it is evident that the lower frequency of ch3 is

affected, while the higher frequency of ch9 is nearly unnoticeable. Moreover, the observation of picture on TV receiver show that only the picture and sound of ch3 is distorted. This can be explained from Eq.(4.8) that the power density of wave at the receiving antenna due to scattering by airplane (P_{Dr}) is small when λ is short (λ of Ch3 = 5 m while λ of Ch9 = 1.4 m).

The effects of speed and altitude on the duration time of signal variation and the maximum variation can be explained using our proposed model. The speed and altitude of the airplane directly affects the duration time and signal variation. The longer duration is caused by slower speed. At higher altitude, the maximum signal variation is reduced, while the duration time increases. The reduction of fluctuation is due to the fact that higher R_{ra} decreases the percentage of reflection.

5.3 Conclusions

In this chapter, we propose a novel approach to simulate the flutter phenomena based on physical and geometrical parameters. The mode of analysis that I did depends on the measurement data obtained from a lot of places and it depends on physical and geometrical parameters. The model for signal variation takes into account of real physical and related parameters such as type of airplane, speeds, altitude, and direction. In addition, transmission and receiving information such as transmitter power, and antenna height, and gain are input to the model. The simulation results are then compared with measurement results at 60.75 MHz and 208.75 MHz.

Mostly measured pattern are cross and cross-range patterns. The results have shown good agreement between simulation and measurement patterns. However, the slightly difference between measured pattern and simulated pattern occurs. This due to slightly mistake assigned the angle of $Rx(\theta,\phi)_{in}$ and $Rx(\theta,\phi)_{out}$. From the simulation results, if input more wide ϕ angle, the interference time is increased. In addition, longer interference time when altitude is higher but signal variation is reduced. Moreover, the

airplane flutter program can use simulated on other frequency in VHF band such as Ch5, Ch7, *etc*.

Chapter 6

Conclusions

In this thesis, we study radio wave propagation of television broadcasting signal. Television broadcasting is widely used as important media in world wide. A wireless method is used as a majority in TV broadcasting. Thus some problems on television receiving signal occurs for example, noise interference in low channel receiving signal, solar noise and airplane flutter phenomena. The study consists of the following pasts there.

Firstly, Electromagnetic interference (EMI) causes high interference to television reception, especially, at low frequency band such as 47-68 MHz. The EMI is the unintended radio frequency emission from electrical and electronic products. In the television reception of VHF frequency channel 2 and 3 (47-68MHz), the received signal is easier interfered by EMI than the high frequency channel. From the study, we find that the lowest channels of TV channel 2 (47-54MHz) is easily affected from EMI, although the received signal field strength is high. To reduce the effect from EMI sources, one may change the antenna direction to avoid the EMI source path or using the higher antenna or attenuation of input signal from antenna. In this research, we find that the low frequency should not use in TV broadcasting due to easily disturbed. Moreover, the receiving antenna difficulty setting due to size is larger. In the future, digital broadcasting will setup in Thailand. The frequency of UHF channels shall be considered for digital TV planning in Thailand.

Lastly, airplane flutter phenomena occur when an airplane flies across transmitting and receiving antenna. The reflected signal from airplane reaches the receiving antenna at the same time as the direct signal but with a phase delay. The model for signal variation takes into account of real physical and related parameters such as type of airplane, speeds, altitude, and direction. In addition, transmission and receiving information such as

transmitter power, antenna height, and gain are input to the model. The simulation results are then compared with measurement results. The results have shown good agreement between simulation and measurement patterns. Finally, the research on airplane flutter not only clarifies that the effects on the television signal due to moving scattering objects, but also be useful for the research of the radio wave propagation depends on the frequency response. For its application, the airplane flutter program in MATLAB is easy to use simulate many events of flutter phenomena for research and development work on TV receiving system by changing parameters input. Another application is moving object detected such as airplane or missile in military work.

References

[1] E.L.Bronaugh and W.S. Lambdin, **Electromagnetic Interference Test Methodology and Procedures.** Handbook series on Electromagnetic Interference and Compatibility, Interference Technologies, Inc., USA, 1988, pp.1.22-1.24 & 3.35-3.38.

[2] ANSI C63.4-1981, **American National Standard Methods of Measurement of Radio-noise Emissions from Low-Voltage Electrical and Electronic Equipment in the Range of 10 kHz to 1000 kHz**. pp.3.

[3] E.L. Bronaugh, "Introduction to Electromagnetic Compatibility: Review, History and Trends." **Proceeding of the 17th Electrical/ Electronic Insulation Conference, IEEE EIS, NEMA and ICWA, Boston, MA**, Sept. 30- Oct. 3, 1985, p.177

[4] Ito and Ohta. "Estimation of Fluttering of Field Intensity Caused by Aircraft and its Disturbance to Television Reception." **ITE Journal.**, vol. 40, no. 9, 1986. pp. 899-905

[5] Nishihara, Endo, Hidaka and Takahashi. "Investigation and Countermeasures for TV Reception Interference by Aircraft." **IEICE Technical Report EMCJ97-8.**, 1997

[6] H. Miyazawa. "Evaluation and Measurement of Airplane Flutter Interference." **IEEE Trans. Broadcast.**, vol. 35, no. 4, 1989. pp. 362-367

[7] N. Leelaruji, H. Sakurada and Y. Moriya, "Relation Between Quasi- Periodic Level Fluctuation and Plane Flight on Television Broadcasting Waves." **ITE Technical Report.**, vol. 21, No. 5, pp.21-21, Jan. 1997.

[8] Blake UK. "**Reception Problems.**" [Online]. Available: http://www.blake-uk.com/page/reception-problems. 2008.

[9] BBC News. "**Help Receiving Analogue TV - Interference.**" [Online]. Available: http://www.bbc.co.uk/reception/analoguetv/interference.shtml. 2008.

[10] Office of Communication. "**Guidelines for Improving Digital Television and Radio Reception.**" [Online]. Available: http://www.ofcom.org.uk /static/archive/ra/publication /ra_info/ra415/ra415.htm. 2008.

[11] Federal Communications Commission (FCC). "**Interference Handbook.**" [Online]. Available: http://www.kyes.com/antenna/interference/tvibook.html. 2008.

[12] Self Help and More. "**Cutting Through Television Interference.**" [Online]. Available: http://www.selfhelpandmore.com/interference/tv/. 2008.

[13] E.L.Bronaugh and W.S. Lambdin, **Electromagnetic Interference Test Methodology and Procedures.** Handbook series on Electromagnetic Interference and Compatibility, Interference Technologies, Inc., USA, 1988, pp.1.22-1.24 & 3.35-3.38.

[14] ANSI C63.4-1981, **American National Standard Methods of Measurement of Radio-noise Emissions from Low-Voltage Electrical and Electronic Equipment in the Range of 10 kHz to 1000 kHz.** pp.3.

[15] Duff, Willium G., **Fundamental of Electromagnetic Compatibility.** Interference Control Technology Inc., vol.1, Verginia, 1988. pp.1.1.

[16] Ito and Ohta. "Estimation of Fluttering of Field Intensity Caused by Aircraft and its Disturbance to Television Reception." **ITE Journal.**, vol. 40, no. 9, 1986. pp. 899-905

[17] Nishihara, Endo, Hidaka and Takahashi. "Investigation and Countermeasures for TV Reception Interference by Aircraft." **IEICE Technical Report EMCJ97-8.**, 1997

[18] H. Miyazawa. "Evaluation and Measurement of Airplane Flutter Interference." **IEEE Trans. Broadcast.**, vol. 35, no. 4, 1989. pp. 362-367

[19] A. Wongkeeratikul, P. Sangonchat, S. Noppanakeepong, N. Leelarruji, and Y. Moriya, "The Observation and Simulation of the Airplane Flutter on Low Band TV signal," **Int. Conf. SCOReD 2003, Putrajaya, Malaysia,** 2003. pp. 23

[20] A. Wongkeeratikul, S. Noppanakeepong, N. Leelarruji, and Y. Moriya, "The Analysis of the Airplane Flutter on Low Band TV signal," **Int. Conf. ICCAS 2003, Gyeongju, Korea**, 2003. pp. 88

[21] K. Takagi, N. Leeraluji, N. Hemmakorn, H. Sakurada and Y. Moriya, "Simulation and Application of Quasi Periodic Fluctuation Caused by Aircraft Scattering Phenomenon," **Proc. Asia-Pacific Symp. on Broadcast. and Commun. (APSBC'2000)., KMITL, Thailand,** 2000, pp. 186-191

[22] J. I. Glaser, "Bistatic RCS of Complex Objects Near Forward Scatter," **IEEE Trans. Aerosp. and electron. Syts.,** vol. AES-21, no. 1, Jan. 1985

[23] A. David, C. Brousseau and A. Bourdillon, "Simulation and Measurement of a Radar Cross Section of a Boeing 747-200 in the 20-60MHz Frequency Band," **Radio Science,** vol. 38, no. 4, 2003, pp.1064

[24] M. L. Bucher, "Simulation of Multipath Fading/Ghosting for Analog and Digital Television Transmission in Broadcast Channels," **IEEE Trans. Broadcast.,** vol. 38, no. 4, Dec. 1992, pp. 256-262

[25] Bassem R. Mahafza. **Radar Systems Analysis and Design Using MATLAB.** Chapman & Hall/CRC. 2000.

[26] Albert A. Smith. **Radio Frequency Principle and Applications.** Chapman&Hall publishers. 1998. pp. 46-50.

[27] J. Kraus and D. Fleish. **Electromagnetics with applications.** McGraw-Hill international editions. 1999. pp. 24-30.

Appendices

IEEE TRANSACTIONS ON

BROADCASTING

A PUBLICATION OF THE IEEE BROADCAST TECHNOLOGY SOCIETY

MARCH 2007 VOLUME 53 NUMBER 1 IETBAC (ISSN 0018-9316)

PART I OF TWO PARTS

PAPERS

BRIEF PAPERS

CORRESPONDENCE

CALLS FOR PAPERS

IEEE TRANSACTIONS ON BROADCASTING

Transactions on Broadcasting Publications Office

Reply to:
IEEE Technical
Activities
445 Hoes Lane
Piscataway, NJ 08854
Tel: +1 732 562 3905
Fax: +1 732 981 1769
bt-pubs@ieee.org

21 January 2008

Anuchit Wongkeeratikul
W_anuchit@yahoo.com

RE: BTS-06-074: "Modeling and Measurement of Airplane Flutter Phenomena on TV Broadcasting Signal"

Dear Anuchit Wongkeeratikul:

I am pleased to inform you that your manuscript, referenced above, has been accepted for publication in the *IEEE Transactions on Broadcasting* as a Transaction paper. It is likely that your paper will appear in the June 2008 Issue.

For additional information on submitting final manuscripts for publication, please see to the GUIDE FOR TRANSACTIONS AUTHORS at web site:
http://www.ieee.org/organizations/pubs/transactions/information.htm

Please provide these materials to the IEEE/BTS Publications Office at the address below as soon as possible to ensure publication as scheduled. We appreciate your interest in the *IEEE Transactions on Broadcasting*.

Sincerely,

Jennifer Barbato
BT Publications Office

Modeling and Measurement of Airplane Flutter Phenomena on TV Broadcasting Signal

A. Wongkeeratikul, *Student Member, IEEE*, P. Supnithi, *Member, IEEE*, S. Noppanakeepong, N. Leelaruji, and N. Hemmakorn

***Abstract*—This paper presents a novel approach to model TV signal due to airplane flutter phenomena. The three components of the modeling are based on 1) Bistatic radar cross sections (RCS) of an ellipsoid, 2) 3-dimensional geometry consideration technique to calculate the distance difference between direct and reflected waves due to airplane, and 3) Ray theory, based on physical and geometrical consideration. Unlike previous works, the model takes into account of realistic parameters such flying height, distance from the airport, flying angle, altitude, aircraft body type and others. The simulation results are then compared with measurement results at 60.75 MHz and 208.75 MHz. The results have shown good agreement between simulation and measurement patterns.**

***Index Terms*— airplane flutter phenomena, interference on TV signal, quasi-periodic phenomena, modeling and measurement on TV signal**

I. Introduction

Airplane flutter phenomena [1][2] occur when an airplane flies across transmitting and receiving antenna. The reflected signal from airplane reaches the receiving antenna at the same time as the direct signal but with a phase delay. The phenomena naturally affect the signal quality of both analog and digital transmission systems [3]. Accurate model of the signal variation caused by the phenomena is thus necessary for flutter prediction and compensation. The signal measurement is crucial for comparison with the simulation results of the developed model.

Previous works on flutter modeling can be found in [1][4] [5][6]. In [1], the reflected signal from aircraft is measured from different angles using scaled aircraft in an echoic chamber. A Quasi-periodic (QP) fluctuation of signals is observed. In [6], a sinusoidal approach is used to replicate the signal attenuation in the VHF and UHF band as a result of the airplane flying near an airport. It indicates that directivity of the antenna does not affect the pattern of received TV signal. In [1], a geometrical aspect is, however, not used to generate the signals.

Manuscript received May 24, 2006; revised April 13, 2007.

A.Wongkeeratikul, P. Subnithi, S. Noppanakeepong, N. Leelaruji, and N. Hemmakorn are with the Faculty of Engineering and Research Center for Communications and Information Technology (ReCCIT), King Mongkut's Institute of Technology Ladkrabang (KMITL), Chalongkrung Road, Ladkrabang, Bangkok 10520, THAILAND.Tel.+66-2-7373000 ext.3326 (e-mail:w_anuchit@yahoo.com, ksupornc@kmitl.ac.th, knsuthic@kmitl.ac.th, klnipa@kmitl.ac.th,khnarong@kmitl.ac.th)

To obtain more accurate flutter models, aircraft modeling is required. Radar cross section (RCS) technique has been used to model complexed objects. In [7], approximation of an airplane dimensions based on bistatic RCS of spheres and cylinder agree approximately with predictions obtained via exact techniques. In [8], the RCS of Boeing 747-200 aircraft is developed using the Numerical Electromagnetic Code (NEC). The paper presents RCS variations of an aircraft along different flight routes at the 20-60MHz frequency band. The simulation result is not compared with the actual flying route, but with the experiment of scaled aircraft in the echoic chamber. In this case, although the experiment offers better understanding of fluttering, it is based on unrealistic parameter values. For example, the airplane is scaled to 1:100 operating at frequency of 20-60 MHz. In addition, the speeds under study differ from actual values at 400-500km/hour.

The signal variation from fluttering is the result of multipath propagation of direct waves, reflected waves from the airplane and ground. Multipath propagation from the airplane fluttering has recently been discussed in the literature [4][5][9]. In [4-5], a single scatter multipath model and Doppler shift effect are included to model the VHF signal. In [9], the modeling of fading and ghosting of both digital and analog signals are reported. The paper describes simulation of multipath effects with the result of picture distortion in various environment conditions ranging from fixed path between transmitters and receivers to moving reflectors with and reception under mobile condition, but the paper does not compare simulation from equipment with measurement data.

In this paper, we develop a novel model to produce signal fluctuation due to the airplane flutter phenomena. Our contributions are three folds. Firstly, the bistatic *ellipsoid* RCS backscattered method is used to approximate the airplane body. Secondly, the distance and phase difference between direct and reflected waves are computed using the 3-dimensional geometrical technique. Finally, we calculate the total electric field strength at the receiving antenna by modifying the Ray theory and using multipath propagation. Most importantly, realistic parameters such as flight altitude, speed, direction, body type, frequency among others are included in the model. The simulated results are compared against the measured data with the actual flying routes based on two modes of flying patterns: cross and cross-range pattern. Furthermore, the model clearly shows the effect of airplane fluttering on low frequency signal.

In section II, we review the theory of RCS and how

ellipsoid aids the aircraft modeling. The proposed model of fluttering based on physical and geometrical approach is then described in Section III. In Section IV, we present the simulation results and compare those with measured signal variation level are presented. The discussions is in Section V. Finally, a conclusion is in Section VI.

II. Background Theory

In this section, the radar cross section (RCS) back scattered of a simple object and wave propagation on the plane earth are reviewed in relation with the flutter phenomena.

A. Radar Cross Section (RCS)

The electromagnetic waves with any specified polarization diffract scattered signals in all directions when incident on a target. These scattered waves are broken down into two parts; the first part is made of waves that has the same polarization as the receiving antenna, the other has a different polarization to which the receiving antenna does not respond. These two polarizations are orthogonal. The target RCS is defined as effective cross section of the target causing the intensity of the back scattered energy with the same polarization as the radar's receiving antenna. It is expressed with the unit of m^2.

An approximate method is often used to predict RCS of complexed and extended targets such as aircraft, ships, and missile [10]. When experimental results are available, they can be used to validate and verify the approximations.

We consider using RCS of ellipsoid with dimensions (width and length) relative to the body of an airplane. In fact, other shapes of objects such as spheres and cylinders have been used to model the airplane flutter, but the case in this paper produces results closer to measured data

RCS Back Scattered of Ellipsoid: The RCS back scattered determines the proportion of intensity of waves reflected from the target. Consider an ellipsoid centered at the coordinate (0,0,0) as shown in Fig.1. It is used to model the body part of an airplane defined by

$$\left(\frac{x}{a}\right)^2+\left(\frac{y}{b}\right)^2+\left(\frac{z}{c}\right)^2=1, \qquad (1)$$

where a and b are the widths and c is the length of an ellipsoid.

The direction to the receiving signal has aspect angle θ from the z-axis, and φ is the angle between the y-axis and the incoming wave incident on the ellipsoid. One widely accepted approximation RCS back scattered of ellipsoid (σ) is given by [11]

$$\sigma=\frac{\pi a^2b^2c^2}{\left(a^2\sin^2\theta\cos^2\varphi+b^2\sin^2\theta\sin^2\varphi+c^2\cos^2\theta\right)^2}. \qquad (2)$$

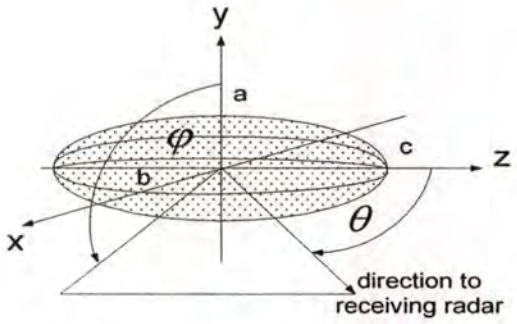

Fig.1. Geometry of ellipsoid RCS back scattered

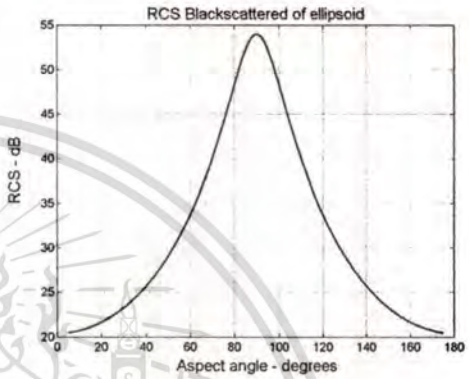

Fig.2. The RCS back scattered of ellipsoid size are a=10 m, b=10 m, and c=70 m.

When $a = b$, the ellipsoid becomes roll symmetric, thus, the RCS back scattered is independent of φ, and (2) is reduced to

$$\sigma=\frac{\pi a^4c^2}{\left(a^2\sin^2\theta+c^2\cos^2\theta\right)^2}. \qquad (3)$$

In Fig.2, the plot of the ellipsoid RCS back scattered in dB versus θ with φ = 45°, a = 10m, b = 10m, and c = 70m is shown. This dimension in fact approximates the body of a Boeing 747-200. The aspect angle θ ranges from 0 to 180 degrees. Observe that the peak of ellipsoid RCS back scattered occurs at about 54 dB for the aspect angle θ at 90°, *i.e.*, when the waves are transmitted directly to the target.

B. Radio Wave Propagation

Free space propagation: Consider an isotropic radiator in free space. By definition, an isotropic radiator produces identical radiation intensity in all directions. In free space, the resultant spherical wave spreads out with uniform intensity in all directions. If P_o is the power radiated from the isotropic source, the electric field strength (E_o) at a radial distance r is given by [11]

$$E_o=\frac{\sqrt{30P_o}}{r}\varepsilon^{-j\beta r} \quad \text{V/m}, \qquad (4)$$

Fig.3. Radiator with directional gain pattern.

where $\beta = 2\pi/\lambda$ is the free-space wave number or phase constant (β is the space rate of decrease of the phase of the field in the direction of propagation), the subscript on E_o denotes the free space field. Note that the electric field strength E_o scales with $1/r$.

Consider a source with a directional gain pattern $D(\theta,\phi)$ and surface area far field power density is related by $S(\theta, \phi)$ as shown in Fig.3. In this case, the radiated power is concentrated in some direction as it spreads out over the surface of a surrounding imaginary sphere. The far-field electric field strength is given by

$$E_o(\theta,\phi) = \frac{\sqrt{30 P_o D(\theta,\phi)}}{r} \varepsilon^{-j\beta r} \quad \text{V/m.} \qquad (5)$$

Ground-wave propagation over plane earth: The geometry for ground wave propagation over plane earth is used for analysis of airplane flutter phenomena as both direct and indirect wave of multipath interfering signal. For the method used to calculate the ground wave electric field strength $E(r)$ depends on the geometry and wavelength given by

$$E(r) = E_o(R_1) + \rho E_o(R_2), \qquad (6)$$

where

$E(r)$ = total electric field strength at receiving antenna at a radial distance r,

E_o = electric field strength of the direct wave at a radial distance r,

R_1 = distance traveled by direct wave between source and point,

R_2 = distance traveled by ground reflected wave between source and points,

ρ = magnitude of reflection coefficient.

III. Proposed Method

In this section, we explain a proposed method to compute the electric field strength of the ground wave based on two techniques: 3-dimensional geometry and ellipsoid RCS back scattered. The RCS of ellipsoid with appropriate dimensions (width and length) relative to the body of an airplane can be used in the model of flutter phenomena. In this paper, we focus on the body part of airplane only because it is the biggest part and scatters most of the signals. The signal is, in fact, scattered from the body at all time, independent of the direction and pattern of the flying routes. For other parts such as wing and tail, however, the amount of reflected waves is typically quite small and dependent on the flying angles. They do not always affect the TV signal due to the flatness and relatively small size [1].

A. Basic Parameters

The basic parameters, which affect the signal variation patterns, can be classified into 3 categories as follow.

1. Amplitude of variation depends on the parameters including percentage of reflection by airplane (Γ_{airp}), RCS back scattered (σ), size of airplane, and distance from airplane to receiving antenna (R_{ra}).
2. Frequency of variation pattern depends on the wavelength (λ) of the TV signal.
3. Duration time of variation pattern depends on the parameters including speed, altitude, directivity of antenna, and direction of airplane.

A simple multipath scattering model is used to describe the airplane flutter phenomena. It is formulated with the objectives of increasing the understanding of some of the measured signal behavior and also predicting its patterns. This requires a fundamental description of the causes of the signal variation and is the reason why this model is based on both physical and geometrical considerations. The method used to calculate the field strength at the receiving antenna is modified from Ray theory by A. A. Smith Jr. [11], which depends on the geometry and signal wavelength. In the case of reflection by airplane, some parameters such as radar cross section (RCS), airplane altitude, speed and direction of airplane are considered.

B. Cross pattern

Consider the geometry of wave propagation reflected from airplane flying with *cross pattern* as shown in Fig. 4 (a), (b), and (c). The signal multipath is composed of the direct wave (e_1), reflected wave by ground (e_2), and reflected wave from airplane (e_3), respectively. Figure 4(a) is a front view showing the transmitted and received angle θ and the signal at receiving antenna that is composed of e_1, e_2 and e_3, respectively. Fig 4(b) is a top view showing the angle ϕ at receiving and transmitting sites, and Fig 4(c) shows a 3-dimensional geometry.

For the cross pattern, vertical angle θ on the receiving side during interference is constant at 45 degrees, while the horizontal angle ϕ varies from around 45 to 135 degrees as shown in Fig.4 (a), (b), and (c).

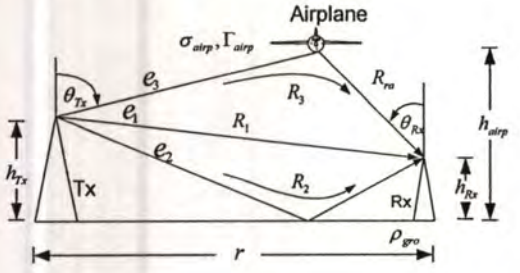

(a)

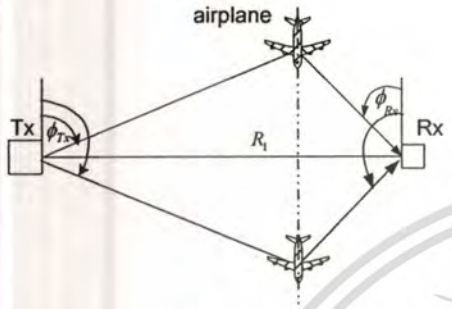

(b)

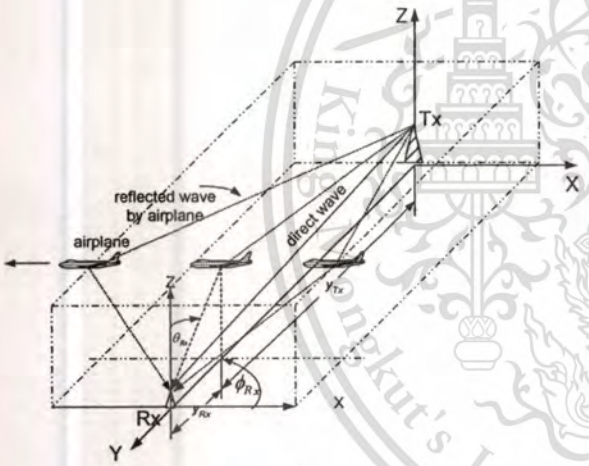

(c)

Fig.4. The geometry of the wave propagation in the airplane flutter, composed of the direct wave (e_1), reflected wave by ground (e_2), and reflected wave by airplane (e_3). (a) front view, (b) top view, and (c) 3-dimensional view

In Fig.4,

R_1 is distance traveled by direct wave between source and field point by [13]

$$= \left[r^2 + (h_{Tx} - h_{Rx})^2\right]^{\frac{1}{2}} \quad ,$$

R_2 is distance traveled by ground reflected wave between source and field points and can be computed by

$$= \left[r^2 + (h_{Tx} + h_{Rx})^2\right]^{\frac{1}{2}} \quad ,$$

R_3 is distance traveled by airplane reflected wave between source and field points can be computed by

$$= \left(\frac{y_{Rx}}{\sin\theta_{Rx}\sin\phi_{Rx}} + \frac{y_{Tx}}{\sin\theta_{Tx}\sin\phi_{Tx}}\right) \quad ,$$

y_{Tx}, y_{Rx} = distance from transmitting and receiving antennas to airplane in y plane, respectively ,

r = distance between source and field point measured on the plane,

h_{Tx} = height of transmitting antenna above earth plane ,

h_{Rx} = height of receiving antenna above earth plane,

θ_{Tx}, θ_{Rx} = angle between antenna and reflected wave by airplane in vertical plane at transmitting and receiving side (degrees), respectively,

ϕ_{Tx}, ϕ_{Rx} = angle between antenna to reflected wave by airplane in horizontal plane at transmitting and receiving side (degrees), respectively, and

R_{ra} = distance between receiving antenna to airplane given by $\left(\frac{y_{Rx}}{\sin\theta_{Rx}\sin\phi_{Rx}}\right)$

The total electric field strength at the receiving antenna $E(r)$ can be computed from the sum of the direct wave (e_1), ground reflected wave (e_2), and airplane reflected wave (e_3), each of which can be computed based on (5), *i.e.*,

$$E(r) = e_1 + e_2 + e_3$$
$$= \sqrt{(30P_o D(\theta,\phi))}\left[\frac{\varepsilon^{-j\beta R_1}}{R_1} + |\rho_{gro}|\frac{\varepsilon^{-j\beta R_2}\varepsilon^{-j\varphi_1}}{R_2} + |\sigma_{airp}||\Gamma_{airp}|\frac{\varepsilon^{-j\beta R_3}\varepsilon^{-j\varphi_2}}{R_3}\right] \quad , \qquad (7)$$

where

P_o = power output of transmitter,

$D(\theta,\phi)$ = directivity of antenna,

ε = permitivity of the earth (F/m),

ε_0 = permitivity of free space, $8.854*10^{-12}$ F/m,

k = $\varepsilon/\varepsilon_0$ = the relative permitivity of the earth (k=15 for good earth),

β = $2\pi/\lambda$,

ρ_{gro} = reflection coefficient by ground respectively ($\rho_{gro} \cong$ 0.8% for VHF [11]),

φ_1, φ_2 = reflection coefficient phase by ground and airplane, respectively,

σ_{airp} = RCS back scattered of an airplane, and

Γ_{airp} = percentage of reflection by airplane (%).

Equation (7) can be used to calculate the signal variation caused by airplane at the receiving antenna. The RCS back scattered σ_{airp} is based on an ellipsoid of dimension relative to the body of an airplane. The phase difference (φ) is determined from the different paths of direct and reflected wave and based on 3-dimensional geometry due to the;

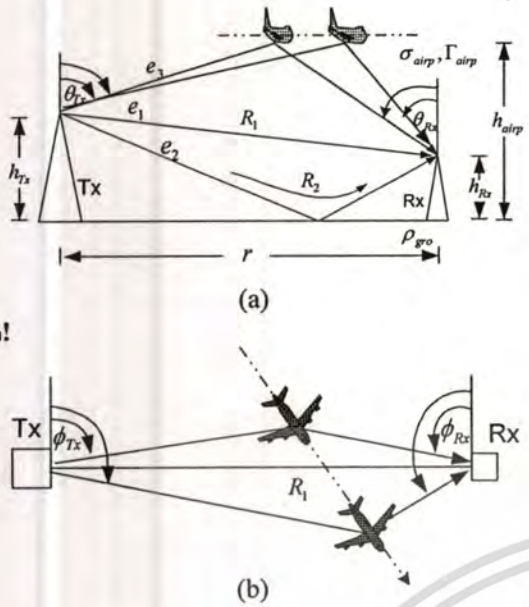

Fig.5. The flying geometry of cross-range pattern. The direction of the flying airplane did not fly perpendicular with the line-of-sight signal (a) front view and (b) top view

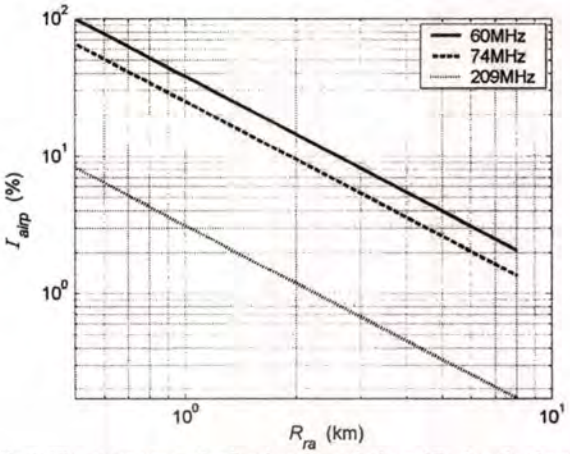

Fig.6. The percentage of reflection from airplane (Γ_{airp}) at the frequency of 60 MHz, 100 MHz, and 209 MHz

airplane movement at all time. Percentage of airplane reflection (Γ_{airp}) is dependent on the size of airplane, R_{ra}, and frequency of signal. The directivity (D) depends on the type of antenna, for high-gain transmitting and receiving antennas, the directivity needs to be accounted for in (7).

C. Cross-range pattern

In Fig. 5 (a) and (b), the geometry of cross-range pattern of an airplane is shown. The airplane makes an angle that is not perpendicular to the line-of-sight signal. In this case, both angle of θ_{Rx} and ϕ_{Rx} vary, while for the case of cross pattern, θ_{Rx} is constant. From the view of receive antenna, the angle θ_{Rx} decreases as the plane approaches the antenna, while, the angle ϕ_{Rx} increases.

D. Percentage of Reflection Wave Caused by Airplane (Γ_{airp})

The power density of wave at the receiving antenna due to scattered by airplane (P_{Dr}) by [10] is

$$P_{Dr} = \frac{G_r \lambda^2 P_t G_t \sigma_B}{(4\pi)^3 R_t^{\,2} R_{ra}^{\,2}}, \qquad (8)$$

where P_t is transmitted power, R_{ra} is distance between receiving antenna to airplane, G_t and G_r are transmitting and receiving antenna gain, respectively, σ_B is the radar cross section, in this case, with $\sigma_B = \sigma_{airp}$, and R_t is the range from the transmitting antenna to a target.

The percentage of reflection of wave by airplane is defined as

$$\Gamma_{airp} = \frac{P_{Dr}}{P_{Dr(\max)}} \times 100 \quad (\%), \qquad (9)$$

where $P_{Dr(max)}$ is maximum power intensity of reflected wave from the airplane measured at the receiving antenna. The relationship between Γ_{airp} and R_{ra} is illustrated in Fig. 6 at the frequency of 60 MHz, 74 MHz, and 209 MHz, respectively. From the figure, it can be observed that at the distance of R_{ra} equal to 1400 m (equivalent to the altitude of 1000 m in cross pattern experiment), the percentages of reflection at 60 MHz and 209 MHz are 25 % and 2 %, respectively. The higher frequency, the lower proportion of reflection Γ_{airp} is found. The value of Γ_{airp} is an essential parameter used in the airplane flutter model in (7).

IV. Measurement and Simulation Results

In this section, the measurement and simulation results of airplane flutter phenomena on TV signals are presented. The signal variation caused by airplane was measured at King Mongkut's Institute of Technology Ladkrabang (KMITL) campus, Bangkok, Thailand. The airplane took off from Donmuang International Airport and flew past the line-of-sight signal between Tx and Rx points at KMITL. The obtained data were then compared with the simulation results using the parameters relevant to the measurement.

A. Measurement Setup:

The measurement parameters are listed in Table 1. The TV signals from local stations of channel 3 (Ch3) at 60.75 MHz and channel 9 (Ch9) at 208.75 MHz are selected in the test. For Ch3, the output power is 60 kW with 230-m height antenna and for Ch9, the output power is 20 kW with 250-m height antenna height. Both channels are transmitted from the same antenna tower at Nongkam station, located on the western rim of the city. On the receiving side, Anritsu WI-208 field strength meter is used with standard 3-meter and 3.5-meter dipole antennas above ground for Ch3 and Ch9, respectively. The received signal is collected using Keyence data acquisition system, and Yokogawa Hokushin Electric;

TABLE 1. MEASUREMENT PARAMETERS

Transmitting side	
Ch3 frequency	60.75 MHz
Ch9 frequency	208.75 MHz
Ch3 transmitting antenna height	230 m
Ch9 transmitting antenna height	250 m
Output power of Ch3	60 kW
Output power of Ch9	20 kW
Antenna gain	13 dB
Polarization	Horizontal
Receiving side	
Distance from Tx (Nongkam) to Rx(KMITL)	45 km
Field strength meter	Anritsu(WI-208)
Data acquisition	Keyence(NR-2000)
Paper recorder	Yokogawa- Hokushin Electric
Standard dipole height,(60.75 MHz and 208.75 MHz, with gain of 2.15 dB)	3 m, 3.5 m
Polarization	Horizontal
Airplane parameters	
Airplane	Boeing747
Altitude	1000-2000m
Speed	400-500km/h
Direction	cross, cross-range

paper recorder. The data acquisition rate is 100 samples per second. The equipment is setup in the middle of the football field on KMITL campus, located on the eastern rim of the city the football field location is chosen to prevent signal reflection from the buildings in the vicinity.

The TV signals of Ch3 and Ch9 were recorded as the airplane flied over the observation point. The receiving antenna Rx at KMITL is approximately 45 km from transmitting antenna Tx at Nongkam station. Note that strong line-of-sight signals exist.

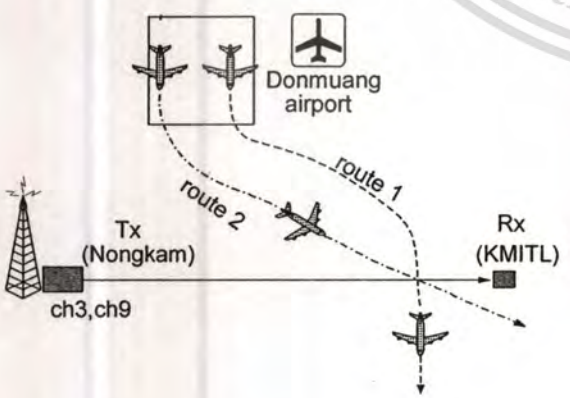

Fig.7. The airplane route of cross and cross-range patterns at KMITL measured point.

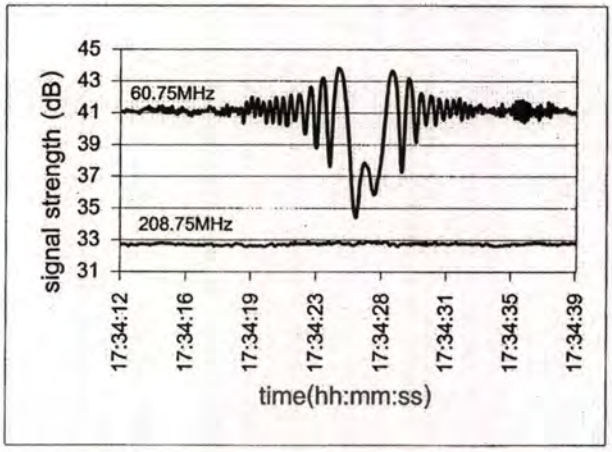

Fig.8. Measured signal strengths of Ch3 (60.75 MHz) and Ch9 (208.75 MHz) for cross airplane route.

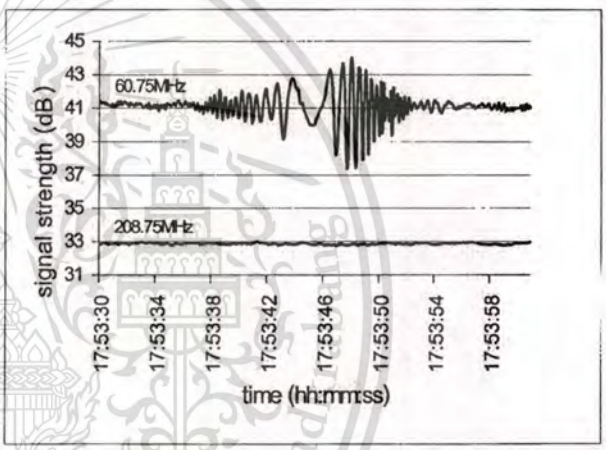

Fig.9. Measured signal strengths of Ch3 (60.75 MHz) and Ch9 (208.75 MHz) for cross-range airplane route.

In Fig. 7, two possible airplane routes over KMITL measured points are shown. The Boeing 747 typically flies with cross (Route 1) and cross-range (Route2) patterns between the Tx and Rx antennas. There are many flights per day. The flight information such as airplane altitude, speeds, of model are obtained from Aeronautical Radio of Thailand, Ltd.

B. Measurement Results:

The TV signal strengths of the cross, and cross-range patterns are shown in Fig. 8, and Fig.9, respectively. The signal variations of both patterns shown here are typical among all the collected data.

Cross pattern: In Fig. 8, the measured signal of the cross-pattern flight on Oct 28, 2003 from 17:34:12 to 17:34:39 hr is shown. The airplane took off from Donmuang International Airport and flied across the line-of-sight signal between Tx and Rx antennas (direction is perpendicular with the line-of-sight signal). The speed and altitude of the aircraft are

approximately 450 km/h and 1,000 m, respectively. Typical signal levels of Ch3 and Ch9 are about 41 dB and 33 dB, respectively. With fluttering phenomena, however, the maximum signal variation of Ch3 was 9.9 dB over a 14-second interval, while the signal of Ch9 is relatively unaffected. Observe that symmetry of the signal patterns exists in this case.

Cross-range pattern: In Fig. 9, the measured data from the cross-range pattern on Oct 28, 2003 from 17:53:30 to 17:53:58 hr is shown. The airplane took off from Donmuang airport and flied cross-range over the line-of-sight signal. The speed of airplane was 450 km/h with an altitude of 1800 m. Maximum signal variation of Ch3 was 7.2 dB over a 15-second interval. Similar to the cross pattern case, the signal at 208.75 MHz was, not noticeable.

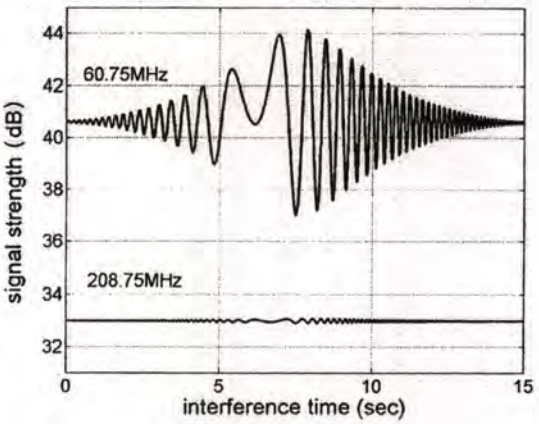

Fig.11. Cross-range pattern simulation results of Ch3 (60.75 MHz) and Ch9 (208.75 MHz).

C. Simulation Results:

The signal levels of cross and cross-range flying patterns at KMITL depending on the geometry of the airplane and related flight parameters can be simulated.

Cross pattern simulation: The simulation of TV signals due to cross pattern route is done using the RCS of ellipsoid with dimension of 10x10x70 m. The altitude is 1,000 m (R_{ra} = 1400 m) with the aircraft speed of 450 km/h. The percentage of reflection for Ch3 and Ch9 are computed using (2), (8) and (9) to yield 25 % and 2 %, respectively. The vertical angle θ on the receiving side during interference is constant at 45 degrees, while the horizontal angle ϕ varies from 45 to 135 degrees. From Fig. 10, the simulated signal variation of Ch3 is around 9 dB over a 14-second time interval, while the Ch9 signal shows some signal variation but with very small proportion to the Ch3 case. The simulated patterns closely resemble the measured patterns in Fig. 8.

Cross-range pattern simulation: The simulation of TV signals due to a cross-range pattern route is done using the same size of RCS back scattered. The altitude is 1,800 m (R_{ra} = 2100 m) with the aircraft speed of 450 km/h.

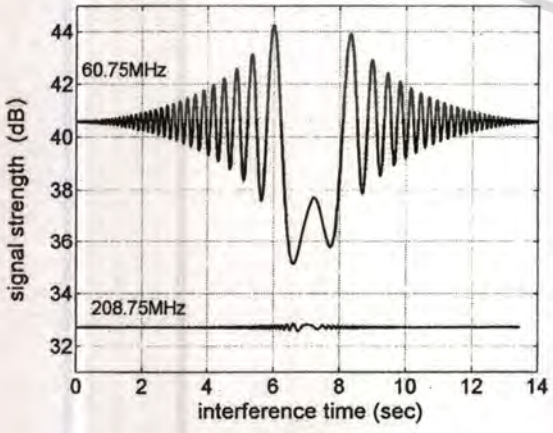

Fig.10. Cross-pattern simulation results of Ch3 (60.75 MHz) and Ch9 (208.75 MHz).

The percentage of reflection for Ch3 and Ch9 are similarly computed to yield 15% and 1.1%, respectively. The ellipsoid makes the vertical angle θ at the receiving side during interference from 28 down to 24 degrees, while the horizontal angle ϕ on receiving side varies from 55 to 120 degrees. From Fig. 11, the simulated signal variation of Ch3 is 7 dB over a 15-second time interval. The Ch9 signal shows small change of amplitude.

Figure 12, we study the effects of speed and altitude on the characteristics of simulated flutter signal on cross pattern route. For all four cases, The vertical angles are roughly fixed, while the horizontal angle varies, specifically, $Rx(\theta,\phi)_{in}$ = [45°, 48°] and $Rx(\theta,\phi)_{out}$ = [44.9999 °, 133 °]. The frequency of Ch3 and the distance d_0 = 45 km is used.

From Fig. 12(a), with the speed of 450 km/h and altitude of 1,000 m, the duration time of signal variation is around 14 seconds and the maximum variation is around 9.1 dB. As the speed is reduced to 350 km/h with same altitude, the duration time is increased to 18 seconds as seen in Fig. 12 (b). When altitude is increased to 2,000 m with the speed of 450 km/h, the maximum signal variation reduces to 3.5 dB but the duration time increases to 29 seconds as shown in Fig. 12(c). As the altitude is increased to 3,000 m with the speed of 450 km/h, the maximum signal variation reduces to 2.028 dB but the duration time increases to 43.9 seconds as shown in Fig. 12(d).

The relationship of between the simulated maximum signal variation and the distance R_{ra} can be seen in Fig. 13. The maximum signal variation is dependent on the TV frequency. In this figure, four frequencies 61, 74, 181, and 209 MHz are plotted. The measured maximum signal levels at 61MHz (denote by •) and 209MHz (denoted by ×) at the R_{ra} of 1,400 m (at altitude of 1,000 m) are plotted and compared with the simulation results. For Ch3 (61 MHz) and Ch9 (209 MHz), the signal variation levels are around 9.9 dB and 0.3 dB, respectively. With R_{ra} of about 2100 m (at altitude of 1,800 m), the signal variation levels are around 7 dB and 0.2 dB, and

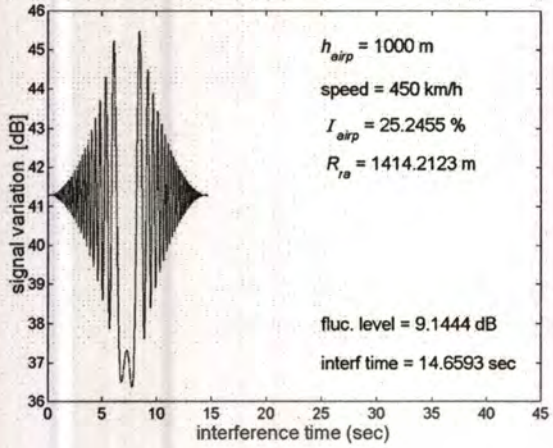

(a)

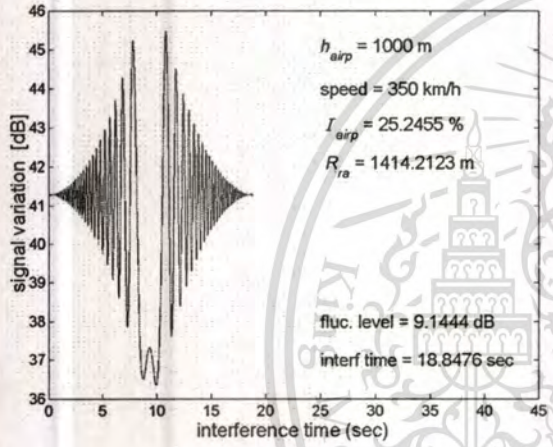

(b)

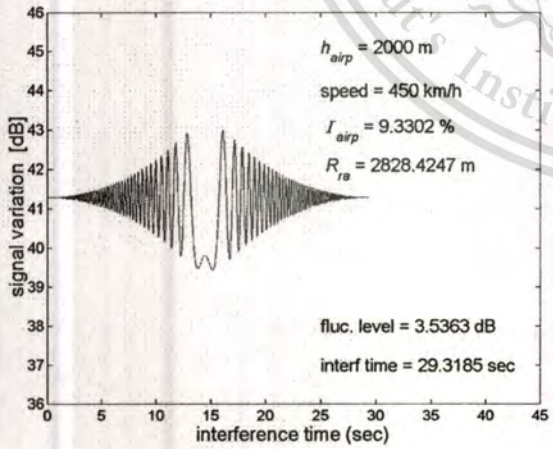

(c)

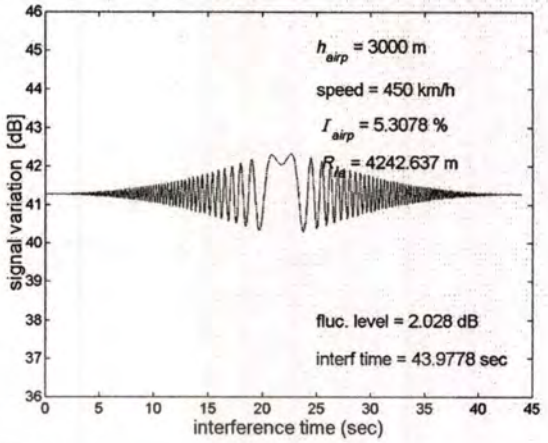

(d)

Fig.12. Simulation results of cross flutter pattern of Ch3 when parameters are changed. (a) The speeds of 450km/h with altitude of 1000 m, (b) The speeds of 350km/h with altitude of 1000 m, (c) The speeds of 450km/h with altitude of 2000 m, and (d) The speeds of 450km/h with altitude of 3000 m

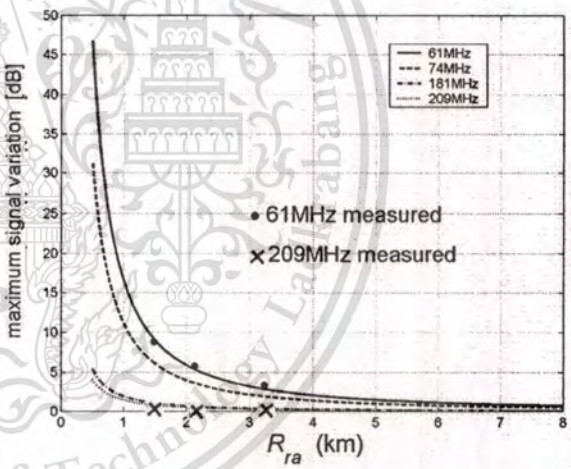

Fig.13. The maximum signal variation for the frequencies of ch3 (61 MHz), ch5 (74 MHz), ch7 (181 MHz) and ch9 (209 MHz).

at R_{ra} of about 3,200 m the signal variation levels are around 3 dB and 0.1 dB, respectively. The measured values are close to the simulated ones.

A 3-dimensional simulation plot of relationship between maximum signal variation, frequency and R_{ra} is also shown in Fig. 14. The frequency varies from 50 to 300 MHz, and R_{ra} ranges from 500 to 8,000 m. The figure shows that as R_{ra} and frequency increase, the maximum signal variation decreases. The KMITL measured points of R_{ra} equal to 1,400 m, 2,100 m, and 3,200 m of 61 MHz and 209 MHz respectively are also plotted. It is evident that the measured results are close to the simulation results.

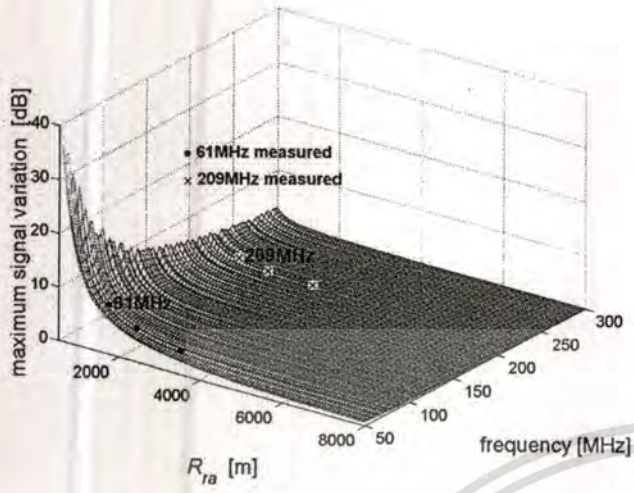

Fig.14. A 3-dimensional plot of relationship between maximum signal variation, frequency and R_{ra}.

V. Discussions

The observation and measurement of airplane flutter was performed at KMITL as the distance between transmitting and receiving side is 45 km. The signal was measured when the Boeing 747 flew with cross, and cross-range patterns between line-of-sight with altitudes of around 1,000-3,000 m and speeds of around 400-500 km/h. Symmetry of the variation patterns occurred when an airplane flew across between line-of-sight signal. Asymmetry of the variation pattern occurs as an airplane flew cross-range between the line-of-sight signal. The measurement pattern results, mostly 80% from about 100 measured data are cross and cross-range patterns are used in the analysis in this paper.

From the experimental results, it is evident that the lower frequency of ch3 is affected, while the higher frequency of ch9 is nearly unnoticeable. Moreover, the observation of picture on TV receiver show that only the picture and sound of ch3 is distorted. This can be explained from (8) that the power density of wave at the receiving antenna due to scattering by airplane (P_{Dr}) is small when λ is short (λ of Ch3 = 5 m while λ of Ch9 = 1.4 m).

The effects of speed and altitude on the duration time of signal variation and the maximum variation can be explained using our proposed model. The speed and altitude of the airplane directly affects the duration time of signal variation. The longer duration is caused by slower speed. At higher altitude, the maximum signal variation is reduced, while the duration time increases. The reduction of fluctuation is due to the fact that higher R_{ra} decreases the percentage of reflection.

VI. Conclusions

Flying object such as airplane could scatter wave from TV transmission signal. The scattered wave caused by airplane disturbs direct wave from transmission and the result appears in the reception of TV signals. The flutter phenomena also occur at a point considerably far from the airport. When the airplane flew across the line-of-sight path between the television signal and the receiving antennas, received signal strength cause a flutter or quasi-periodic fluctuation.

In this paper, we propose a novel approach to simulate the flutter phenomena based on physical and geometrical parameters. The Ray-theory is used due to suitability of analysis of physical and geometrical aspects of direct and reflected wave. Bistatic RCS of ellipsoid is used due to the geometry shape closed to airplane body, facilitate and accurate for analysis. In fact, other shapes of objects such as spheres and cylinders have been used to model the airplane flutter, but the case in this paper produces results closer to measured data.

The model for signal variation takes into account of real physical and related parameters such as type of airplane, speeds, altitude, and direction. In addition, transmission and receiving information such as transmitter power, and antenna height, and gain are input to the model. Thus, the simulation can be performed for various scenarios.

In future works, we intend to obtain measurement results for the aircraft of different sizes, digital TV signal, longer distance and higher frequency. Coincidentally, the KMITL campus is very close to the new Suvarnabhumi International Airport of Thailand scheduled to be open in 2007, thus it is ideal for the experimental study of flutter phenomena. In addition, efforts will be directed toward combining a number of scattered and more complex objects. Thus, the model should be capable of predicting the position, direction, and speed of airplane.

Acknowledgements

The authors would like to thank the Department of Air Traffic Control; Aeronautical Radio of Thailand Ltd., for the flight information. We also would like to thank Prof. Dr. Monai Krairiksh of the Department of Telecommunication Engineering, KMITL, for his comments on the paper and especially, Prof. Dr. Yoshiaki Moriya for his incessant kindness to advise and support this work.

References

[1] Ito and Ohta, "Estimation of Fluttering of Field Intensity Caused by Aircraft and its Disturbance to Television Reception," *ITE Journal*, vol.40, no.9, pp.899-905, 1986.

[2] Nishihara, Endo, Hidaka and Takahashi, "Investigation and Countermeasures for TV Reception Interference by Aircraft," IEICE Technical Report EMCJ97-8.

[3] H. Miyazawa, "Evaluation and Measurement of Airplane Flutter Interference," *IEEE Trans. Broadcast.*, vol.35, no.4, pp. 362-367, Dec. 1989.
[4] A. Wongkeeratikul, P. Sangonchat, S. Noppanakeepong, N. Leelarruji, and Y. Moriya, "The Observation and Simulation of the Airplane Flutter on Low Band TV signal," in *Int. Conf. SCOReD 2003*, Putrajaya, Malaysia, 2003, pp.23.
[5] A. Wongkeeratikul, S. Noppanakeepong, N. Leelarruji, and Y. Moriya, "The Analysis of the Airplane Flutter on Low Band TV signal," in *Int. Conf. ICCAS 2003*, Gyeongju, Korea, 2003, pp.88.
[6] K. Takagi, N. Leeraluji, N. Hemmakorn, H. Sakurada and Y. Moriya, "Simulation and Application of Quasi Periodic Fluctuation Caused by Aircraft Scattering Phenomenon," in *Proc. Asia-Pacific Symp. on Broadcast. and Commun. (APSBC'2000).*, KMITL, Thailand, 2000, pp.186-191.
[7] J. I. Glaser, "Bistatic RCS of Complex Objects Near Forward Scatter," *IEEE Trans. Aerosp. and electron. Syts.*, vol.AES-21, no.1, Jan. 1985.
[8] A. David, C. Brousseau and A. Bourdillon, "Simulation and Measurement of a Radar Cross Section of a Boeing 747-200 in the 20-60MHz Frequency Band," *Radio Science*, vol.38, No.4, pp.1064, 2003.
[9] M. L. Bucher, "Simulation of Multipath Fading/Ghosting for Analog and Digital Television Transmission in Broadcast Channels," *IEEE Trans. Broadcast.*, vol.38, no.4, pp.256-262, Dec. 1992.
[10] Bassem R. Mahafza, "Radar Systems Analysis and Design Using MATLAB," Chapman & Hall/CRC, 2000.
[11] Albert A. Smith, "Radio Frequency Principle and Applications," Chapman&Hall publishers, 1998, pp. 46-50.

Nipa Leelaruji was born in Bangkok, Thailand in June 1948. She received B.Eng. and M. Eng. from King Mongkut's Institute of Technology Ladkrabang (KMITL), Bangkok, Thailand in 1975 and 1999, respectively. In 1969, she joined the KMITL and she is presently an Associate Professor in the Department of Telecommunication Engineering. Her main research interests are in broadcasting, scintillation and rain attenuation of satellite signals. Assoc. Prof. Leelaruji presently serves as the chief of satellite laboratory at KMITL.

Narong Hemmakorn was born in Bangkok, Thailand in March 1942. He received the B.Eng. and M.S in Eng. degree from Tokai University, Tokyo, Japan in 1968 and 1973, respectively. In 1968 he joined the KMITL. Currently, he is an Associate Professor in the Department of Telecommunication Engineering, Faculty of Engineering, King Mongkut's Institute of Technology Ladkrabang. His main research interests include radio-wave propagation, scintillation and rain attenuation of satellite signals.

Anuchit Wongkeeratikul (Student Member, IEEE) was born in Nakornratchasima, Thailand in July 1968. He received B.Eng. from Vongchavalitkul University, Nakornratchasima, Thailand, in 1992 and M.Eng. from Khonkaen University, Khonkaen, Thailand, in 1996. He is currently pursuing the D.Eng. degree at King Mongkut's Institute of Technology Ladkrabang (KMITL), Bangkok, Thailand. His main research interests are in television broadcasting and satellite communication.

Pornchai Supnithi (Member, IEEE) was born in Bangkok, Thailand. He received a Ph.D. from Georgia Institute of Technology, Atlanta, USA, in 2002. In 2003, he joined the Department of Telecommunications Engineering, KMITL. He is at present an Assistant Professor. At present, he is also a Deputy Director of I/U CRC in Data Storage Technology and Applications aimed at strengthening Thailand Hard Disk Drive industry. His main interests are in communication theory, coding/signal processing for communications and data storage, and hard disk drive technology.

Suttichai Noppanakeepong was born in Bangkok, Thailand. He received B. Eng. and M. Eng. from King Mongkut's Institute of Technology Ladkrabang (KMITL), Bangkok, Thailand and Ph.D. degree from Tokyo Institute of Technology, Tokyo, Japan. He joined the KMITL and is presently an Assistant Professor in the Department of Telecommunication Engineering. His main research interests include fiber-optic communication, radio-wave propagation and satellite communication.

Appendix B

```
%Thes_propose_new_1.m
%Input parameters of model

fprintf('\n');
fprintf('\n');
fprintf('**************************************************************************
**************************************\n');
fprintf('\n');
fprintf('          The program simulates Airplane flutter phenomena.\n');
fprintf('\n');
fprintf('**************************************************************************
**************************************\n');
%fprintf('\n');
fprintf(' Please, input other parameters or used default\n');

%freq  = input(' 1. Frequency (ch3=60MHz,ch9=208MHz) = ');
%thetaRXin=input(' 2. Theta angle at start point[45(cross) or 65(cross-range) in degrees] = ');
%thetaRXout=input(' 3. Theta angle at stop point[ 45(cross) or 45(cross-range) in degrees] = ');
%phiRXin=input(' 4. Phi angle at start point[45(cross),55(cross-range)]in degrees = ');
%phiRXout=input(' 5. Phi angle at stop point[135(cross),120(cross-range)]in degrees = ');
%Po=input(' 6. Power output of TV transmitter (ch3=60kW,ch9=20kW) = ');
%h_airp=input(' 7. Height of airplane (1000m) = ');
%v_airp=input(' 8. Velocity of airplane (450km/h) = ');
%d0=input(' 9. Distance between TX and RX (45km) = ');
%h_tx=input(' 10. TX antenna height (ch3=230,ch9=250m) = ');
%h_rx=input(' 11. RX antenna height (4m) = ');
%h_airp_max=input(' 12. Maximum of airplane height[rho=0]: 5000m =');
%fprintf('\n');

%next=input(' THANK YOU and press enter \n');

freq=60.75
Po=60
thetaRXin=45
thetaRXout=45
phiRXin=45
phiRXout=134
h_airp=1000
v_airp=450
d0=45
h_tx=230;
h_rx=2;
h_airp_max=8000

%*****************************************************************
freq_phase_adj=7.011
ampli_adj=2.6
level_adj=18.7
sec_adj=400
aa=2;bb=2;cc=70
freq = freq*1e6;          %CH3 frequency
lambda = 3.0e8 /freq;
```

```
%*****************************************************************
% function [rcs_db] = rcs_ellipsoid (a, b, c, phi)
% This program computes the back-scattered RCS for an ellipsoid.
% The angle phi is fixed, while the angle theta is varied from 0-180 deg.
% A plot of RCSversus theta is generated
%*****************************************************************
eps = 0.00001;
% Enter the ellipsiod size
%aa = 2;% 20 m
%bb = 2;% 20 m

%cc = 70;% 70 m  %++++++++++++++++++++++++++++++++++++++++++++
% Enter angle phi
phi = pi / 4.;
sin_phi_s = sin(phi)^2;
cos_phi_s = cos(phi)^2;
% Generate aspect angle vector
theta_e = 5.:.1:175;
theta_ee = (theta_e .* pi) ./ 180.;
if(aa ~= bb & aa ~= cc)
  rcs = (pi * aa^2 * bb^2 * cc^2) ./ (aa^2 * cos_phi_s .* (sin(theta_ee).^2) + ...
  bb^2 * sin_phi_s .* (sin(theta_ee).^2) + ...
  cc^2 .* (cos(theta_ee).^2)).^2 ;
else
  if(aa == bb & aa ~= cc)
    rcs = (pi * bb^4 * cc^2) ./ ( bb^2 .* (sin(theta_ee).^2) + ...
      cc^2 .* (cos(theta_ee).^2)).^2 ;
  else
    if (aa == bb & aa ==cc)
      rcs = pi * cc^2;
    end
  end
end
rcs_db =ampli_adj*(20+10.0 * log10(rcs)); %ellipsoid RCS
%rcs_db =(20+10.0 * log10(rcs)); %ellipsoid RCS


%*****************************************************************
%
%To calculate the distance between reflected wave and
%direct wave by rectangular&sepherical cordinate.
%
%*****************************************************************
%Receiver(Rx) side
%Define theta angle at Rx side
%thetaRXin=45.001;thetaRXout=45; %Cross
%thetaRXin=65,    thetaRXout=45; %Cross-Range
%thetaRXin=65.000
%thetaRXout=45.000
if  thetaRXin == thetaRXout
  thetaRXout=thetaRXout-.0001;
```

```
end
cc2=thetaRXin-thetaRXout;
dd2=abs(cc2/1700);
theta_rx_deg=thetaRXin:-dd2:thetaRXout;        %theta_rx_deg
theta_rx_rad=(theta_rx_deg.*pi)/180;

%To calculated the distance between Rx to airplane in y-axis and theta_rx_deg
%h_airp=1000 %Define airplane height; 1000, 546.5m.....
RX1=h_airp/tan((90-thetaRXin)*pi/180)
RX2=h_airp/tan((90-thetaRXout)*pi/180)
cc1=RX2-RX1;
dd1=cc1/1700;
x_rx= RX1:dd1:RX2;    %find x_rx for same matrix dimension

%Define phi angle value at Rx side
%phiRXin=45;phiRXout=135; %Cross
%phiRXin=55,phiRXout=120; %Cross-Range
%phiRXin=55
%phiRXout=120
cc3=phiRXin-phiRXout;
dd3=abs(cc3/1700);
phi_rx_deg=phiRXin:dd3:phiRXout;
phi_rx_rad=(phi_rx_deg.*pi)/180;

%To calculated distance from rx to airplane (r_rx) in sphererical cordinate
r_rx=x_rx./(sin(theta_rx_rad).*sin(phi_rx_rad)); %**************

%Transmitter(Tx) side
%To calculate distance between Tx to airplane in y-axis and theta_tx
d0=d0*1e3
total_dis=d0;
TX1=total_dis-RX1
TX2=total_dis-RX2
cc4=TX1-TX2;
dd4=abs(cc4/1700);
x_tx= TX1:dd4:TX2;    %find x_tx for same matrix dimension

%To calculated theta angle at Tx side
%thetaTXin;thetaTXout
angle_1=(h_airp/TX1*180/pi); %in degrees
thetaTXin=90-angle_1
angle_2=(h_airp/TX2*180/pi); %in degrees
thetaTXout=90-angle_2
cc5=thetaTXin-thetaTXout;


dd5=abs(cc5/1700);
theta_tx_deg=thetaTXin:dd5:thetaTXout;        %theta_tx_deg
theta_tx_rad=(theta_tx_deg.*pi)/180;

%To calculate phi angle at Tx side
```

```
%phiTXin;phiTXout
dphi_1=tan((90-phiRXin)*pi/180)*RX1;
dphi_2=tan((phiRXout-90)*pi/180)*RX2;
angle_3=(dphi_1/TX1*180/pi);
phiTXin=90-angle_3
angle_4=(dphi_2/TX2*180/pi);
phiTXout=90+angle_4
cc6=phiTXin-phiTXout;
dd6=abs(cc6/1700);
phi_tx_deg=phiTXin:dd6:phiTXout;
phi_tx_rad=(phi_tx_deg.*pi)/180;

%To calculated the distance from Tx to airplane (r_tx)
r_tx=x_tx./(sin(theta_tx_rad).*sin(phi_tx_rad)); %**************

%total of reflected wave distance(m)
total_r_refl=r_rx+r_tx;

%Line of sight wave distance(m)
%Defind hight of Tx, Rx antenna and distance between Tx and Rx
%h_tx=230;                    %hight of Tx
%h_rx=4;                      %hight of Rx antenna
r_direct=sqrt((h_tx-h_rx)^2+d0^2)

%Distance difference between direct and reflected wave (m)
r_diff=total_r_refl-r_direct;


%To calculate the interference distance (interf_dis)in meters
phi_rx_rad1=((90-phiRXin)*pi)/180;
d_1=(RX1/cos(phi_rx_rad1));
phi_rx_rad2=((phiRXout-90)*pi)/180;
e_1=((RX2)/cos(phi_rx_rad2));
interf_dis=sqrt(d_1^2+e_1^2-2*d_1*e_1*cos(phi_rx_rad1+phi_rx_rad2))
incre1=abs(interf_dis/1700);
interf_dis_1=0:incre1:interf_dis;

%To calculate the interference time (interf_time) in seconds
v_airp=v_airp*1e3; %velocity of airplane 450km/hour
sec_hour=3600
meter_sec=v_airp/(sec_hour-sec_adj);
interf_time=interf_dis/meter_sec
incre2=abs(interf_time/1700);
interf_time_1=0:incre2:interf_time;


%Phase differnce between direct and reflected path
lambda=3e8/freq;
phase_diff=((2*pi)/lambda)*r_diff;

figure (1)
plot(phi_rx_deg,r_rx,'k');
```

```
%title('total of reflected wave distance(m)', 'FontSize',16);
xlabel('\phi Angle at receiving side [degrees]', 'FontSize',14);
ylabel(' Distance to airplane [meters]', 'FontSize',14);
figure (2)
plot(phi_tx_deg,r_tx,'k');
%title('total of reflected wave distance(m)', 'FontSize',16);
xlabel('\phi Angle at transmitting side [degrees]', 'FontSize',14);
ylabel('Distance to airplane[meters]', 'FontSize',14);

figure (3)
plot(phi_rx_deg,total_r_refl,'k');
title('total reflected distance of airplane(m)', 'FontSize',16);
xlabel('\phi Angle at receiving side [degrees]', 'FontSize',14);
ylabel('Total distance [meters]', 'FontSize',14);

%To calculate percentage of reflection Gamma
Pt=Po*1e3; %output power of transmitter
Gt=100;    %antenna gain of Tx
Gr=2.5;    %atenna gain of Rx
v=3e8;
freq=freq;
freq_min=60.75e6;
lambda_max=v/freq_min;
lambda_1=v/freq;
sigma=max(rcs_db)
Rt=44; %Rt is distance between Tx antenna to airplane of cross range in km.
r_rx_min=min(r_rx)/1000        % r_rx is Rra in km.
Rt_1=min(r_tx)/1000            %Rt_1 is distance between Tx antenna to airplane in km.


Rra= [.5:.1:8];
  PDr=(Pt*Gt*Gr.*lambda_max^2*sigma)./((4*pi)^3*Rt^2*Rra.^1.4)
        PDr_max=max(PDr)

        Gamma=(PDr*100)/PDr_max

Rra_1=r_rx_min
  PDr_1=(Pt*Gt*Gr.*lambda_1^2*sigma)./((4*pi)^3*Rt_1^2*Rra_1.^1.3);
  Gamma_1=(PDr_1*100)/PDr_max


figure(4)
plot(PDr,Rra,'*-')
xlabel('\sl P_{Dr} \rm (mW/m^2) ','FontSize', 13)
ylabel('\sl R_{ra} \rm (km)','fontsize',13)
legend('60.75MHz')

hold on
axis tight

figure(5)
plot(Gamma,Rra,'.-k')
```

```
xlabel('\sl \Gamma_{airp} \rm (%) ','FontSize', 18)
ylabel('\sl R_{ra} \rm (km)','fontsize',18)
legend('60.75MHz')
hold on
axis tight


%*****************************************************************
%
%To calculate field strength at receiving antenna.
%
%*****************************************************************
%Defind parameters of model
%rho_1=rho_use        %reflection coefficient (%)
Po=Po*1e3;                    %Tx output power of ch9,ch3
Direc=1.64;     %directivity of standard dipole
lambda = 3e8 /(freq/freq_phase_adj);
beta=(2*pi/lambda);     %phase constance
sigma_2=rcs_db;         %RCS of ellipsoild
%ex=15*8.854*10^-12;
%ex=2*8.854*10^-5;



 Eref_02 = exp(-i*beta*r_direct)./r_direct +Gamma_1*sigma_2.*(exp(-
i*beta.*total_r_refl).*exp(-i*beta*r_diff))./total_r_refl;


Eo= 4*(sqrt(30*Po*Direc))/r_direct *((pi*h_tx*h_rx)/(lambda*r_direct)); %eq(3.16)
Eo=Eo*1e6;              %V/m to uV/m
Eo_dBuV=level_adj+10*log10(Eo)  %in dBuV
Eo1 =sqrt(30*Po*Direc)*1e6;
Eo1_dBuV=10*log10(Eo1);

Er_02 =Eo_dBuV+ Eo1_dBuV * Eref_02; %used RCS Ellipsoild

dB_max=abs(max(Er_02));
dB_min=abs(min(Er_02));
div=dB_max-dB_min

figure (6);
plot((theta_ee*180/pi),rcs_db);
xlabel ('Aspect angle - degrees');
ylabel ('RCS ');
title (' RCS Blackscattered of ellipsoid ')
grid;



figure (9);
plot(phi_rx_deg,Er_02);
axis tight
xlabel('\phi Angle at receiving side [degrees]','FontSize',14);
```

```
ylabel('Field strength  [dB]','FontSize',14);


figure (11);
plot(interf_dis_1,Er_02);
axis tight
%axis([32 3500 25 40])
xlabel('Interference distance (meters)','FontSize',14);
ylabel('Field strength  [dB]','FontSize',14);


figure (13);
plot(interf_time_1,Er_02);
axis tight


xlabel('interference time (sec)','FontSize',14);
ylabel('field strength  [dB]','FontSize',14);

Title(['\sl{h_{airp}}\rm ',num2str(h_airp),(' m  '),' speed ',num2str(v_airp),(' m/h')...
    '  \slRx(\theta,\phi)_{in}\rm','[',num2str(thetaRXin),'\circ',',',num2str(phiRXin),'\circ',']'...
    '  \slRx(\theta,\phi)_{out}\rm','[',num2str(thetaRXout),'\circ',',',num2str(phiRXout),'\circ',']'])
step=(div/2)/8;
text(.4,dB_max-step,  (['signal freq  ',num2str(freq),' Hz']))
text(.4,dB_max-2*step,  (['interf dist  ',num2str(interf_dis),' m']))
text(.4,dB_max-3*step,(['interf time  ',num2str(interf_time),' sec']))
text(.4,dB_max-4*step,(['\sl d_0\rm   ',num2str(d0),' m']))
%text(.4,dB_max-5*step,(['RXin   ',num2str(RX1),' m']))

%text(.4,dB_max-6*step,(['RXout   ',num2str(RX2),' m']))
text(.4,dB_max-11*step,(['\sl \Gamma_{airp}\rm  ',num2str(Gamma_1),' %']))
text(.4,dB_max-12*step,(['fluc. level ',num2str(div),' dB']));
text(.4,dB_max-13*step,(['\sl R_r_a\rm ',num2str(min(r_rx)),' m']));

figure (14);
plot(interf_time_1,Er_02);
axis tight
axis([0 14 32 46])
grid on
xlabel('interference time (sec)','FontSize',22);
ylabel('signal strength  [dBuV]','FontSize',22);
```

Author Biography

Name	**Mr. Anuchit Wongkeeratikul**
Date of Birth	**July 12, 1968 at Nakornratchasima**
Address	**148 Muban Silichon Village, T. Pralub, A. Muang, Khon Kaen, THAILAND 40000**
E-mail Address	**w_anuchit@yahoo.com**
Education	**1992 B.Eng. of Electrical Engineering from Vongchavalitkul University**
	1996 M.Eng. of Electrical Engineering from Khon Kaen University
Proficiency	**1) Television Broadcasting**
	2) Satellite Communication
Experience	**1988-1992 Broadcasting Technicians**
	1998-2002 Part-time Lecturers at North-eastern University, Khon Kaen
	1992-Present Broadcasting Engineer and Chief of TV Station of Thai TV Color Channel 3 Khon Kaen